AN AIRBORNE INVESTIGATION OF THE STRUCTURE OF THE ATMOSPHERIC BOUNDARY LAYER OVER THE TROPICAL OCEAN

by

MARK ANTHONY DONELAN

B.Eng., McGill University, 1964

A THESIS SUBMITTED IN PARTIAL FULFILMENT OF THE

REQUIREMENTS FOR THE DEGREE OF

DOCTOR OF PHILOSOPHY

in the Department

of

Physics

and the Institute of Oceanography

We accept this thesis as conforming to the required standard

THE UNIVERSITY OF BRITISH COLUMBIA

October, 1970

In presenting this thesis in partial fulfilment of the requirements for an advanced degree at the University of British Columbia, I agree that the Library shall make it freely available for reference and study. I further agree that permission for extensive copying of this thesis for scholarly purposes may be granted by the Head of my Department or by his representatives. It is understood that copying or publication of this thesis for financial gain shall not be allowed without my written permission.

Department of Physics and the Institute of Oceanography

The University of British Columbia
Vancouver 8, Canada

Date October 15, 1970

ABSTRACT

Across the air-sea interface there is a transfer of momentum, heat and moisture. Knowledge of these is essential to the understanding of oceanic and atmospheric circulations.

This study is an investigation of the vertical turbulent transfers of momentum, heat and moisture in the boundary layer of the atmosphere using an instrumented light aircraft. The data were collected at several altitudes between 18 m and 500 m in the Atlantic trade wind zone east of the island of Barbados. Since the tropical ocean is the primary source of heat input to the atmospheric heat engine, good estimates, in this region, of the transfers of heat and moisture and their vertical variations are essential to any global numerical atmospheric prediction scheme.

The fluctuations of the velocity components, temperature and humidity and the transfers of momentum, heat and moisture were investigated, primarily by means of their spectra and cospectra. It was found that: ninety percent of the heat input to the atmosphere was in the form of latent heat; the sensible heat flux was positive (upward) at the small scales generated near the surface and negative at the large scales due to subsiding air; the latent heat flux was positive at all scales and similar in spectral distribution to the momentum flux; the flow appeared to be anisotropic even at scales one hundred times smaller than the distance from the boundary; the drag coefficient, from direct measurements of the momentum flux (or stress), was $(1.45 \pm 0.08) \times 10^{-3}$; shear generated turbulence was not entirely dissipated locally.

TABLE OF CONTENTS

	page
ABSTRACT	ii
TABLE OF CONTENTS	iii
LIST OF TABLES	vi
LIST OF FIGURES	vii
ACKNOWLEDGEMENTS	x
CHAPTER 1: INTRODUCTION	1
1.1 Airborne turbulence measurements	1
1.2 Previous work	1
1.3 Objectives of this study	2
CHAPTER 2: OBSERVATIONAL SCHEME AND ANALYSIS METHODS	4
2.1 The experiment	4
2.2 Flight patterns	4
2.3 Data gathering procedure	11
2.4 Data processing	12
CHAPTER 3: EXPERIMENTAL RESULTS AND DISCUSSION	13
3.1 Introduction	13
3.1.1 The data	13
3.1.2 Synoptic conditions	13
3.1.3 Methods of presentation	18
3.2 Measurements along the wind	23
3.2.1 Vertical velocity	23
3.2.2 Horizontal velocity	31
3.2.3 Temperature	40
3.2.4 Humidity	46
3.2.5 Momentum flux	50

3.2.6 Heat flux 59

3.2.7 Moisture flux 65

3.3 Comparison of crosswind measurements with measurements along the wind 73

3.3.1 Introduction 73

3.3.2 Vertical velocity 74

3.3.3 Horizontal velocity 78

3.3.4 Temperature and humidity 80

3.3.5 Heat flux 80

3.3.6 Moisture flux 85

3.4 The turbulent kinetic energy budget 88

3.4.1 Introduction 88

3.4.2 Height dependence of terms in kinetic energy budget 90

3.4.2.1 Mechanical production 90

3.4.2.2 Buoyancy production 90

3.4.2.3 Dissipation 90

3.4.2.4 The residual term 93

3.4.3 The budget for flights 1 and 3 95

3.5 The temperature-humidity correspondence 98

3.6 Discussion of a possible pattern of convective organization 108

CHAPTER 4: SUMMARY OF CONCLUSIONS 112

LIST OF REFERENCES 117

APPENDIX A: THE INSTRUMENTS 120

A.1 Introduction 120

A.2 The temperature sensor 120

A.3 The humidiometer 124

APPENDIX B: DATA PROCESSING 128

B.1 Introduction 128

B.2 Selection of data segments 128

B.3 Machine processing 129

APPENDIX C: COMPARISON OF SIMULTANEOUS MEASUREMENTS FROM FLIP AND THE AIRCRAFT 135

C.1 Introduction 135

C.2 Data outline 135

C.3 Spectra and cospectra 137

APPENDIX D: STATISTICS 142

LIST OF TABLES

		page
1.	Flight summary	14
2.	Normalizers for spectra and cospectra of flights 1 and 3	20
3.	Statistics of flights 1 and 3	27
4.	Drag coefficients	37
5.	The data used in the Flip/Aircraft comparison	136
6.	Variances	143
7.	Stability	144
8.	Similarity ratios	145
9.	The Kinetic Energy Budget	146

LIST OF FIGURES

		page
1.	The Bomex array	5
2.	The research aircraft, Beechraft Queen Air 304D	6
3.	FLIP	7
4.	The flight patterns	9
5.	Temperature and humidity profiles	15
6.	Wind profiles from the airborne Doppler radar	16
7.	Satellite photographs of the Bomex area	17
8.	Vertical velocity spectra (upwind)	24
9.	Vertical velocity traces (upwind)	25
10.	σ_w vs. Z (upwind)	26
11.	$(L_M)_w$ vs. Z (upwind)	28
12.	B_w vs. Z (upwind)	30
13.	Longitudinal velocity traces	32
14.	Longitudinal velocity spectra	33
15.	'4/3' test for isotropy	35
16.	σ_u/u_* vs. Z	39
17.	Temperature spectra (upwind)	41
18.	σ_T vs. Z (upwind)	42
19.	$(L_M)_T$ vs. Z (upwind)	43
20.	Temperature traces (upwind)	45
21.	Humidity spectra (upwind)	47
22.	σ_Q vs. Z (upwind)	48
23.	Humidity traces (upwind)	49
24.	Momentum traces (upwind)	51

25. Momentum cospectra (upwind) 52

26. u_*^2 vs. Z 53

27. $-r_{uw}$ vs. Z 55

28. $(L_M)_{uw}$ vs. Z 57

29. B_{uw} vs. Z 58

30. Heat flux traces (upwind) 60

31. Heat flux cospectra (upwind) 62

32. Heat flux vs. Z (upwind) 64

33. Moisture flux traces (upwind) 66

34. Moisture flux cospectra (upwind) 67

35. $(L_M)_{wQ}$ vs. Z (upwind) 69

36. r_{wQ} vs. Z (upwind) 70

37. Moisture flux vs. Z (upwind) 71

38. Vertical velocity traces (crosswind) 75

39. Vertical velocity spectra (crosswind) 76

40. Lateral velocity spectra 79

41. σ_T vs. Z (crosswind) 81

42. σ_Q vs. Z (crosswind) 82

43. $(L_M)_Q$ vs. Z (crosswind) 83

44. Heat flux cospectra (crosswind) 84

45. Moisture flux traces (crosswind) 86

46. $(L_M)_{wQ}$ vs. Z (crosswind) 87

47. Mechanical production vs. Z 91

48. Dissipation vs. Z 92

49. Divergence vs. Z 94

50. Kinetic Energy Budget for flight # 1 96

51. Kinetic Energy Budget for flight # 3 97

52. T'Q' (t) (upwind) 99

53. T'Q' (t) (crosswind) 100

54. $r_{TQ}(k)$ (upwind) 101

55. r_{TQ} (k_v) (crosswind) 103

56. $(L_+)_{TQ}$ vs. Z (upwind) 104

57. $(L_+)_{TQ}$ vs. Z (crosswind) 105

58. Cross-spectra of T' and Q' (upwind) 107

59. A possible pattern of convective organization 110

60. The frequency response of the thermistor 122

61. The frequency response of the humidiometer 126

62. Block diagram of machine processing steps 130

63. Comparison of w spectra from the aircraft and Flip 138

64. Comparison of u spectra from the aircraft and Flip 139

65. Comparison of the momentum cospectra from the aircraft and Flip 140

ACKNOWLEDGEMENTS

The writer wishes to express his indebtedness to the many members of this Institute who in one way or another helped make this thesis possible: in particular to Dr. M. Miyake whose guidance shortened many paths, Dr. R.W. Stewart and Dr. R.W. Burling from whom help and encouragement were never wanting, Ron Wilson, John Garrett, Gordon McBean and Mary Lou Marotte who put many painstaking hours into computer programming for the general good, and to Ernie Jerome with whom data collecting was never a chore. Mr. Don Hume designed and built some of the electronic packages and Mr. Heinz Heckl did much of the structural construction and repairs.

This thesis is based on information collected from an aircraft owned and operated by the U.S. National Centre for Atmospheric Research. The author would like to thank all the pilots who were involved in this programme and especially Mr. L.M. Zinser and Mr. R. Burris who flew an average of one mission a day for 30 long, hot, consecutive days in sunny Barbados.

The ancillary data was collected with NCAR instruments using NCAR recording equipment, and some preliminary data preparation was handled by NCAR personnel. Consequently, the list of persons who have contributed to the groundwork of this thesis is long; the author is grateful to them and especially to Mr. Richard Garrellts, who did much outside the line of duty and whose patience appeared to be inexhaustible.

To my wife, June, I offer my gratitude for the many ways in which she has made my years as a graduate student happy ones.

This study was directly supported by contract E22-78-70 (N) of the U.S. Environmental Science Services Administration. The research is conducted as part of the Air-Sea Interaction programme of this Institute, which receives general support from: the National Research Council of Canada, the Defence Research Board of Canada, the Meteorological Branch of the Canadian Department of Transport, and the U.S. Office of Naval Research.

While engaged in this study the author received personal support from the National Research Council of Canada.

CHAPTER 1

INTRODUCTION

1.1 Airborne turbulence measurements

The airplane is an eminently suitable platform for the investigation of atmospheric turbulence primarily because of its mobility. Paradoxically enough, it is just this mobility which poses the most serious problems in the interpretation of airborne turbulence measurements. That is, the data must be corrected for the motion of the platform. The central problem, however, is the measurement of vertical velocity; a task which has been tackled in several different ways over the past fifteen years.

1.2 Previous work

Bunker (1955, 1957, 1960) used an 'airplane acceleration' technique to estimate the vertical velocity. In this method the airplane itself is the sensor and the relative vertical air velocity is related to the vertical acceleration of the aircraft through the lift equation (von Mises, 1945). Of course this method is severely band limited by the aircraft's phugoidal oscillations at low frequencies and its inertia at high frequencies. In terms of measurable gust sizes, Bunker (1957) estimated a range of 20 m to 2000 m for the Woods Hold Oceanographic Institution's PBY-6A (Catalina) aircraft.

Lappe et al (1959), Telford and Warner (1962), Dutton and Lenschow (1962) and Myrup (1965) all used either a vane or pitot tube array angle of attack sensor to estimate the vertical velocity components down to much smaller scale sizes.

The development of the sonic anemometer provided another method of getting at the cross-stream velocity components (Kuprov and Tsvang, 1965; Miyake et al 1970b), and, since the instrument's calibration is uniquely related to the speed of sound in air and the acoustic path length, this method is particularly well suited to the delicate study of isotropic turbulence.

The question of correction of the measured velocity components for the aircraft's motion has been handled by the previous investigators cited in much the same manner: the details of each method and the differences among them can be found in many of the references listed. In general the integrated outputs of accelerometers furnish the aircraft's velocity components and a gyroscope senses the variations of attitude angle. In this way the air velocity components are deduced within an accuracy of a few percent; however, corrections at frequencies lower than 0.005 Hz are rather uncertain due to gyroscopic drift. Today these problems are being eliminated by the use of inertial platforms on turbulent flux measuring aircraft.

1.3 Objectives of this study

In 1967 a programme of development of turbulence sensors for use on light aircraft was launched at the Institute of Oceanography of the University of British Columbia. The programme culminated in April 1969 with the sensor system described by Miyake et al (1970b) and used in this investigation. At that time it was considered that the developmental programme had achieved its objective, which was the capability of measurement of the vertical turbulent fluxes of momentum, heat and moisture over scale sizes from 2 m to 20 km. A subsequent comparison against other flux measurements (see Appendix C) indicated that this was indeed the case. The use of hot-wire anemometry extended the measurement of the horizontal velocity fluctuations to scales as

small as 5 mm.

The completion of the developmental programme coincided with the commencement of a large meteorological and oceanographic field experiment near the island of Barbados. The central purpose of the Barbados Oceanographic and Meteorological Experiment 'BOMEX' (Davidson, 1968) was the measurement of the interchange of mass, momentum and energy across the air-sea interface. Thus this experiment provided an excellent opportunity to directly measure the turbulent transfers in a region where the upward flux of heat is the primary driving force for the atmospheric heat engine. In addition, the Bomex organization handled many of the logistical field problems inherent in any large experimental programme, and facilitated the exchange of information between the various participants.

This study is an experimental investigation into the structure of the atmospheric boundary layer in the Atlantic trade wind zone, using data gathered during Bomex. Measurements were made at several altitudes between 18 m and 500 m. Ground based measurements indicate that a flight altitude of 18 m is sufficiently low to obtain good estimates of the transports in the surface boundary layer. Data were collected at higher altitudes to investigate the variability with height of the turbulent fluxes and of the mechanisms responsible for their variability. The data are analysed through the cospectra of the fluxes of heat, moisture and momentum and the spectra of the four turbulent parameters required to compute these fluxes. Both the total integral under the spectra and cospectra and the distribution of the energy among scale sizes are examined for the data gathered during flights in the wind direction. Several crosswind traverses were also made to explore the possibility of convective organization.

CHAPTER 2

OBSERVATIONAL SCHEME AND ANALYSIS METHODS

2.1 The Experiment

In May 1969, some 1500 scientists and technicians converged on the island of Barbados to participate in the Barbados Oceanographic and Meteorological Experiment (BOMEX).

The organization and objectives of Bomex are described by Davidson (1968) and Kuettner and Holland (1969), but the aspects which pertain directly to this work are summarized briefly here. Bomex's primary objective was a thorough investigation of the air-sea interaction problem over an area of 500 km x 500 km (see Figure 1). Various well instrumented research platforms including 25 aircraft probed the atmosphere to an altitude of 20 km and the ocean to a depth of 500 m. Several of the platforms were equipped to measure vertical turbulent transports beneath cloud base. Of these only a few were capable of simultaneous direct measurement of the fluxes of momentum, sensible heat and moisture: NCAR'S aircraft, Beechraft Queen Air 304D (see Figure 2) instrumented as described in Miyake et al (1970b) and Appendix A; 'FLIP' (see Figure 3) the manned spar buoy of Scripps Oceanographic Institution (Rudnick, 1964), instrumented with turbulence sensors similar to those on the Queen Air; and a DC-6 of the Research Flight Facility of the U.S. Environmental Science Services Administration.

2.2 Flight Patterns

The experiment was designed to investigate the vertical structure of the boundary layer. Therefore each flight was divided into sections of level flight (henceforth called 'levels') at three or four different

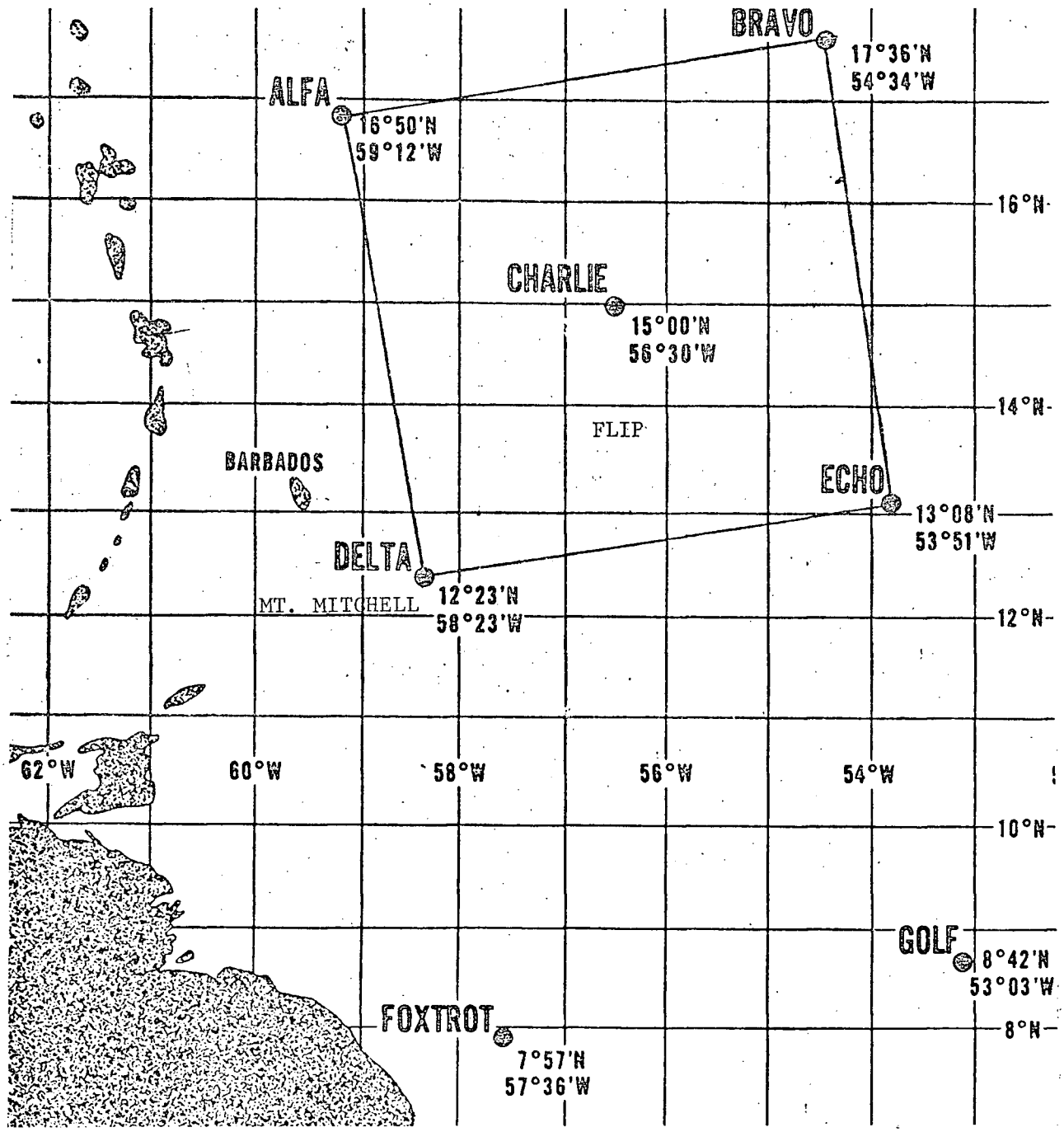

FIGURE 1. THE BOMEX ARRAY

(from Bomex Bulletin No.3, 1969)

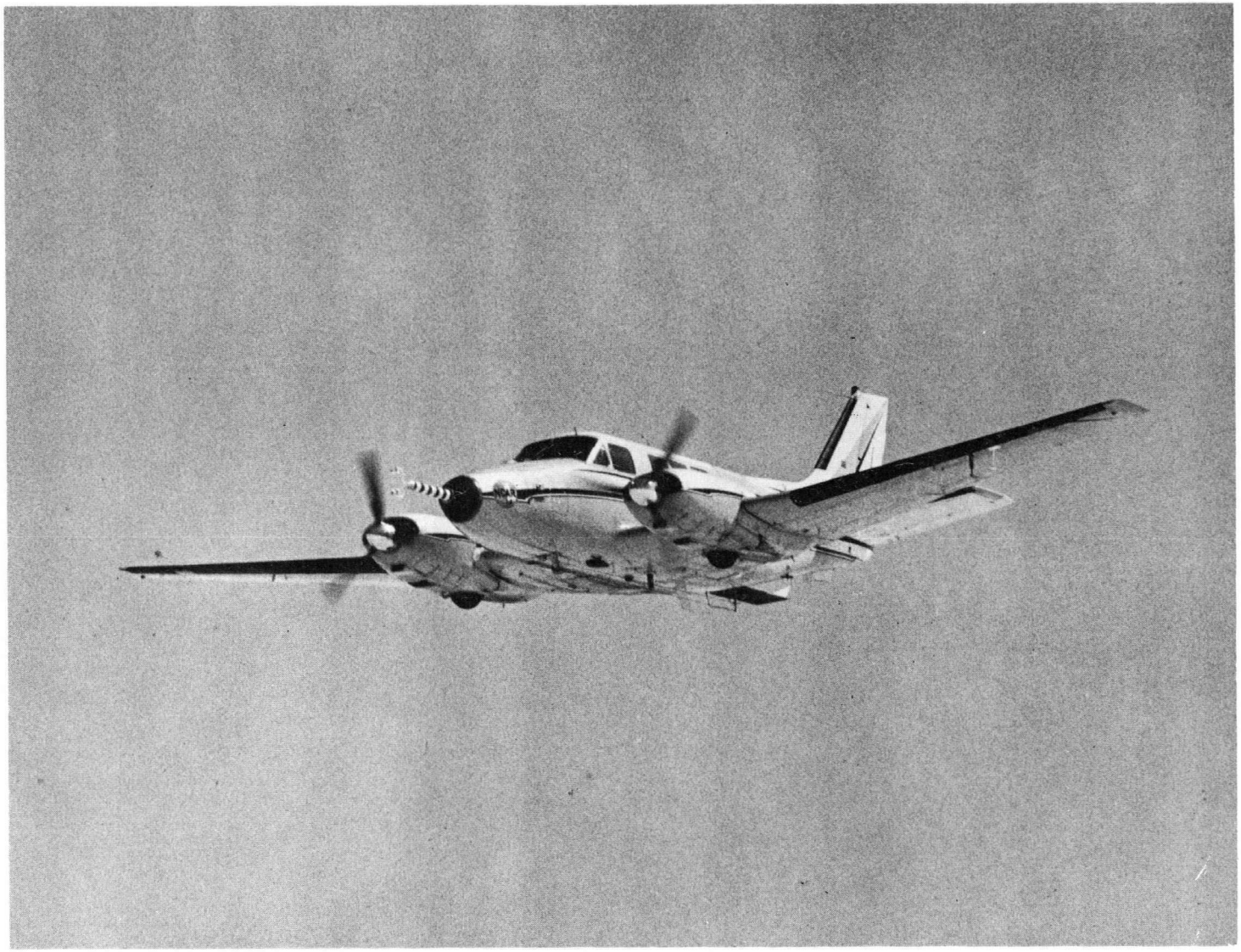

FIGURE 2. THE RESEARCH AIRCRAFT, BEECHCRAFT QUEEN AIR 304D

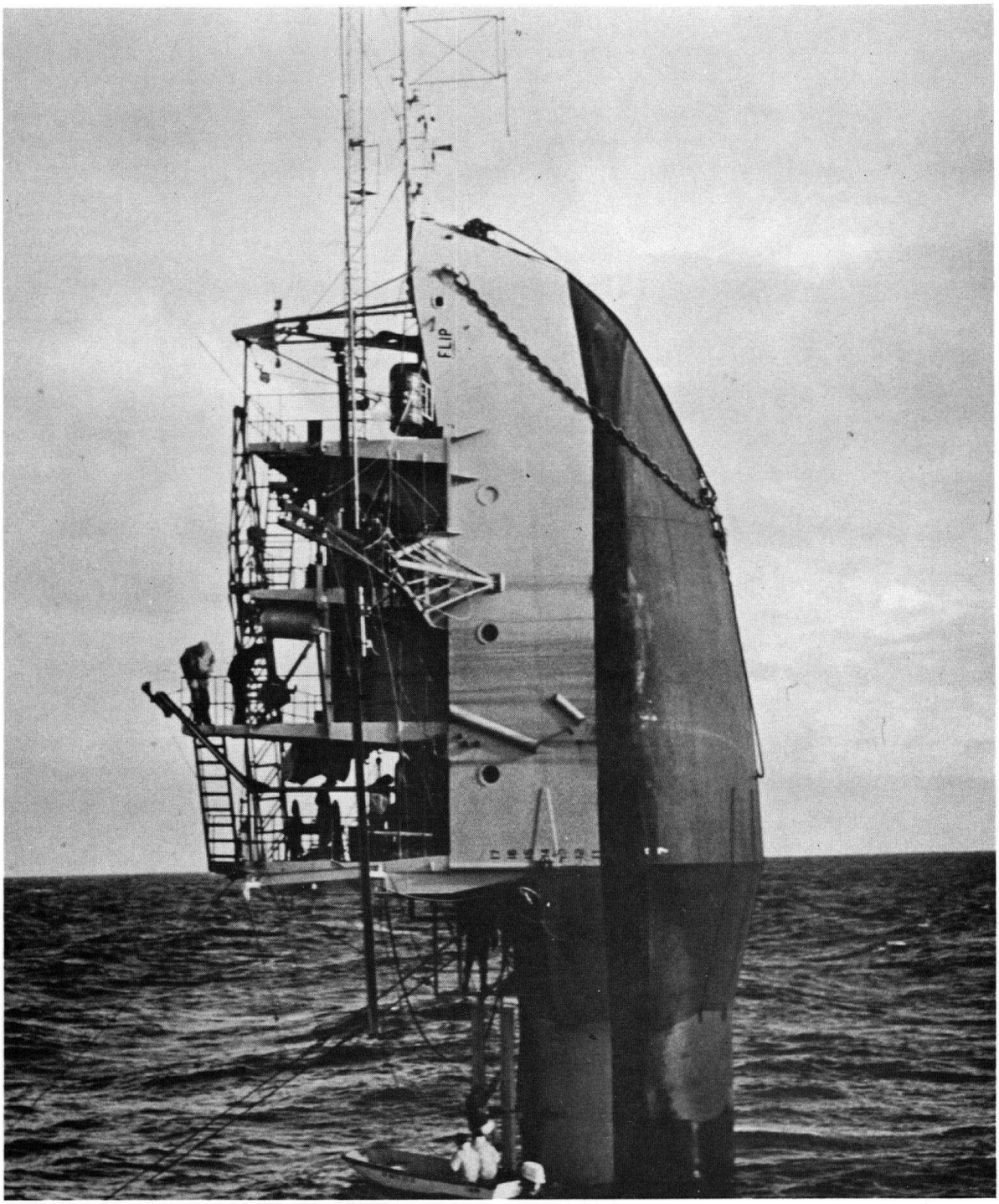

FIGURE 3. FLIP

altitudes. And, because it was believed that the turbulence structure changes less rapidly with height the greater the distance from the boundary, the altitude of successive levels was chosen to increase in equal logarithmic steps from the lowest level of about 18 m. To avoid the possibility of confusing temporal variation with systematic height dependence, the patterns were not flown at steadily increasing or decreasing altitude. Generally the first level flown was at an altitude of approximately 50 m because it was at this level that the pilot and observer estimated the wind direction. This was done in the following fashion. As the aircraft approached the surface craft, over which the pattern was to be flown, the altitude was held at about 50 m and the pilot altered the heading to coincide with the direction of the windrows. The Doppler radar drift angle was then amplified and monitored on the chart recorder in the cabin. Following the observer's instructions the pilot made fine adjustments to the heading until the trace of the drift angle averaged zero over a period of about 30 seconds. At this point the aircraft had always just passed over the vessel, and its heading was taken to be representative of the wind direction at that level in the vicinity. As the aircraft made a standard 180 degree turn to begin the first downwind leg, the observer hastened to make adjustments to the instruments.

The pilot then guided the aircraft in one of the flight patterns of Figure 4 by changing the heading in 90 degree standard turns to port. At the completion of a turn the aircraft autopilot was set to the 'altitude hold' mode except along the leg 'A' in which the pilot altered the altitude to enter the pattern at a new level. Each level was completed with legs either parallel with or perpendicular to the previously

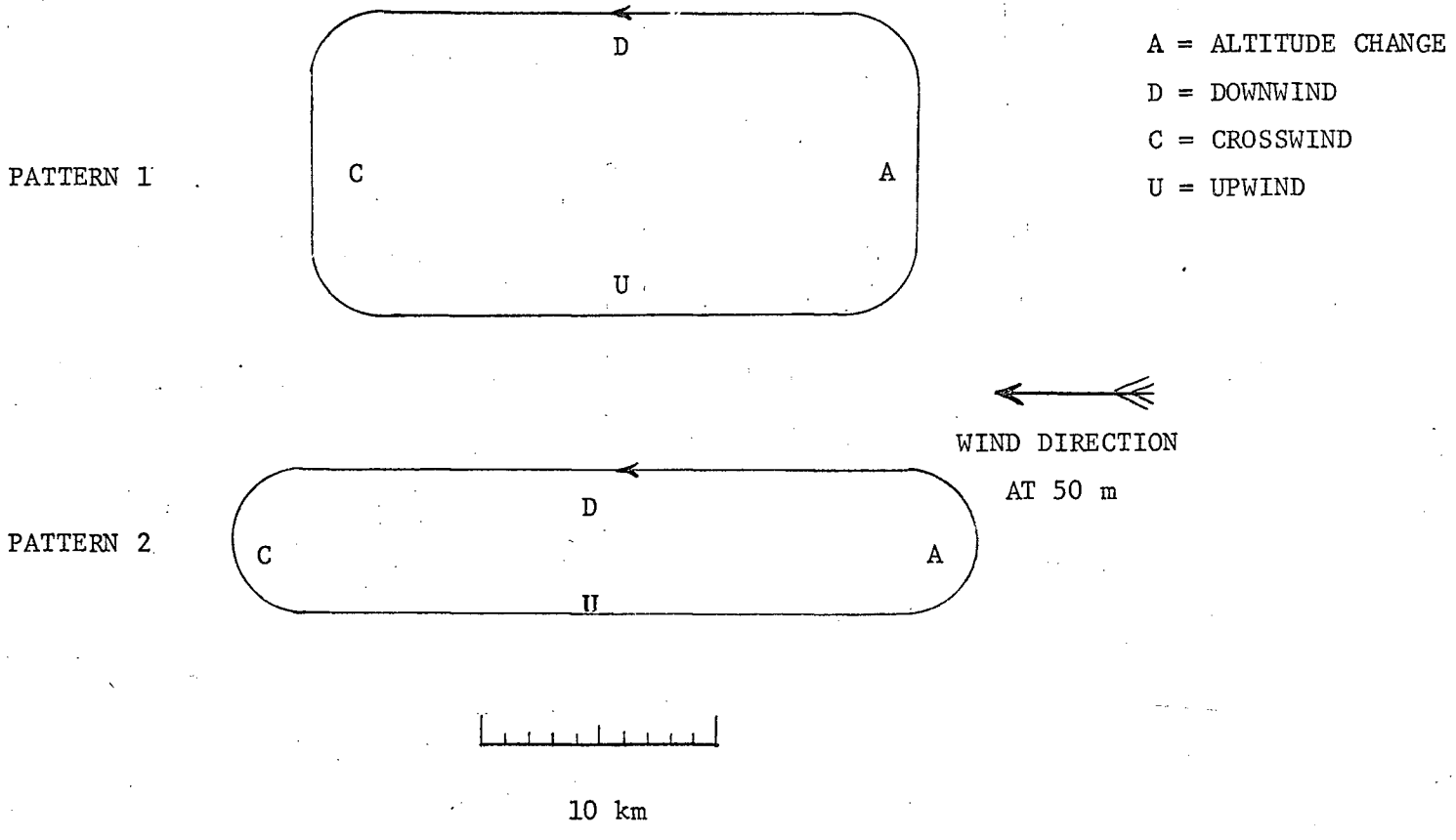

FIGURE 4. THE FLIGHT PATTERNS

determined wind direction at 50 m. To compensate for the difference in ground speed between the upwind and downwind legs, the latter occupied a shorter time interval than the former.

Each flight was in the vicinity of either Flip or the ship, "Mt. Mitchell" (see Figure 1). Throughout the month of May aboard Flip a team of investigators from this Institute collected turbulence data; therefore the flights over Flip were designed to provide direct comparisons of statistics of the turbulence near the surface (see Appendix C) as well as to obtain data at higher levels. Since the flights to Flip severely taxed the Queen Air's range capabilities, the ship "Mt. Mitchell" was selected as an alternate 'ground truth' station.

One of the important considerations in the design of the flight patterns is the choice of a suitable length for both the along wind and cross wind legs. Very long legs are desirable to be able to consider the larger turbulent scales. On the other hand, since temporal variations are not being considered, the shorter the interval between levels the better. The duration of flights over Flip was limited by the range of the Queen Air; heavily loaded as she was it was just possible to fly to Flip, spend an hour there gathering data and return to Barbados. The choice of 20 km for the along wind legs was selected as a balance between these considerations and because gyroscopic limitations make for uncertainty in the computation of the velocity components over longer distances; also it is known from ground based measurements that sampling intervals corresponding to a scale size of 10 km are adequate to estimate the fluxes near the surface. A somewhat shorter distance was traversed across the wind Figure 4) so that the flight duration of each level was limited to fifteen minutes or the complete flight to one hour, and so that neither the upwind nor the downwind legs would be far from the surface vessel.

2.3 Data gathering procedure

The data were recorded on magnetic tape in both digital and analogue form on two separate tape recorders. Thirty two channels of information were digitized at 32 Hz per channel (with a tape transport speed of 7 1/2 i.p.s.) and recorded on NCAR'S ARIS I digital data logging system (Dascher, 1966). The analogue tape recorder accepted 14 voltage signals and recorded them in frequency modulated form withan upper frequency cut-off of 2.5 kHz (at 7 1/2 i.p.s. also).

The signals recorded in analogue form were 'pre-conditioned' in the following way: each signal was, when necessary, added to an adjustable DC voltage, so as to remove its mean value, then amplified by a second operational amplifier using one of two gain settings in order to use as much of the tape recorder's dynamic range ($\pm$ 1.5 volts) as possible.

The digital data logging system was used to record the outputs from the mean value sensors directly in addition to signals from the turbulence sensors pre-conditioned as described above. This redundancy provided both a safeguard against outright loss of the recorded information, and also permitted recorder calibration checks on many of the channels.

In view of the hectic pace of air-borne data collection, it is important for the observer to be able to quickly determine the status of any of the recorded signals. This facility was provided by several types of monitoring equipment. All of the turbulence signal levels could be viewed at a glance on a panel of voltmeters, and any of the digitally recorded channels could be selected for display on a digital voltmeter. In addition a two-channel chart recorder was used to monitor either the input to or playback from the analogue recorder. Largely as a trouble shooting aid a small dual beam oscilloscope was also used.

In the course of a flight the degree of DC bias had to be altered frequently on some channels, the gain settings less frequently, to achieve the best possible signal to noise ratio without saturating the tape recorder. To keep track of these changes and to record visual synoptic observations, the observer kept a careful flight log on paper and a similar voice log on an edge track of the analogue recorder. The voice log was kept as an emergency measure only, as this observer regards the after-the-fact separation of occasional cryptic comments from the constant drone of an aircraft as among the most tedious of tasks. Fortunately, the written log proved adequate. The logs were tied to the recorded data by means of a digitally recorded clock which also provided a visual output.

2.4 Data Processing

The digital data tapes were made available to us in two forms by the National Centre for Atmospheric Research: 1) Copies of the original tapes in an acceptable I B M format; 2) Smoothed time series of each signal on microfilm in which each frame covered 10 minutes. The microfilm was useful in locating each run on the analogue tape by comparison of the roll angle signals, and in obtaining the mean value of various parameters for each run. The digital tape was used to compute several spectra merely to check the calibration of the analogue tape recorder and subsequent conversion to digital format.

All the spectra and time series presented herein were computed from the original analogue recorded data, which contained information up to frequencies in excess of 2 kHz, whereas the maximum digitization rate used was 128 Hz. The digitization and subsequent processing of the analogue recorded data is described in Appendix B.

CHAPTER 3

EXPERIMENTAL RESULTS AND DISCUSSION

3.1 Introduction:

3.1.1 The Data

The data analysed here were gathered during six flights on five consecutive days (May 25th to May 29th) and the night of the fifth day. The flights are numbered 1 to 6 in chronological order and Table 1 summarizes the flight patterns (Figure 4) used and provides details of the runs within flights 1 and 3, which are to be discussed in detail. The term 'run' refers to a single continuous data segment at constant altitude. In the text and figures a particular run will be denoted by x/y, where x is the flight number and y the run number.

3.1.2 Synoptic conditions

During the 'A' legs of the flight plans of Figure 4 the mean value sensors (Miyake et al 1970b) yielded sections of the profiles of temperature and humidity of Figure 5. The sections were then pieced together and the profiles combined to give the virtual potential temperature profile. The mean wind speed profiles were derived from Doppler radar measurements averaged over all the runs at any level. They are displayed in Figure 6, and the deviation of the wind direction from the orientation of the flight plan is indicated at each level in the table of Figure 6. However, such short term averages of Doppler radar measurements are quite likely to vary by 3% of the ground speed, which in this case is an accuracy of $\pm$ 2 m/sec. Thus, although the detailed behaviour of the profiles cannot be regarded as real, they provide a rough estimate of the mean wind speed.

In addition to these profiles, the daily satellite photographs (Figure 7)

FLIGHT	DATE	LOCAL TIME START	LOCAL TIME END	LOCATION	WIND DIRECTION AT 50 m	FLIGHT PATTERN	RUN	LEVEL in metres	* *	DURATION in secs.
1	25/6/'69	10.50	12.00	Mt. Mitchell	100°	1				
							2	43	C	80
							3	43	U	270
							5	20	C	60
							6	20	U	320
							7	150	D	190
							8	150	C	60
							11	500	C	75
							12	500	U	210
2	26/5/'69	10.15	11.20	Mt. Mitchell	108°	1		18, 46 150, 460		
3	27/5/'69	14.40	15.50	FLIP	100°	1				
							2	49	C	75
							3	49	U	210
							5	18	C	55
							6	18	U	280
							8	150	C	60
							9	150	U	240
							11	500	C	45
							12	500	U	165
4	28/5/'69	15.15	16.20	FLIP	≒95°	1		18, 52 150, 460		
5	29/5/'69	17.15	18.30	Mt. Mitchell	90°	2		26, 49 88, 140		
6	29/5/'69	22.00	23.10	Mt. Mitchell	88°	2		29, 98, 480		

* *
U = Upwind
D = Downwind
C = Crosswind

TABLE 1. FLIGHT SUMMARY

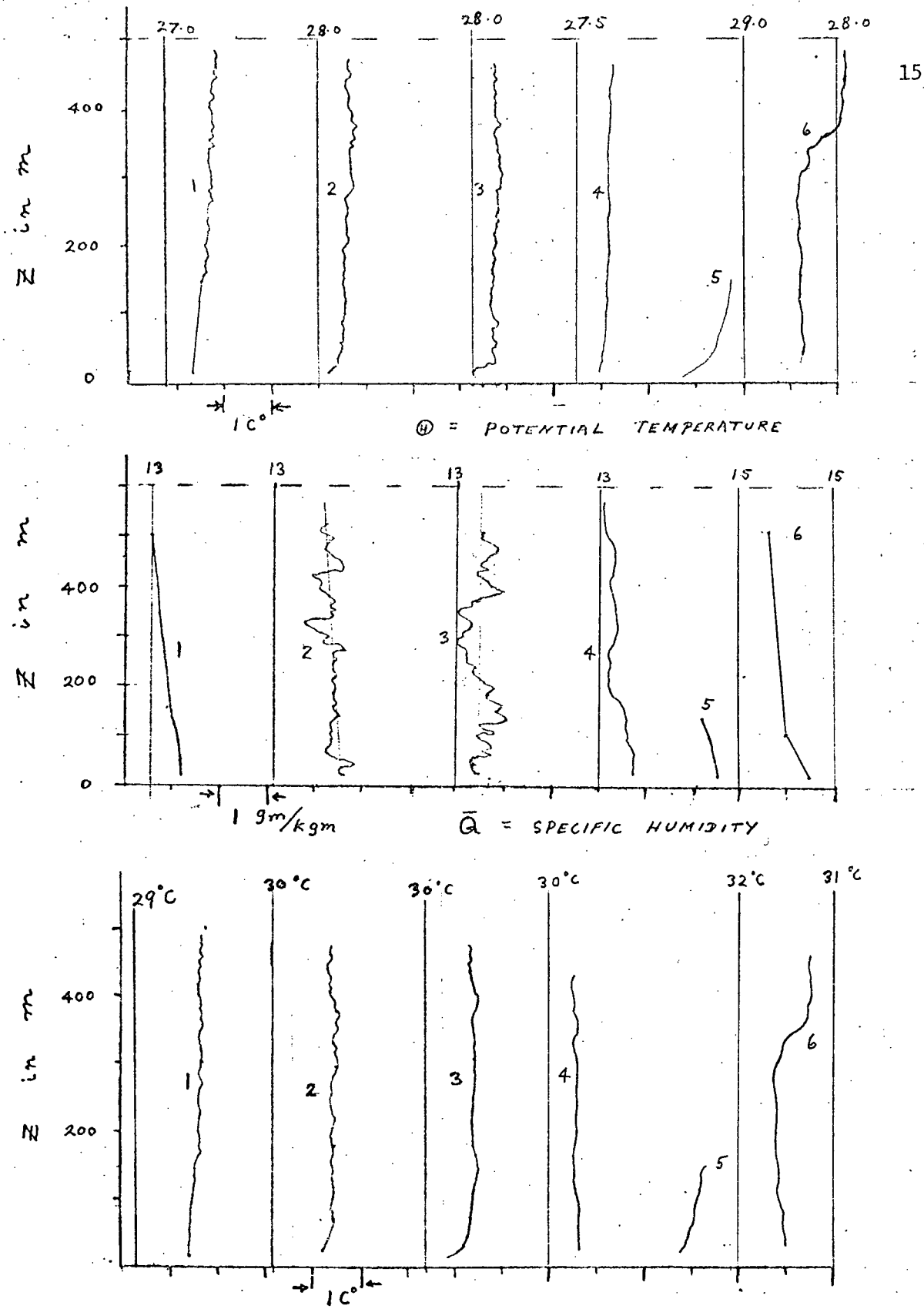

potential virtual temperature = Θ + .183 $\bar{Q}$

FIGURE 5. TEMPERATURE AND HUMIDITY PROFILES

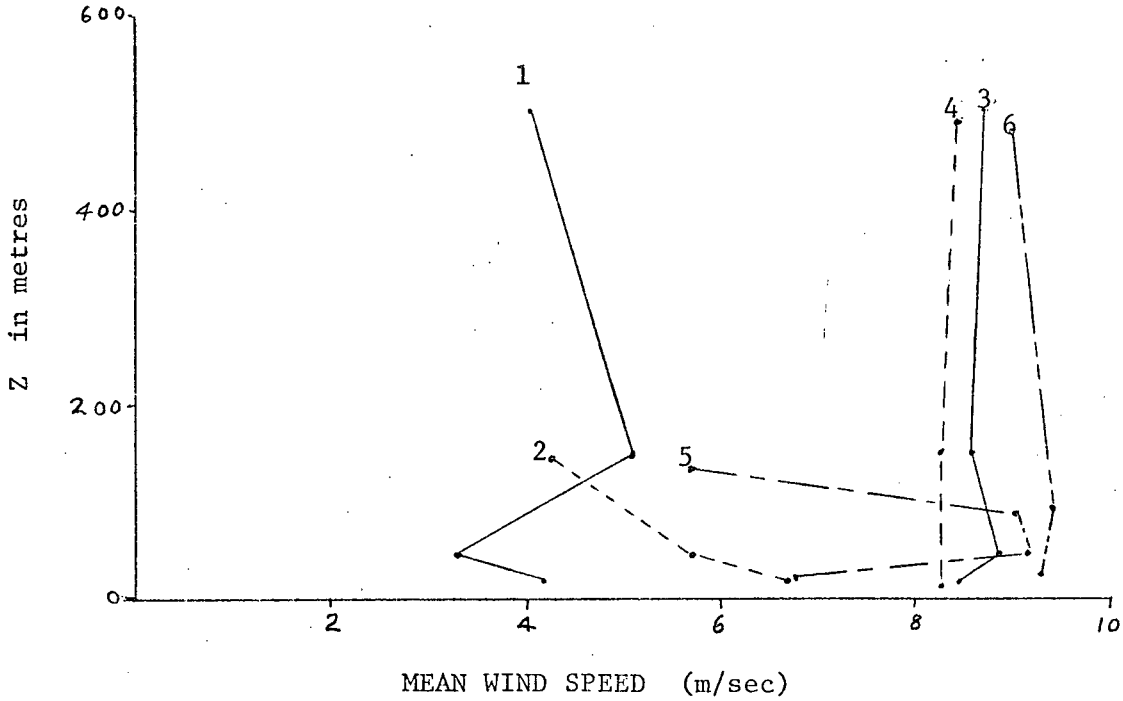

FLIGHT / APPROX. ALTITUDE	1	2	3	4	5	6
18 m	12	11	2	2		
27 m					3	3
50 m	9	13	1		6	
90 m					3	3
150 m	9	12	3	1	7	
500 m	6		-3	9		6

The numbers shown are the wind directions in degrees relative to the orientation of the flight pattern. Clockwise is positive.

FIGURE 6. WIND PROFILES FROM THE AIRBORNE DOPPLER RADAR

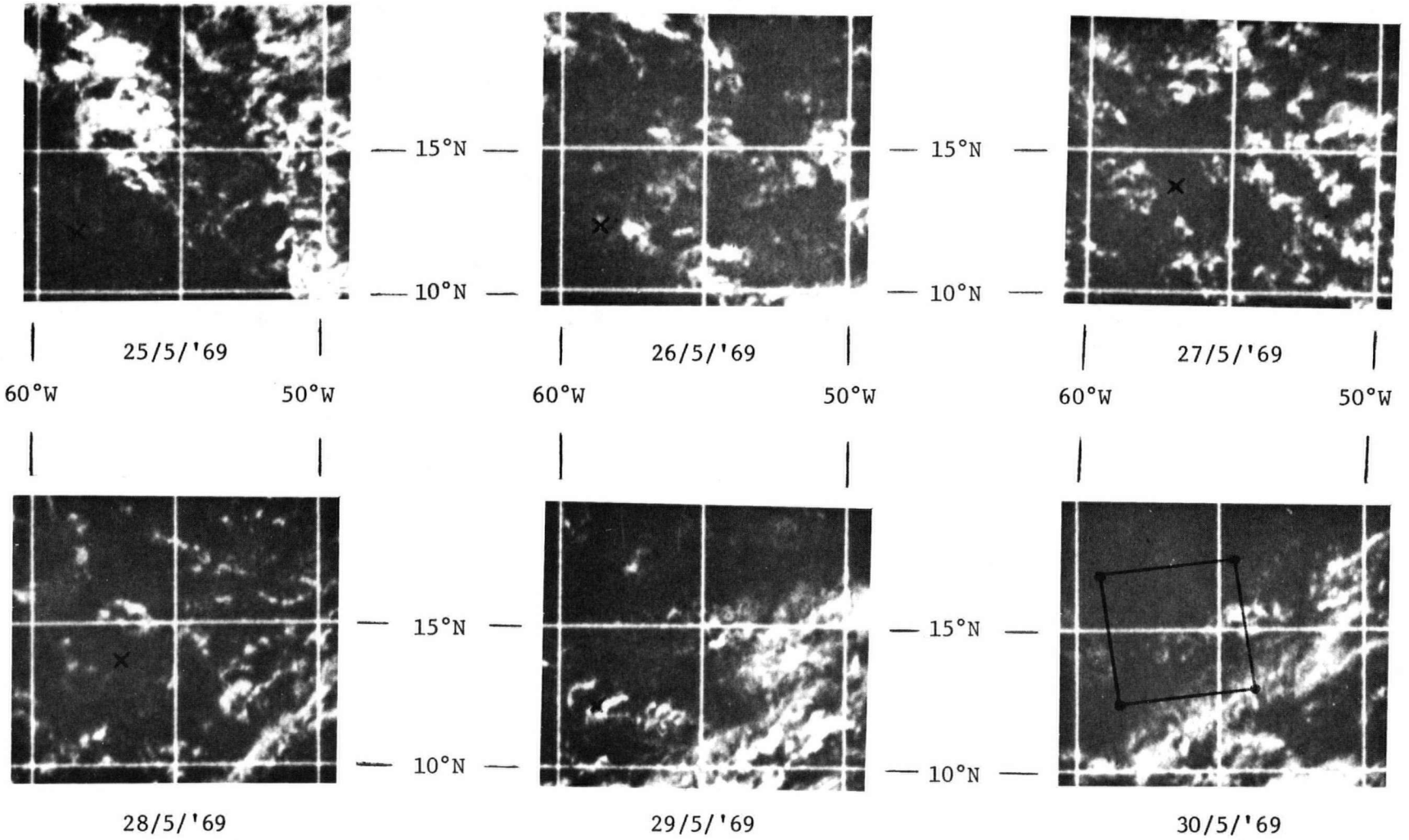

FIGURE 7. SATELLITE PHOTOGRAPHS OF THE BOMEX AREA

These photographs were taken soon after local noon. The Bomex array is shown in the last photograph; in each of the others an 'x' marks the location of the flight pattern on that day.

indicate the prevailling synoptic conditions in the area. Figure 7 consists of 6 enlargements of the Bomex area during the five days of flights 1 to 6 and the following day. These photographs were made from computer composed panoramas of visual range satellite photographs taken by ESSA 9, a satellite of the Environmental Science Services Administration, U.S.A. ESSA 9 passed over the Bomex array in the early afternoon.

From Figures 5 to 7 it is evident that conditions during the six flights were quite similar except with regard to mean wind speed. During all of the flights the potential virtual temperature was nearly constant with height, and meteorological conditions were similar except during flight #6 which was made at night.

Thus the mean surface wind speed is taken as the basis for grouping these flights. It is seen that they fall quite naturally into two groups: (a) flights 1 and 2, having wind speeds lower than 7 m/sec, are called the 'low wind speed group'; (b) flights 3, 4, 5, and 6, having wind speeds in excess of 8 m/sec, are labelled the 'high wind speed' group.

3.1.3 Methods of presentation

In the following sections of this Chapter, flights 1 and 3 are used, as examples of the low and high wind speed groups, in the presentation of time domain and spectral representations of the fluctuations of the vertical and horizontal velocity components, temperature, humidity and the fluxes of momentum, heat and moisture.

Spectra are presented in terms of the product of frequency with the spectral estimates $nS_{xx}(n)$ versus the logarithm of frequency. In such plots equal area increments represent equal increments of the variance of the data. Since it is the product $nS_{xx}(n)$ rather than spectrum itself which is used exclusively in the subsequent chapters, it is convenient and

unambiguous to refer to $nS_{xx}(n)$ as the 'n-spectrum'. The corresponding wave number spectrum times wave number $kS_{xx}(k)$ will be called the 'k-spectrum'.

Normalized k-spectra are presented versus the wave number $k = \frac{2\pi n}{V}$ radians/m; where V in the true air speed of the aircraft averaged over each run. The ordinate is normalized by the indicated parameter evaluated at the lowest upwind run in that flight; see Table 2 for the values of the normalizers. Bi-logarithmic axes are useful, especially in illustrating the high wave number power law dependence and in showing detail in the less energetic spectra on a composite plot. These are used for the k-spectra (for example as in Figure 8), and to avoid confusion the ordinate values are separated by a decade for each successive flight level. On the other hand, log-linear $kS_{xy}(k)$ (see Figure 25) are used for the k-cospectra, because cospectral estimates may be either positive or negative and because it is extremely important to be able to assess the relative importance to the total flux of various scale sizes. In these spectral representations the levels 18 m, 50 m, 150 m, 500 m are identified by the symbols L, C, V, T respectively for flight # 1 and ⅃ , ↄ , ∧ , ⊥ for flight # 3.

From each flight a single run in the wind direction at each level is selected. Because of their greater length, the upwind runs are chosen in all but one case: run #1/7 which is a downwind run (Table 1). Run # 1/7 replaced run # 1/9 (upwind) because the latter suffered from radio pick-up in the thermistor circuit. Thus, in this case only, the sign of the horizontal velocity component in the time domain plots is opposite to the mean wind direction, and as a result the corresponding instantaneous momentum is shown as positive (Figure 24). Due, again, to thermistor pick-up on both upwind and downwind runs, no temperature spectra or heat fluxes appear for run # 3/12. The time series of run # 3/12 have been truncated to exclude the noisy section.

FLIGHT	$[u_*^2]_L$ $(cm/s)^2$	$[\sigma_T^2]_L$ $(C°)^2$	$[\sigma_Q^2]_L$ $(gm/kgm)^2$	$[\sigma_W \sigma_T]_L$ $(\frac{m}{s}) \cdot (C°)$	$[\ w'Q'\ ]_L$ $(\frac{m}{s}) \cdot (\frac{gm}{kgm})$	$[\sigma_T \sigma_Q]_L$ $(C°)\ (\frac{gm}{kgm})$
#1	497	.011	.085	.033	.032	.031
#3	1140	.014	.092	.047	.053	.036
RATIO $\#3/\#1$	2.3	1.24	1.08	1.45	1.66	1.16
LOG $_{10}$ RATIO	.36	.093	.033	.16	.22	.064

TABLE 2. NORMALIZERS FOR SPECTRA AND COSPECTRA OF FLIGHTS 1 AND 3.

Crosswind runs at each level are also presented to illustrate differences between the data thus obtained and the data collected during flights in the wind direction.

The widespread practice of computing the turbulent fluxes from the averages, over 'some' period, of the instantaneous values of the meteorological variables is rather like walking on thin ice - you do not know a priori how far to go. It is considerably more enlightening to compute the spectra and cross-spectra of the variables concerned; on the basis of their behaviour and from a thorough determination of the limitations of the instrumentation and its operation, the measurements can be properly evaluated.

There are two factors which are most easily dealt with by careful inspection of the relevant spectra and cross-spectra. The first, general to all turbulent flux computations by the eddy correlation method. is the question of just what is a suitable time interval or what scale sizes should be included in the flux computation. The second, peculiar to observation platforms which are not fixed to terra firma, is the question of whether the effect of platform motion can be removed from the data. It is primarily the second factor which prompts investigators, seeking to establish the validity of their method, to compare results from their moving platform with those obtained from another type of platform. If the results agree, a reasonable conclusion may be that they are both correct. Such a comparison, between data gathered from the aircraft used in this study and those obtained simultaneously by a manned spar buoy, is presented in Appendix C.

The decision as to what range of scale sizes should be included in the

computation of fluxes hinges on the existence of the so-called 'spectral gap', separating turbulent from mesoscale effects. However, in the atmospheric boundary layer the spectra of several meteorological variables sometimes display a 'plateau' at large scales rather than a distinct gap. Under these conditions the choice of an upper limit of the turbulent scale sizes greatly affects the computed statistical quantities at low frequencies.

For this reason the author chose to define the upper limit to the turbulent flux scale sizes in terms of the vertical velocity. The vertical velocity is, of course, common to the three vertical fluxes (momentum, heat and moisture) being considered and its spectrum times frequency $nS_{ww}(n)$ contains a distinct peak in the turbulent region. The upper scale size limit in terms of measured frequency n_L is taken to be that frequency below which $nS_{ww}(n)$ is less than one tenth of its value at the peak. If the value of $nS_{ww}(n)$ increases as rapidly as is frequently found at sub-peak frequencies (Lumley and Panofsky, 1964), then very little of the variance of vertical velocity is lost and the estimates of other meteorological variables, in particular the vertical fluxes, are defined in a consistent manner among themselves and between runs.

3.2 Measurements along the wind

3.2.1 Vertical velocity

Figure 8 displays the k-spectral behaviour of the vertical velocity for flights 1 and 3. The k-spectral estimates are normalized by the square of the friction velocity u_* at the lowest level, designated $[u_*^2]_L$. It is clear that at the lower two levels the high wave number values are very nearly equal; whereas at the 150 m level flight # 1 is much larger than flight # 3. This difference is evident also in the traces of Figure 9, in which it appears that the extra energy in $kS_{ww}(k)$ of flight # 1 is associated with a series of rather evenly spaced updrafts. The close correspondence of the normalized k-spectra at large k between the two flights and below 100 m is a consequence of the relation between the energy at small scales and the rate of dissipation, which in turn is related to the friction velocity near the surface.

All the k-spectra of vertical velocity analysed displayed a -2/3 power law dependence on k above the peak of the k-spectra. This '-2/3 region' is discussed in the next section (3.2.2).

In Figure 10 the standard deviation of the vertical velocity fluctuations σ_w is plotted against $\log_{10} Z$. There seems to be no systematic height dependence. The ratio $\sigma w/u_*$ is shown in Table 3 for each level of flights 1 and 3; the other flights are tabulated in Appendix D. It is seen that $\sigma w/u_*$ does increase with height, but the scatter is considerable above the 50 m level.

Figure 11 illustrates the dependence of the wave length at the k-spectral peak L_M on height. In spite of the scatter it is evident that in this study the wave length of the peak of the k-spectrum of vertical velocity varies approximately as $Z^{0.75}$ and extrapolated to a height of 10 metres the peak wave

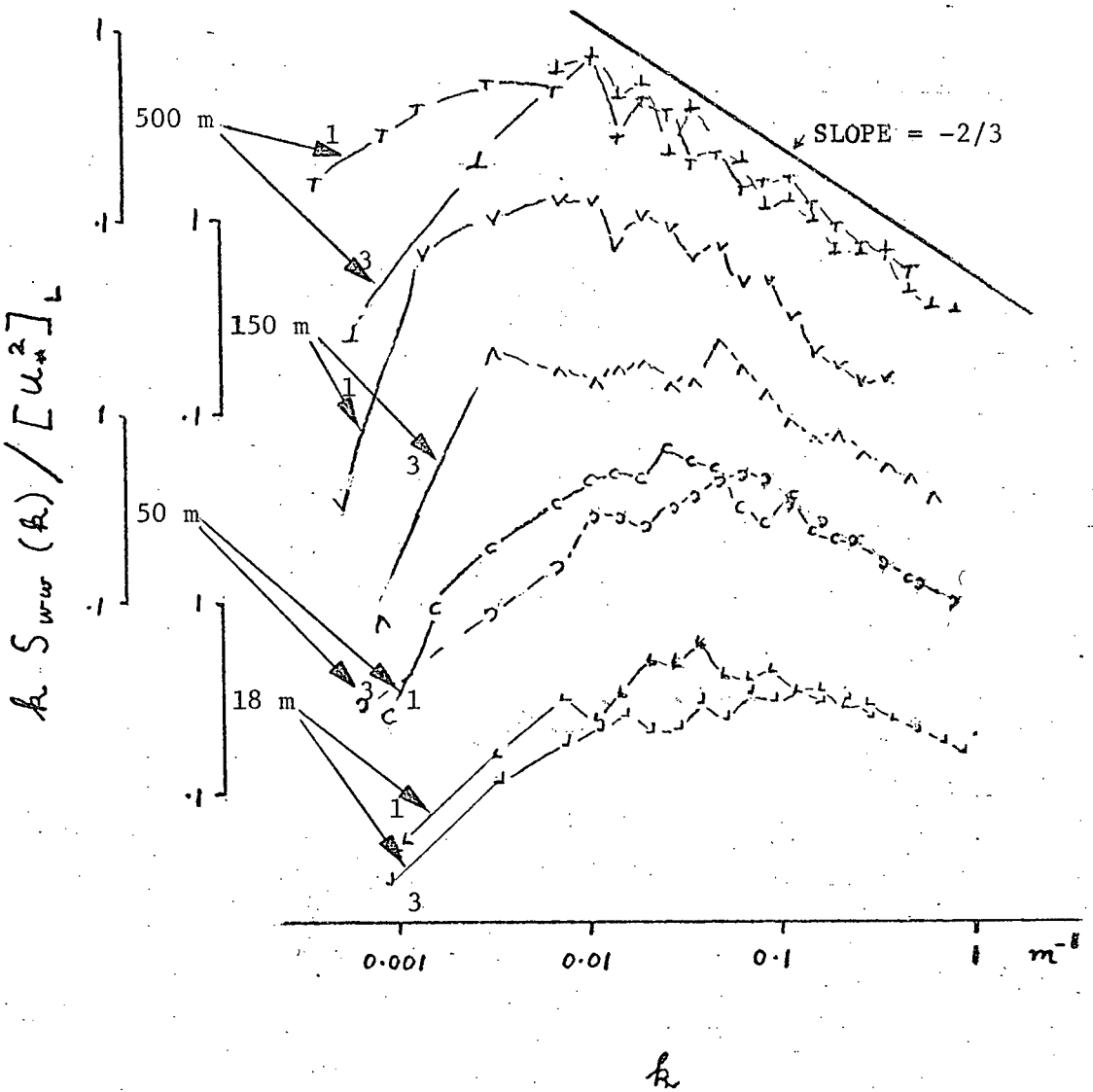

FIGURE 8. VERTICAL VELOCITY SPECTRA (UPWIND)

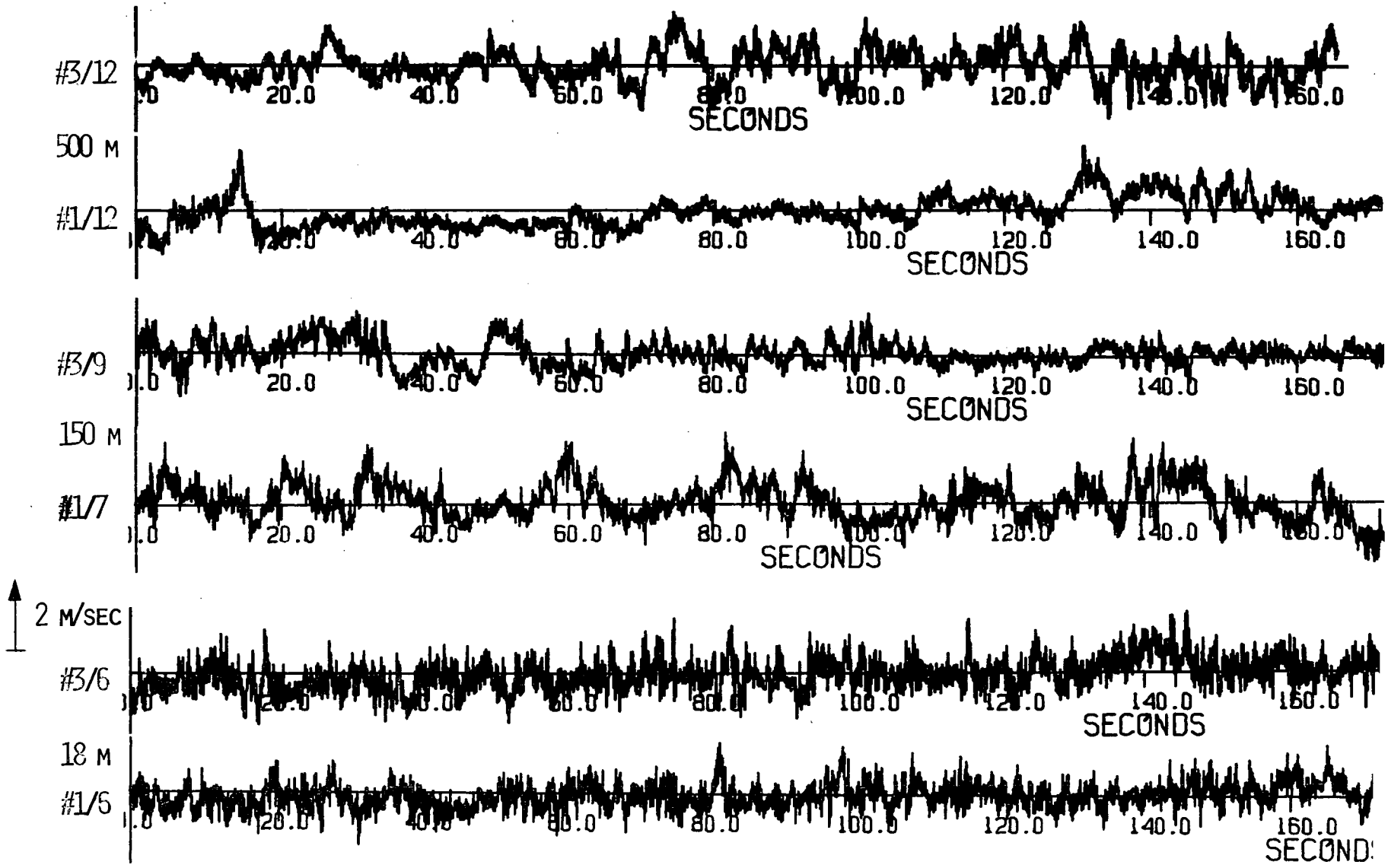

FIGURE 9. VERTICAL VELOCITY TRACES (UPWIND)

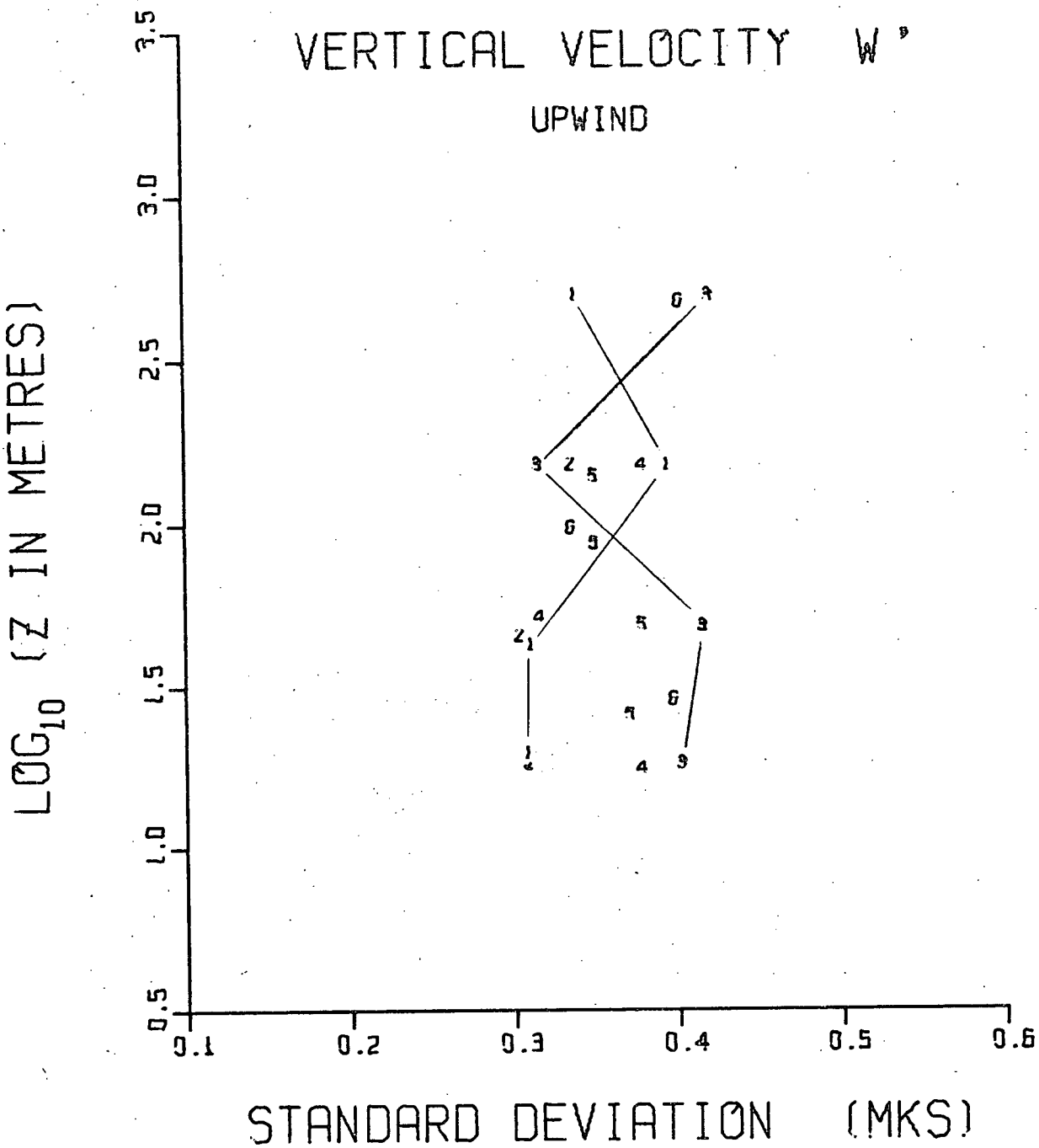

FIGURE 10. σ_w VS. Z (UPWIND)

RUN	**	z	u_*^2	$\overline{w'T'}$	$-z/L_T$	$\overline{w'Q'}$	$-z/L_Q$	$-z/L$
		m	$(m/s)^2$	(m/s)C°		$(\frac{m}{s})(\frac{gm}{kgm})$		
1/6	U	20	.0497	.0059	.14	.0318	.14	.28
1/3	U	43	.0237	.0058	.89	.0293	.83	1.72
1/7	D	150	.0448	-.00083	-.17	.0483	1.9	1.73
1/12	U	500	.0061	-.0094	-130.	.0605	150.	20.
3/6	U	18	.114	-.00042	-.025	.0529	.059	.034
3/3	U	49	.0712	.0049	.16	.0237	.15	.31
3/9	U	150	.061	.0039	.51	.025	.61	1.12
3/12	U	500	.0391	--	--	.0286	4.4	4.4

RUN	σ_w	σ_u	σ_T	σ_Q	τ_{zx}	F_H	F_Q
	cm/s	cm/s	C°	gm/kgm	$\frac{dynes}{cm^2}$	mW/cm^2	mW/cm^2
1/6	30.8	52.2	.105	.291	.643	.77	10.30
1/3	31.0	37.8	.071	.188	.306	.75	9.49
1/7	47.3	38.5	.063	.223	.579	-.11	15.65
1/12	33.8	42.9	.155	.499	.079	-1.22	19.60
3/6	40.2	74.6	.117	.302	1.47	-.05	17.14
3/3	41.5	59.5	.093	.252	.921	.64	7.68
3/9	31.5	56.6	.066	.184	.789	.51	8.10
3/12	42.0	44.4	.527	.198	.504	--	9.27

RUN	u_*	$-T_*$	$-Q_*$	σ_w/u_*	σ_u/u_*	$-\sigma_T/T_*$	$-\sigma_Q/Q_*$
	cm/s	C°	gm/kgm				
1/6	22.3	.066	.357	1.38	2.34	1.59	.82
1/3	15.4	.094	.476	2.01	2.45	.76	.39
1/7	21.2	-.010	.570	2.33	1.82	-6.30	.39
1/12	7.8	-.301	1.939	4.33	5.50	-.51	.26
3/6	33.8	-.003	.391	1.19	2.21	-39.0	.77
3/3	26.7	.046	.222	1.55	2.23	2.02	1.14
3/9	24.7	.039	.253	1.28	2.29	1.69	.73
3/12	19.8	--	.361	2.12	2.24	--	.55

** U = Upwind, D = Downwind

TABLE 3 - STATISTICS OF FLIGHTS 1 and 3

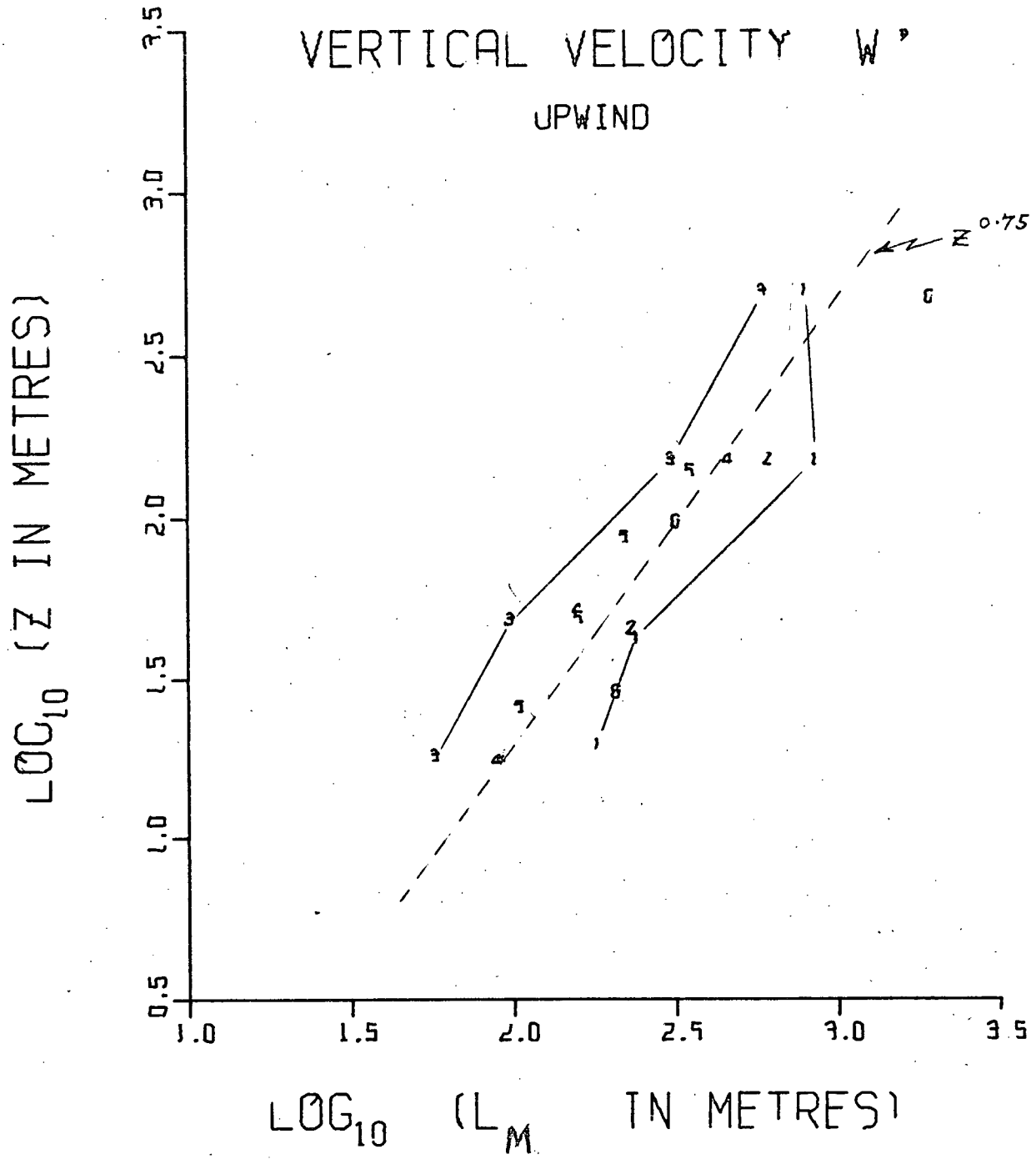

FIGURE 11. $(L_M)_w$ VS. Z (UPWIND)

length is roughly 55 metres;

$\therefore L_M \doteqdot 55\ (Z/10)^{0.75}$ metres, which represents the line shown in Figure 11. Or in terms of the measured frequency n

$$n_M \doteqdot 0.018\ V\ (Z/10)^{0.75}\ \text{Hz}.$$

Far from the boundary where most of the mechanical turbulence is generated, the influence of convective effects is evident in the vertical velocity spectra (Figure 8). The spectra become narrower, both because the buoyant input tends to have a narrow bandwidth and because the boundary is no longer effective in restricting the large scale size generation near the buoyant input peak. In this and subsequent sections the natural logarithmic bandwidth B is defined as the ratio of the variance to the k-spectral peak estimate. The bandwidth variations of the spectra are summarized in Figure 12, in which it is seen that the bandwidth decreases up to the 150 m level; at greater heights any change is less definitely observed.

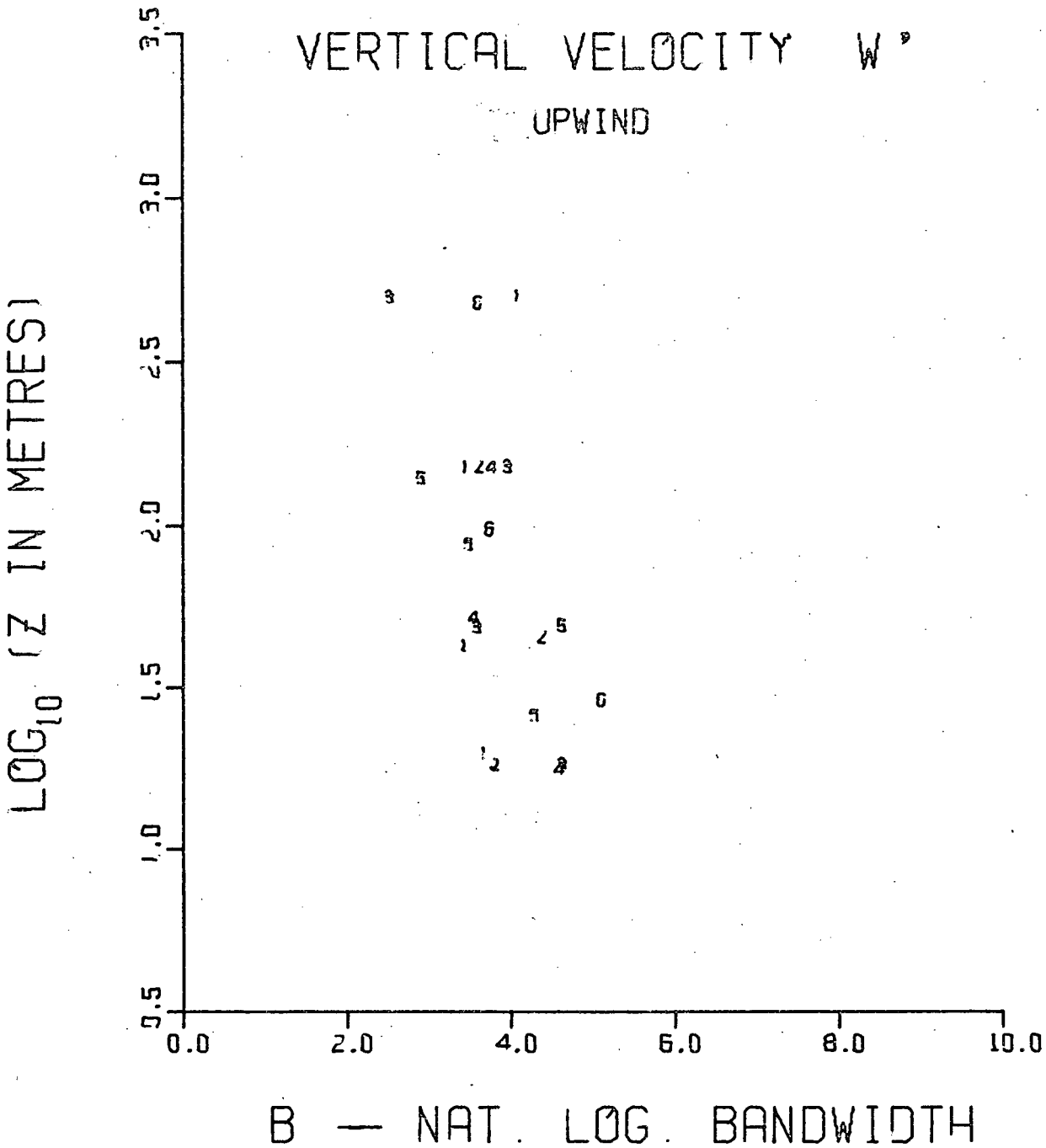

FIGURE 12. B_w VS. Z (UPWIND)

3.2.2 Horizontal Velocity

Figure 13 and the k-spectra of Figure 14 provide a clear description of the evolution of the horizontal velocity component with height. In general there is an overall decrease in the energy of all scale sizes, but the rate of decrease of the small scales is faster than that of the larger scales. This gives the impression in the time series (Figure 13) that the energy at large scales increases with height. In Figure 14 it is seen that the high wave number estimates for flights 1 and 3 agree well except in the case of the runs at 150 metres. However, the difference here is much smaller than in the vertical velocity spectra and appears only above $k = 0.01\ m^{-1}$, whereas the difference in the vertical velocity spectra was largest near this wave number. If the difference is due to the frequency of updrafts, then it is reasonable to expect the vertical velocity spectra to exhibit a larger difference especially in the energy of scale sizes at which the effects of buoyancy are most pronounced.

The k-spectra of Figure 14, and all others computed, display a -2/3 slope at high wave numbers. This slope also obtains at wave numbers corresponding to scale sizes which are three or four times larger than the distance from the boundary, and which transport momentum (Section 3.2.5) and hence are anisotropic. Thus the -2/3 slope of the downwind velocity component's k-spectra is not sufficient evidence for the existence of an 'inertial subrange', which depends on the flow being locally isotropic (Kolmogoroff, 1941). But at sufficiently high wave numbers, where the k-spectra of both vertical and horizontal velocity components display a -2/3 slope and where the momentum transfer is negligible, isotropy may exist.

It can be shown (for example Hinze, 1959) that if the flow is isotropic the ratio of $S_{ww}(k)$ to $S_{uu}(k)$, where k is the wave number component in the

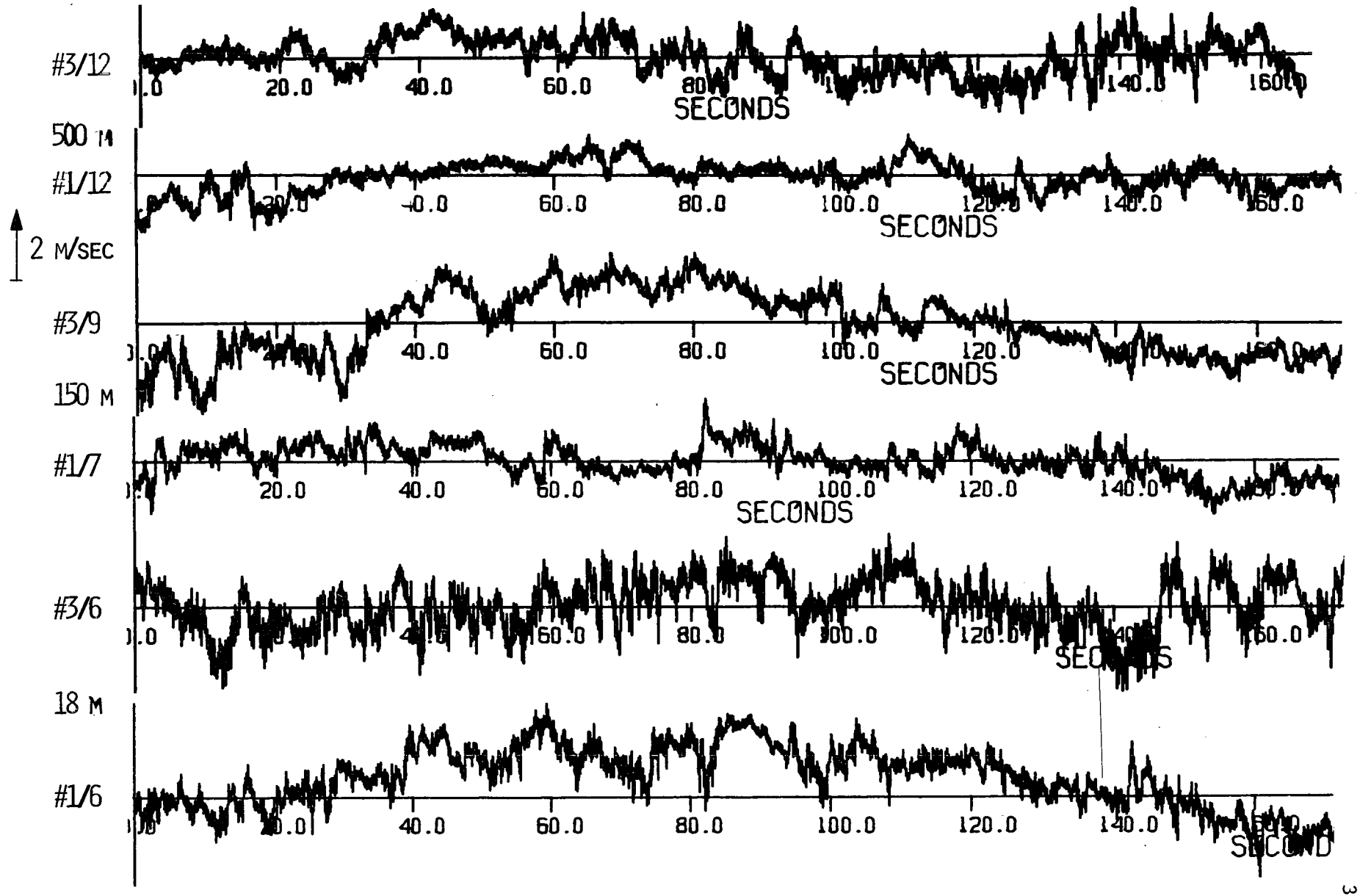

FIGURE 13. LONGITUDINAL VELOCITY TRACES

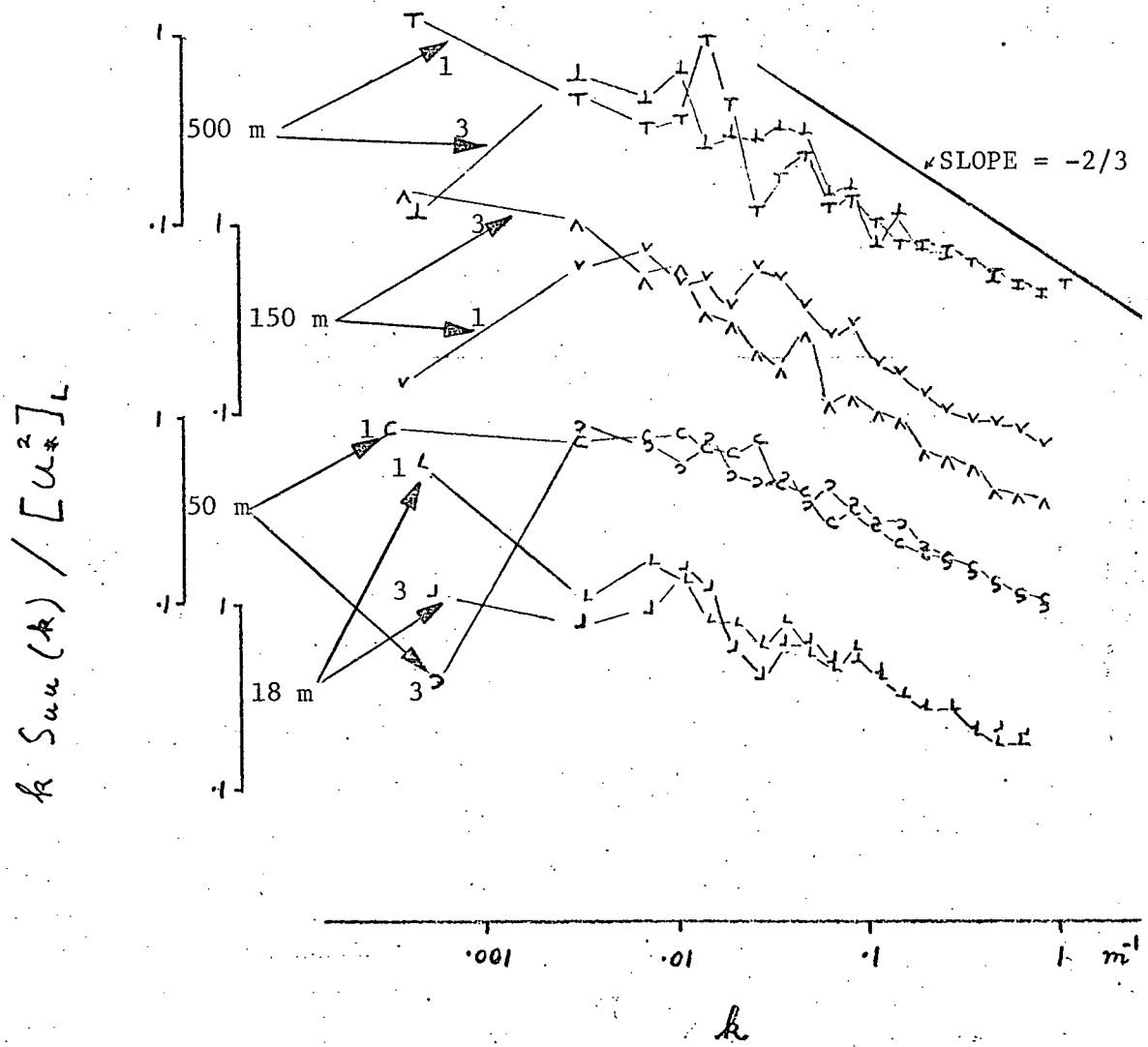

FIGURE 14. LONGITUDINAL VELOCITY SPECTRA

direction of the u component, is 4:3. This ratio is shown in Figure 15, in which it can be seen that, although there is scatter, all of the points correspond to a ratio smaller than 4/3. There is a tendency for the ratio to increase slightly with height, reflecting a reduction in anisotropy as the local shear weakens. However there appears to be no locally isotropic region in the range of scales investigated $0 < k < 1 \quad m^{-1}$, corresponding to a maximum value of kZ of 500. Weiler and Burling (1967) obtained similar values of the ratio of spectral densities using X - wires near the surface over water. Payne and Lumley (1965) used a single hot wire mounted on the wing tip of an aircraft to make measurements both along and perpendicular to the wind direction. Their Figure 1 indicates that the ratio $S_{vv}(k_v)$ to $S_{uu}(k)$, where k_v is the wave number component in the direction of the v component, is about 1.4; the condition of isotropy requires that $S_{uu}(k) = S_{vv}(k_v) = S_{ww}(k_w)$. However, since the measurements of the two horizontal components were separated both in space and time, this result rejects the possibility of local isotropy only if the turbulent field was both stationary and homogeneous over the relevant intervals of time and space. Sheih (1969) using airborne x - wires obtained values of $[S_{ww}(k)]/[S_{uu}(k)]$ ranging from 0.8 to 2.4 for various wave numbers between 1 and 4000 m^{-1}. Although this range of values of $[S_{ww}(k)]/[S_{uu}(k)]$ includes the value (4/3) indicative of isotropy, the scatter is too large to allow the conclusion that the flow was locally isotropic. Apparently, conclusive evidence for the existence of isotropy in atmospheric turbulence is still lacking.

However, since the separate velocity components always exhibit a -5/3 power law in their spectra, the spectral density in this region can be used to estimate the dissipation using the technique first suggested by Obukhov (1951) and the ideas formulated by Kolmogoroff (1941) but related to spectra

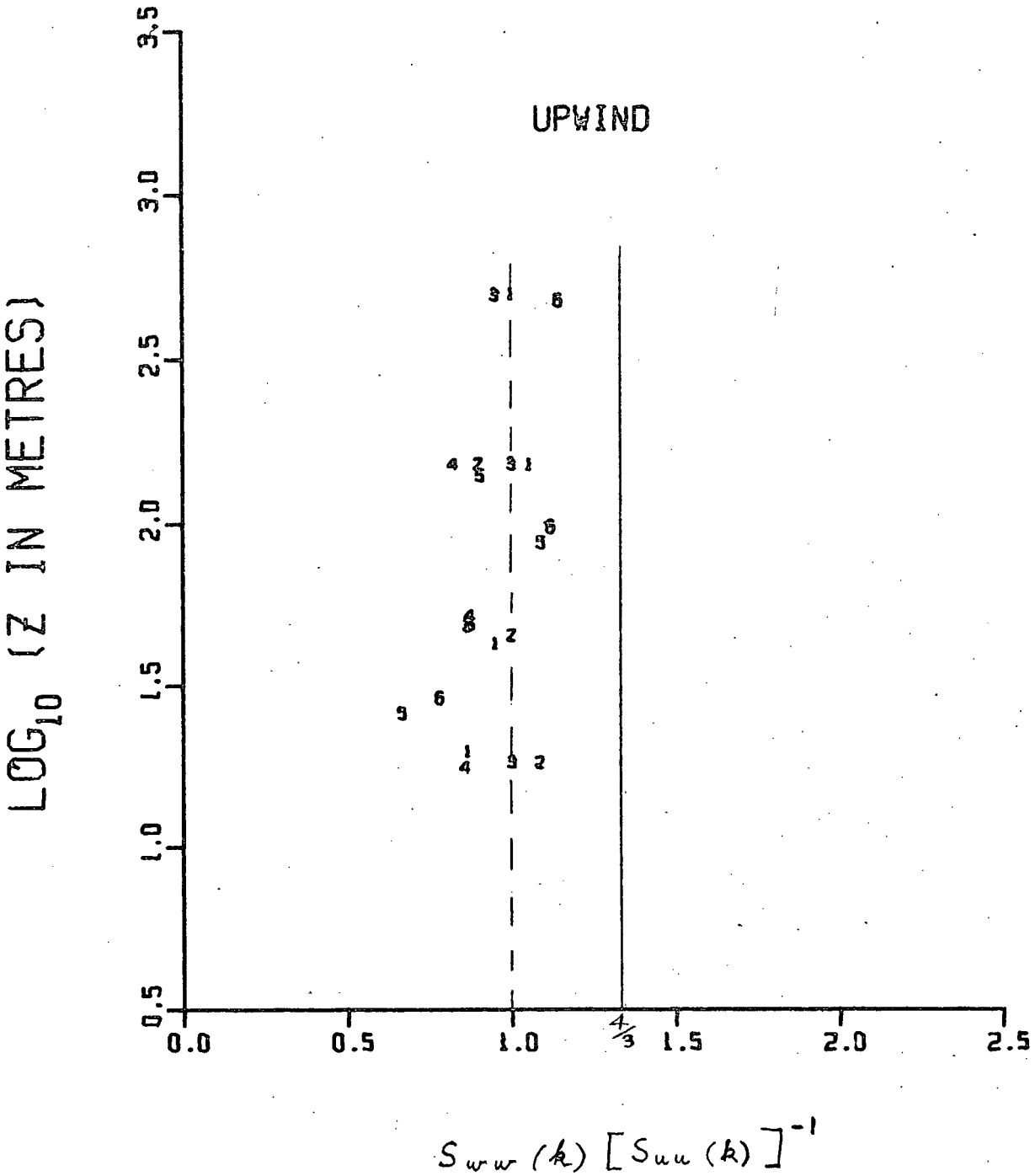

FIGURE 15. '4/3' TEST FOR ISOTROPY

rather than structure functions:

$$S_{xx}(k) = K' \epsilon^{2/3} k^{-5/3} \qquad (3.2.1.)$$

or

$$\epsilon = \frac{2\pi n}{V} K'^{-3/2} [nS_{xx}(n)]^{3/2} \qquad (3.2.2.)$$

where K' is the Kolmogoroff one dimensional wave number constant.

In the past the published values of K' were in the neighbourhood of 0.48 (Grant et al, 1962; Pond et al, 1963). More recent measurements indicate that it may be somewhat higher: perhaps as high as 0.57. However, as there is yet no agreement as to what the revised value should be, the value (K' = 0.48) will be used here.

If it is assumed that production ($u_*^2 \frac{\partial \bar{u}}{\partial Z}$) and dissipation ϵ of turbulent kinetic energy are nearly equal near the surface and that $\frac{\partial \bar{u}}{\partial Z} \doteq \frac{u_*}{KZ} (1 + \frac{5Z}{L})$, (Lumley and Panofsky, 1964, p.107), where $K = 0.4$, von Karman's constant, then the friction velocity u_* and hence the drag coefficient $C_D = u_*^2/U^2$ may be estimated from n-spectrum of the downwind component $nS_{uu}(n)$:

$$u_*^2 = 3.85 (\frac{nZ}{V})^{2/3} nS_{uu}(n) (1 + 5 Z/L)^{-2/3} \qquad (3.2.3.)$$

Table 4 shows u_* and $(C_D)_{20}$ computed from (3.2.3.) and from direct measurements of $\overline{u'w'}$ (Section 3.2.5) for the lowest level of flights 1 to 6. With the exception of flight # 1, the values of $(C_D)_{20}$ computed by the eddy correlation technique ($\overline{u'w'}$) lie between 1.4×10^{-3} and 1.6×10^{-3}. To determine the approximate values of C_D at Z = 5 m the wind profile is assumed to be logarithmic and the surface roughness length is taken to be 0.05 mm or equivalently $(C_D)_5 = 1.2 \times 10^{-3}$. Thus the values of $(C_D)_5$ for

RUN	Z	$\bar{U}_{20}$	from $-u'w'$			Z/L	from $nS_{uu}(n)$		
			$-u'w'$	u_*	$[C_D]_{20}$		u_*^2	u_*	$[C_D]_{20}$
		DOPPLER RADAR			$\times 10^3$				$\times 10^3$
	m	m/s	$(cm/s)^2$	cm/s			$(cm/s)^2$	cm/s	
1/6	20	4.0	497	22.3	3.1	-0.28	-	-	-
2/9	18	6.0	500	22.4	1.4	-0.30	-	-	-
3/6	18	8.6	1140	34.0	1.5	-0.034	1240	35.3	1.7
4/5	18	8.3	990	31.0	1.4	-0.10	2140	46.3	3.2
5/2	26	8.0	1040	32.0	1.6	-0.094	2600	51.0	4.1
6/2	29	9.4	1150	34.0	1.3	-0.093	1520	39.0	1.7

TABLE 4 DRAG COEFFICIENTS

flights 1 to 6 lie between 1.7×10^{-3} and 2.0×10^{-3}. Since these values depend on the accuracy of the wind speed estimates, which are obtained with the airborne Doppler radar, they may be in error by 50% of the values quoted. However they are within the range of values of $(C_D)_5$ obtained over the water by several investigators and summarized by Smith (1967).

The values of $(C_D)_{20}$ from (3.2.3.) are, on average, 85% larger than those computed by the eddy correlation technique. Weiler and Burling (1967) and Miyake et al (1970a) obtained similar results from near surface over water measurements: in the case of the former an over estimate of 40% was obtained while in the latter the over estimate was 25%. Both Weiler and Burling (1967) and Miyake et al (1970) suggest possible reasons for this discrepancy. However, it appears that in these data the assumption that shear production equals dissipation may be the primary reason for the over estimates (see Section 3.4).

Many workers (see, for example, Lumley and Panofsky, 1964) have found that the standard deviation σ_u of the fluctuations of the longitudinal velocity component is proportional to the friction velocity; the ratio σ_u/u_* is usually found to be about 2.5.

In these data the k-spectra of the fluctuations of the longitudinal velocity component are quite flat at large scales; therefore the value of σ_u is very sensitive to the choice of the low wave number limit. In this study a low wave number limit is selected for each run such that more than 90% of the variance of the fluctuations of the vertical velocity component is at larger wave numbers; this limit is used for all the spectra and cospectra of that run. Figure 16 displays the ratio σ_u/u_*; with a few exceptions the points lie between 1.8 and 2.8 and appear not to be height dependent. The values of σ_u/u_* are also listed in Table 3 and Appendix D.

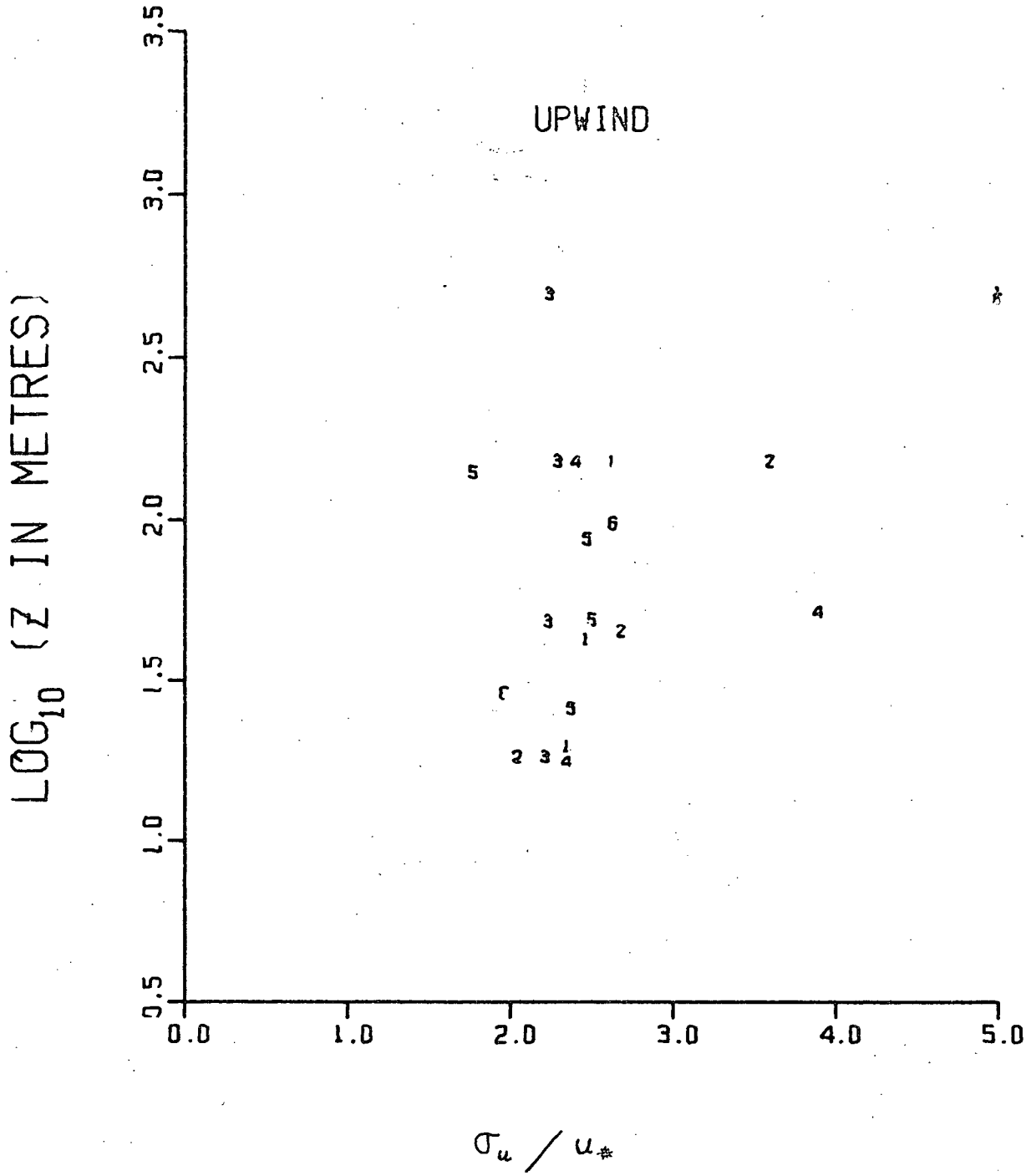

FIGURE 16. σ_u/u_* VS.Z

3.2.3 Temperature

Measurements of temperature fluctuations over water often reveal spectral distributions not unlike those of the longitudinal velocity component (e.g. Miyake et al, 1970C). But the temperature k-spectra of Figure 17 are quite unlike the longitudinal velocity k-spectra of Figure 14. There are two distinct peaks in almost all the temperature k-spectra analysed and, as will be shown in Section 3.5, these peaks are different in origin. The behaviour of the high frequency peak is much the clearer, which is not surprising in view of the low reliability of the spectral estimates at large scales. The wavelength of the high wave number peak shows a steady increase with height, but the amplitude decreases at first up to 150 m; it then appears to increase between 150 m and 500 m (Figure 17 and 18), but with only two useful runs at 500 m no definite pattern can be established. In general the behaviour of the low frequency peak is erratic both with regard to its amplitude and wave length. However the importance of its contribution to the total variance increases steadily with height (Figure 17).

Although there are no previous comparable temperature measurements, it is interesting and useful to search for a convenient description of the height dependence of these k-spectra. Figure 19 shows a clear dependence of L_M of the high frequency hump on height. In fact the dependence as $Z^{0.75}$ is the same as that of the vertical velocity peak. This is not surprising, since, in a convective situation temperature fluctuations are maintained by the action of the vertical velocity on the temperature gradient, it is reasonable to suppose that temperature should scale with height in much the same way as vertical velocity does. For convenience in further discussion, it is of use to state explicitly the dependence of L_M on Z:

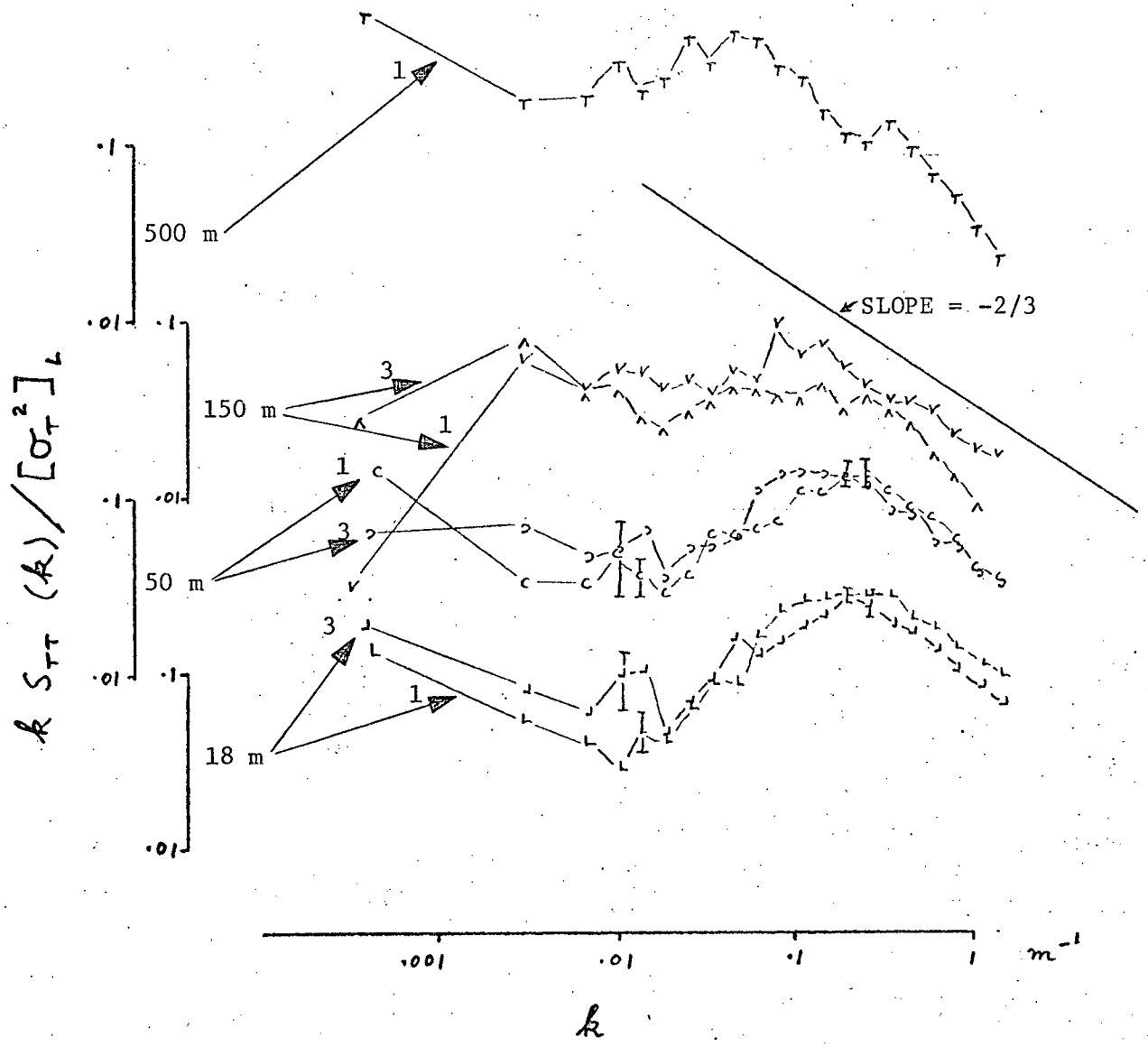

FIGURE 17. TEMPERATURE SPECTRA (UPWIND)

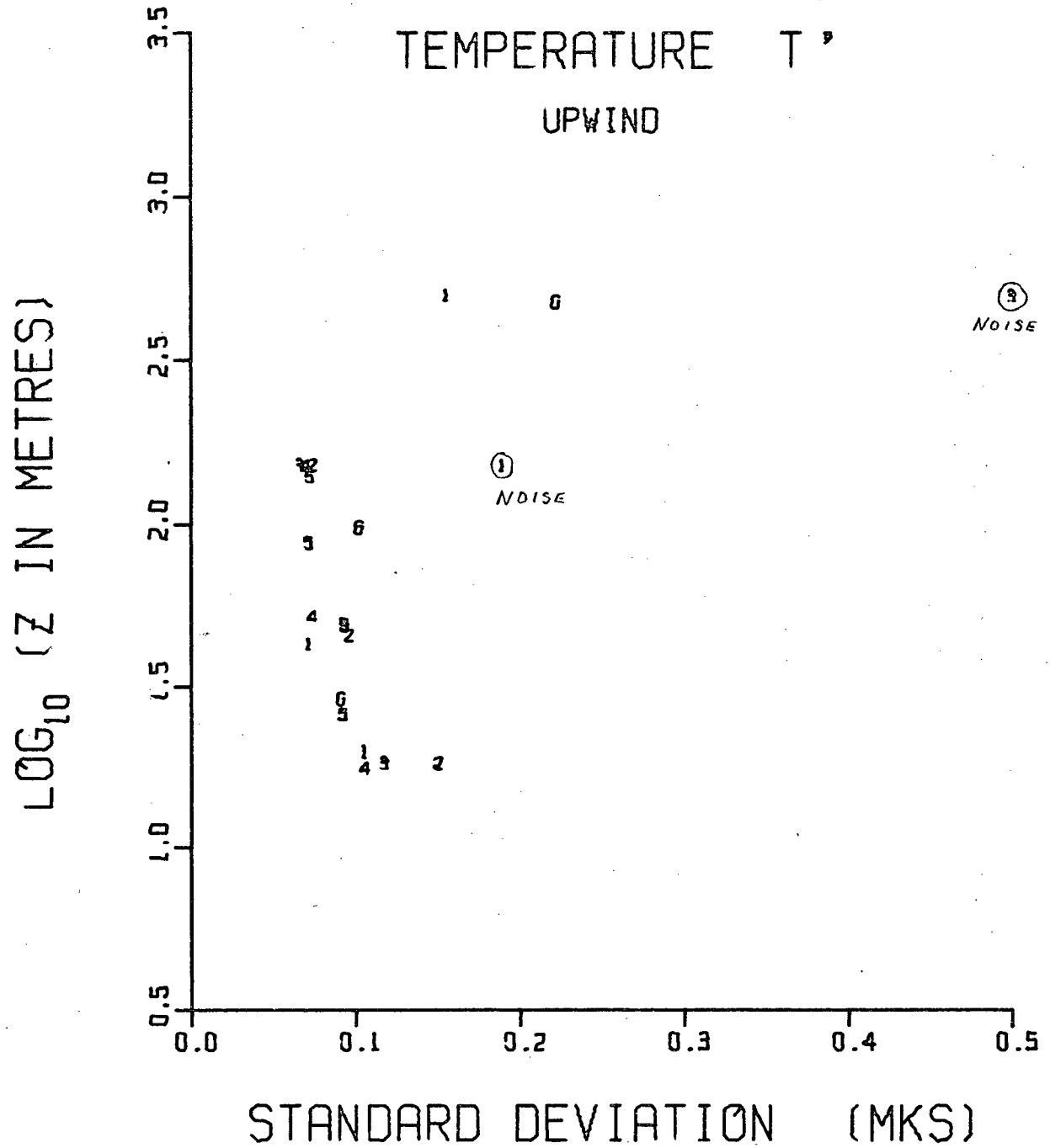

FIGURE 18. σ_T VS. Z (UPWIND)

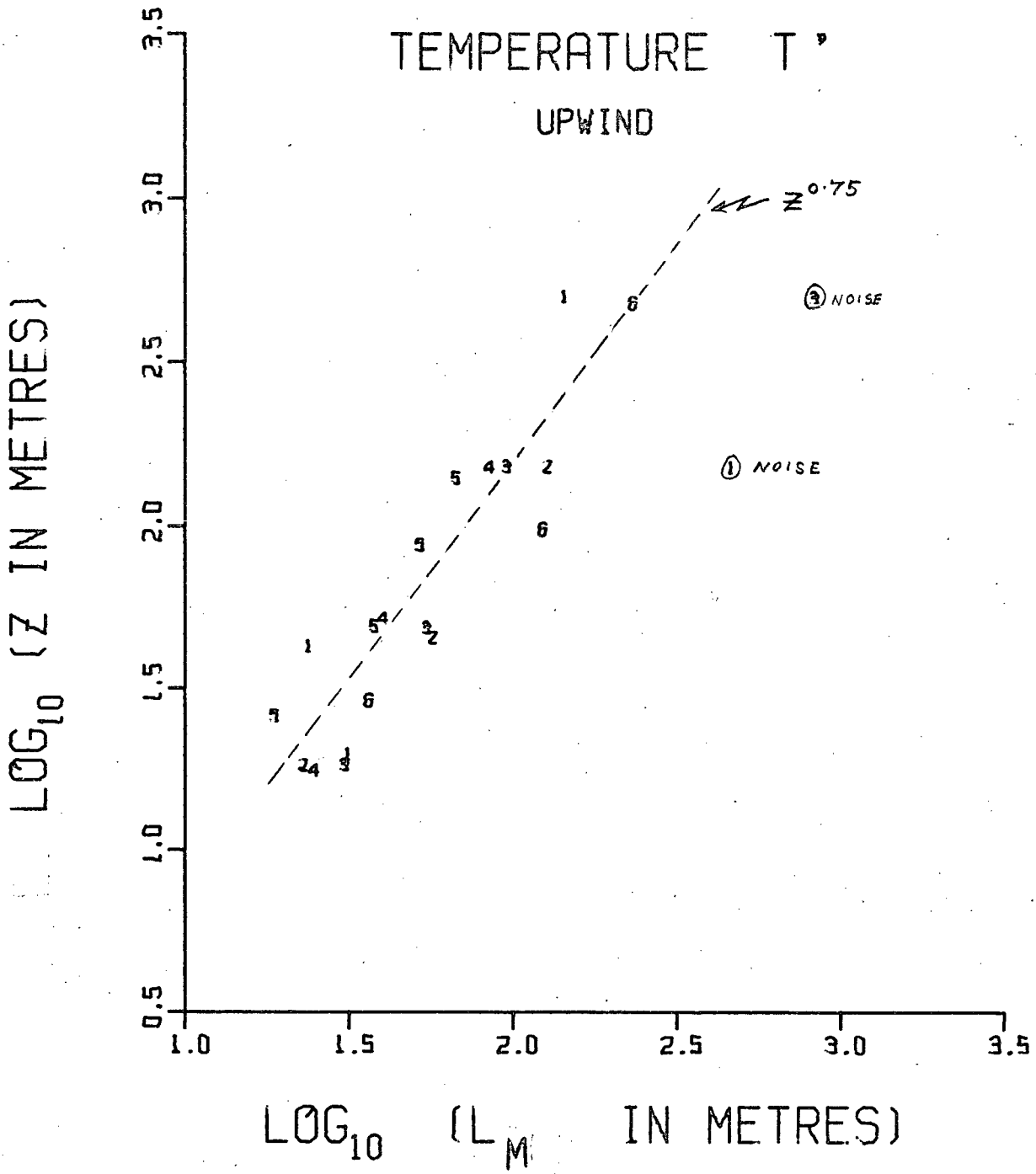

FIGURE 19. $(L_M)_T$ VS. Z (UPWIND)

$L_M = 13\ (z/10)^{0.75}$ metres which represents the line shown in Figure 19.

The standard deviation σ_T (Figure 18) decreases by about 40% from 18 m to 150 m, then increases at much the same rate. Thus there is a minimum of temperature variance at about 150 metres. This conclusion depends on flights 1 and 6 (Figure 18) only, and therefore must be regarded as tentative. However the time series of Figure 20 support this idea to some extent.

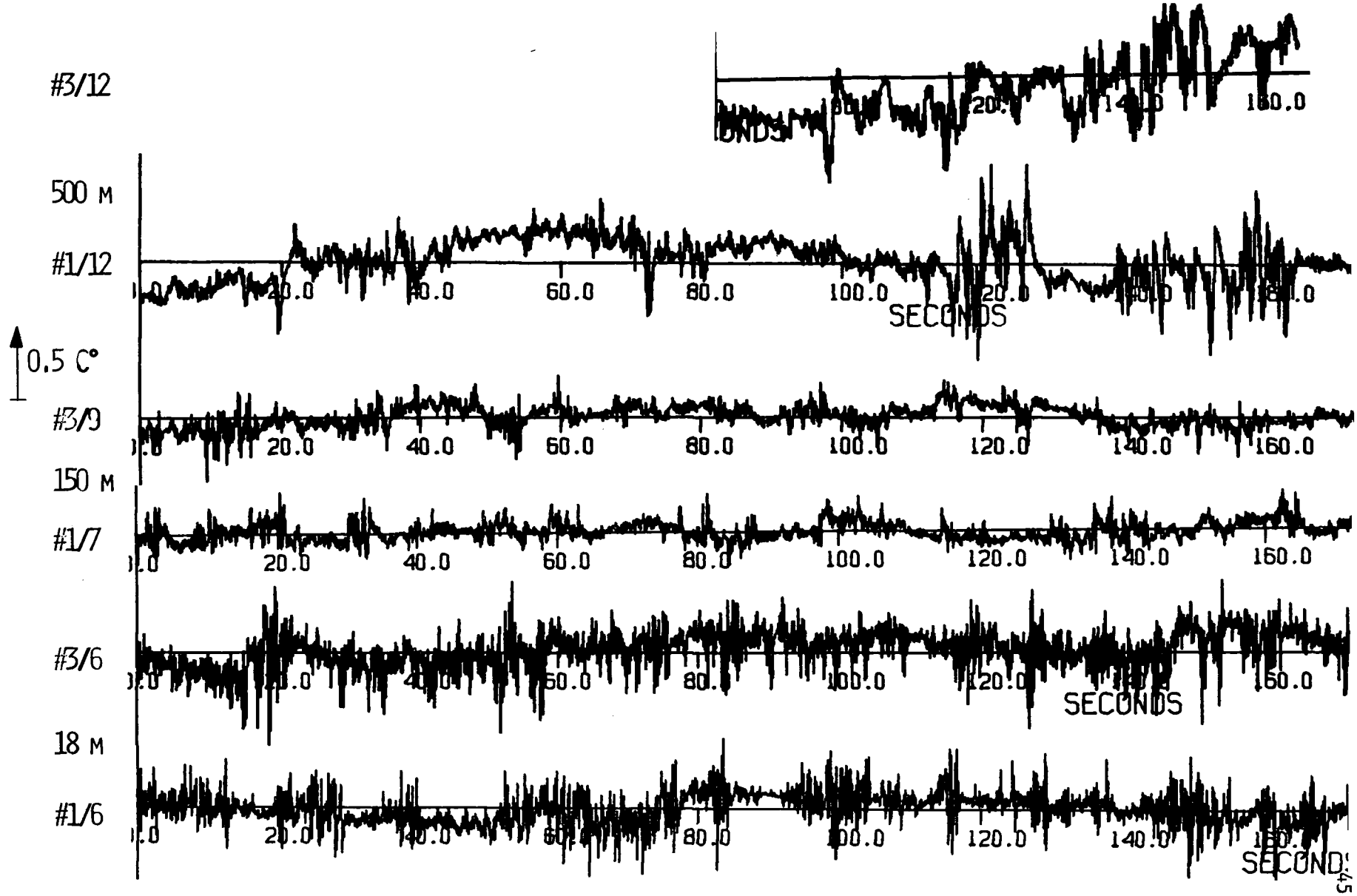

FIGURE 20. TEMPERATURE TRACES (UPWIND)

3.2.4. Humidity

The k-spectra of Figure 21, corrected by the intake tube transfer function, display a -2/3 power law at high frequencies. They are much more like the longitudinal velocity k-spectra, than are the temperature k-spectra, even to the extent of 'obeying' the -2/3 law at anomalously low wave numbers. Alike as they are in spectral shape, humidity and the longitudinal velocity component are quite different in the dependence of their variances on height. σ_u decreases continuously with increasing height, whereas σ_q decreases and then increases again (Figure 22) in the same manner as σ_T, although here too the argument rests on only three points. The greater scatter of the points of Figure 22, compared to Figure 18, reflects the relatively strong dependence of σ_q on the sampling length. However, the minimum of the variances of both temperature and humidity between 50 m and 500 m is very interesting and bears further investigation. This matter will be discussed further in the Section(3.4) dealing with the temperature-humidity correlation.

The humidity traces at 18 m, 150 m and 500 m are displayed in Figure 23 for flights 1 and 3. It is evident that the traces at 150 m are the least energetic; this observation is also reflected in the k-spectra of Figure 21.

Unlike the temperature k- spectrum, $kS_{QQ}(k)$ (Figure 21) appears to retain its shape at all levels, at least in the wave number range $k = .002\ m^{-1}$ to $k = 1\ m^{-1}$.

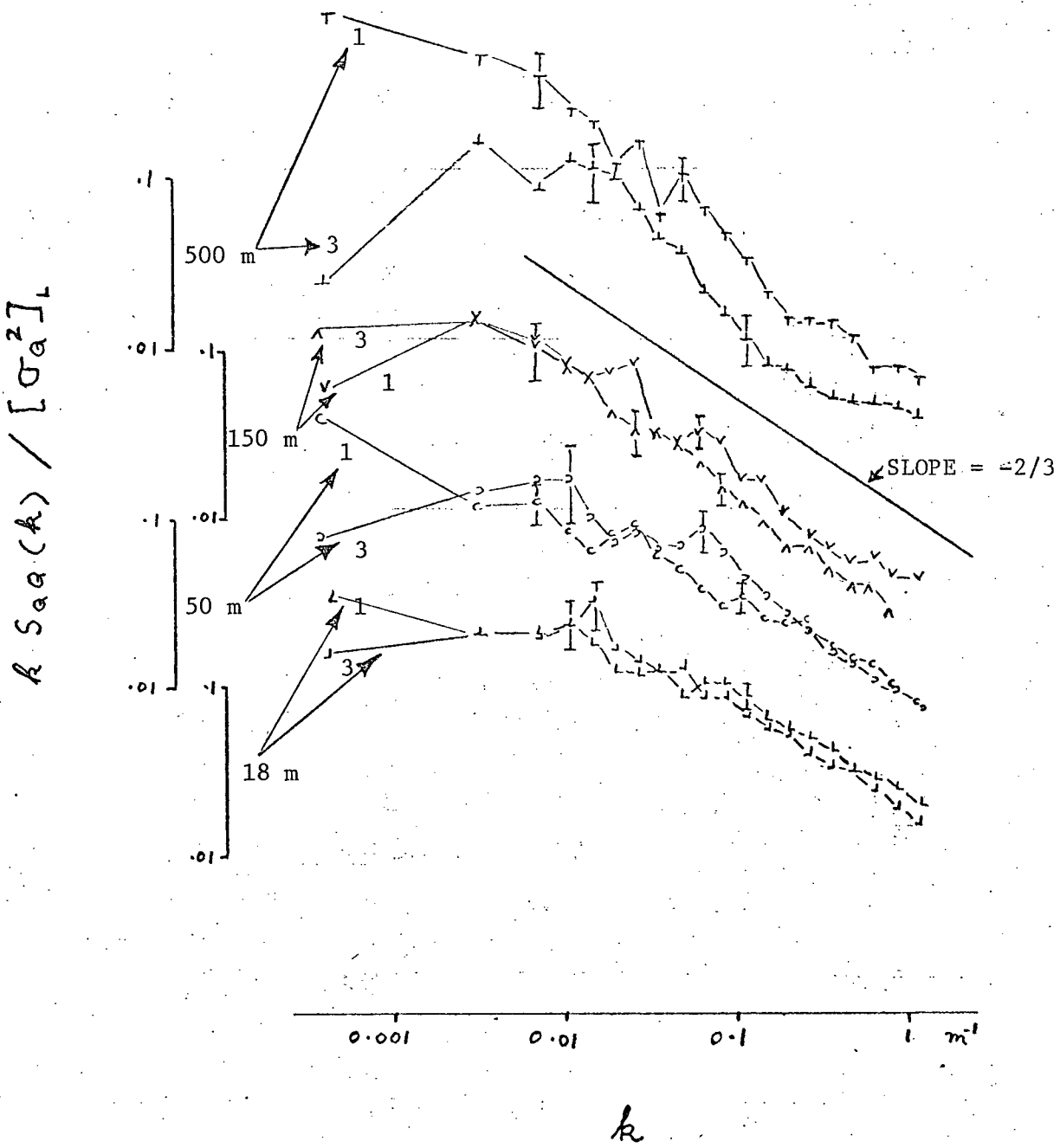

FIGURE 21. HUMIDITY SPECTRA (UPWIND)

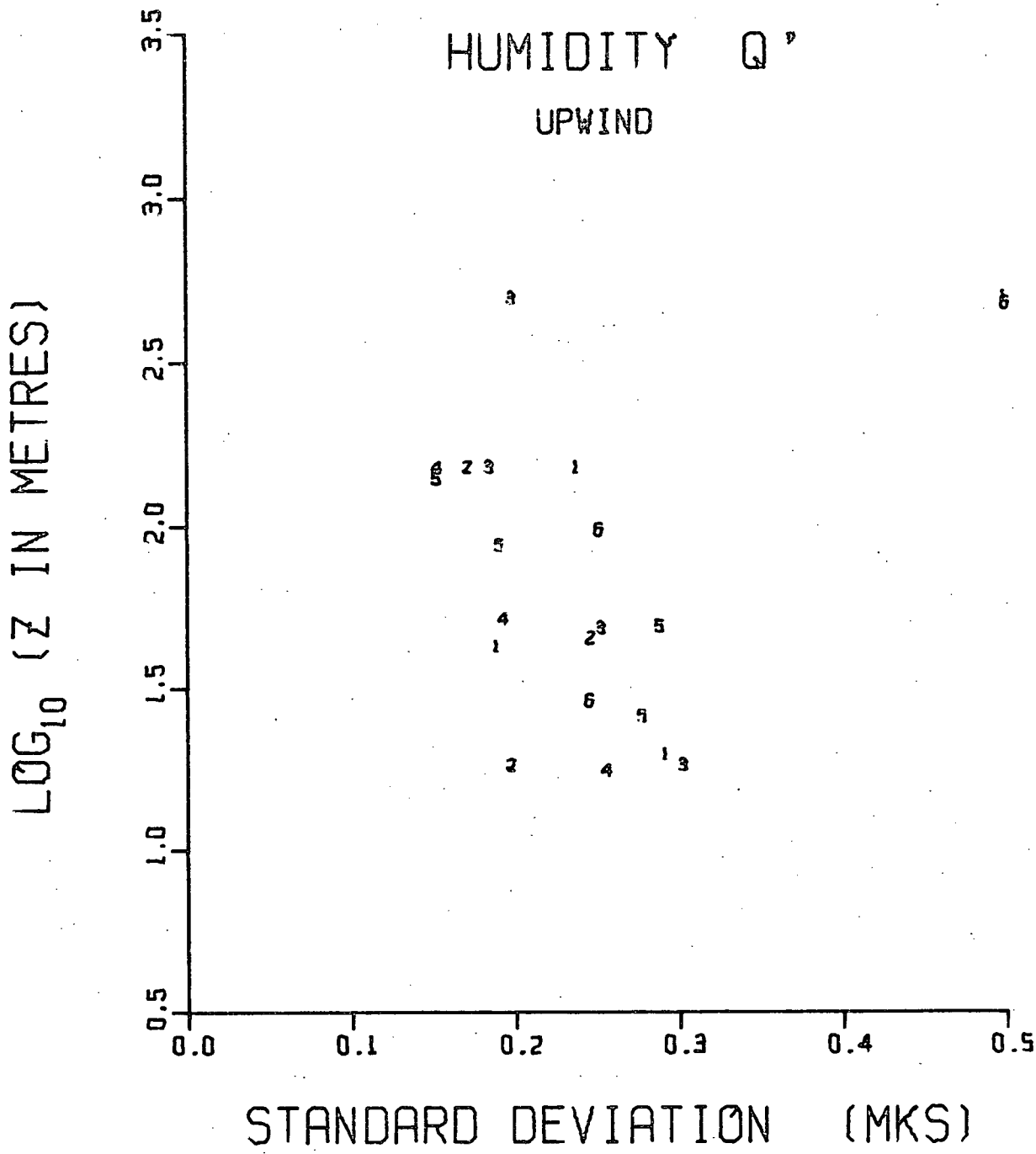

FIGURE 22. σ_Q VS. Z (UPWIND)

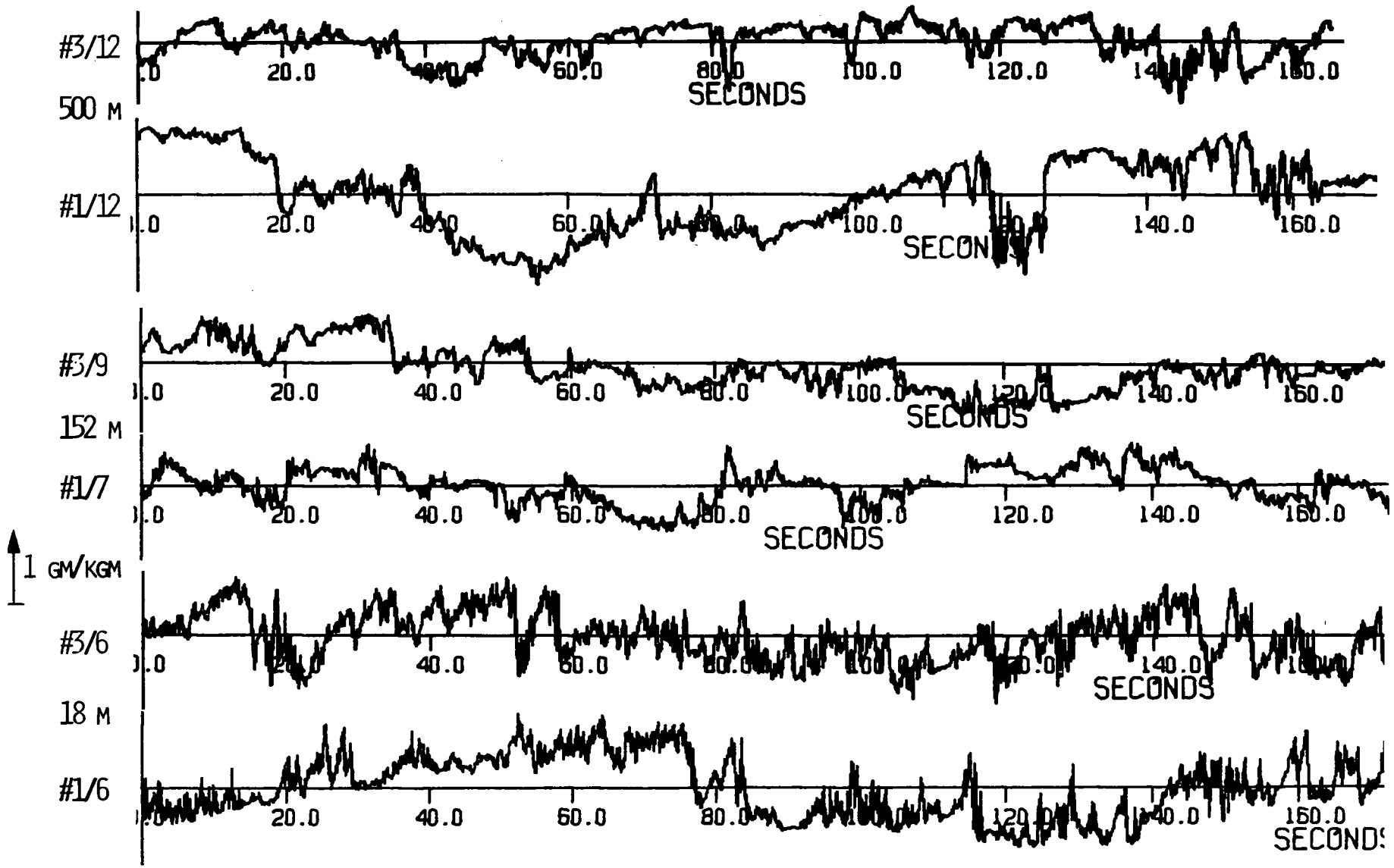

FIGURE 23. HUMIDITY TRACES (UPWIND)

3.2.5. Momentum Flux

The momentum flux can be separated into two parts: the component in the direction of the surface wind (x direction) $\tau_x = -\rho\overline{u'w'}$ and the component in the y direction $\tau_y = -\rho\overline{v'w'}$. Here, as throughout this thesis, the figures are presented in kinematic terms, i.e. the density ρ, which is assumed constant, is omitted. Since there was no evidence of rotation of the mean wind vector with height (Figure 6), only the momentum component in the direction of the surface wind will be considered.

In Figure 24 the instantaneous product u'w' is displayed. In all cases but one (run #1/7) the trace has the correct sign; i.e. a negative value means positive momentum directed downwards. Run # 1/7 was a downwind run, and so the measured u velocity in the coordinate system fixed to the aircraft was anti-parallel with the wind direction.

Figure 25 shows the height dependence of the momentum flux k-cospectra for flight #3, and the integral under these curves ($-\overline{u'w'} = u_*^2$) is displayed for all six flights on linear axes in Figure 26. It must be remembered that in the analysis trends are removed from both velocity components and the lower cut-off of these cospectra is decided by the shape of the vertical velocity k-spectra and justified on the basis of its well established shape near the surface. However, it may be that away from the boundary the vertical velocity contains energy at scales larger than those considered here, and that an appreciable amount of the momentum flux is carried by these large scales. Whether this is so or not cannot be fully examined with the data presented here, but the rapid decrease of the stress (Figures 25 and 26) is consistent with the relative constancy of wind direction and speed with height (see Figure 6) only if other terms in the mean equations of motion were comparable to the vertical stress gradient. For instance, to

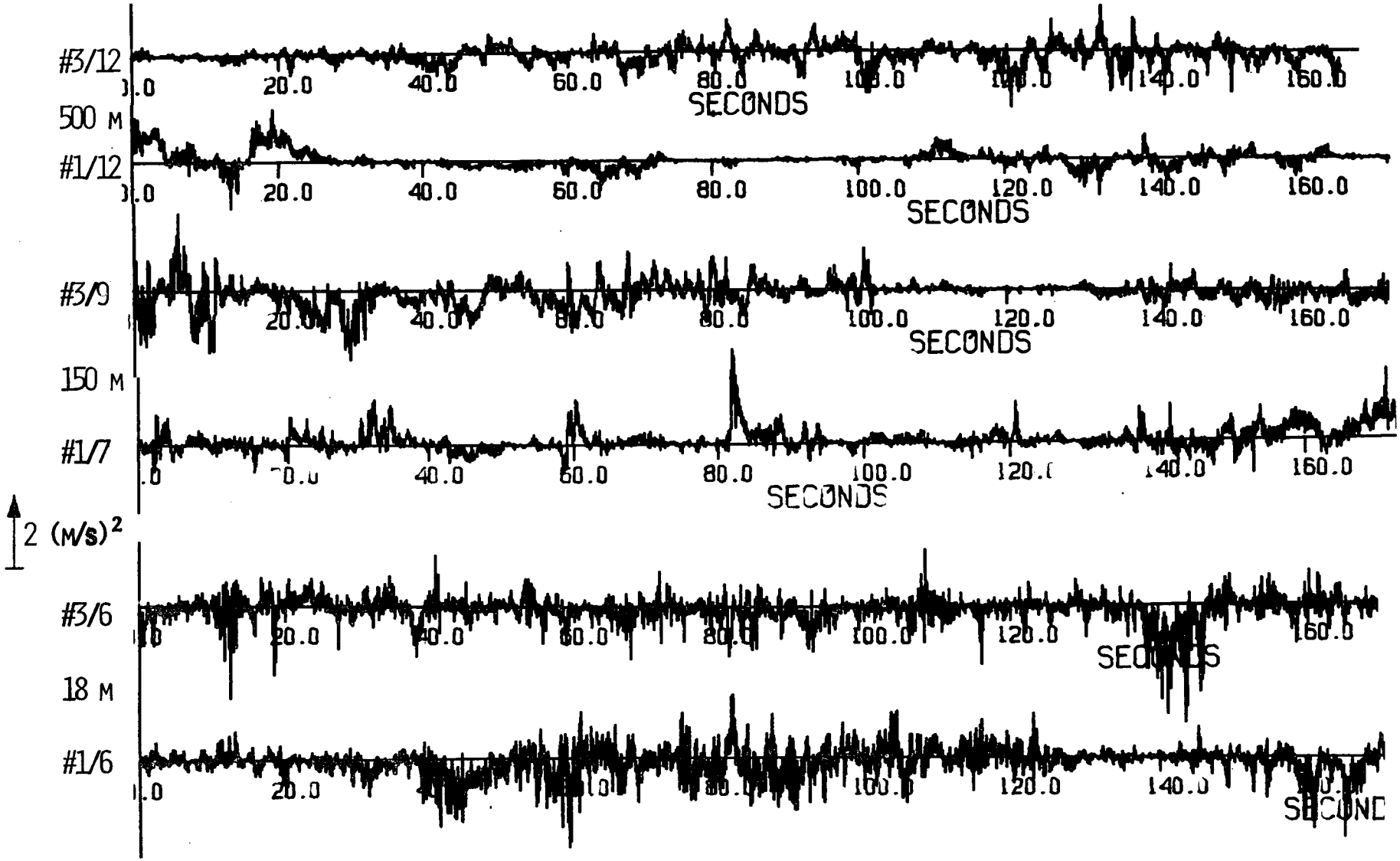

FIGURE 24. MOMENTUM TRACES (UPWIND)

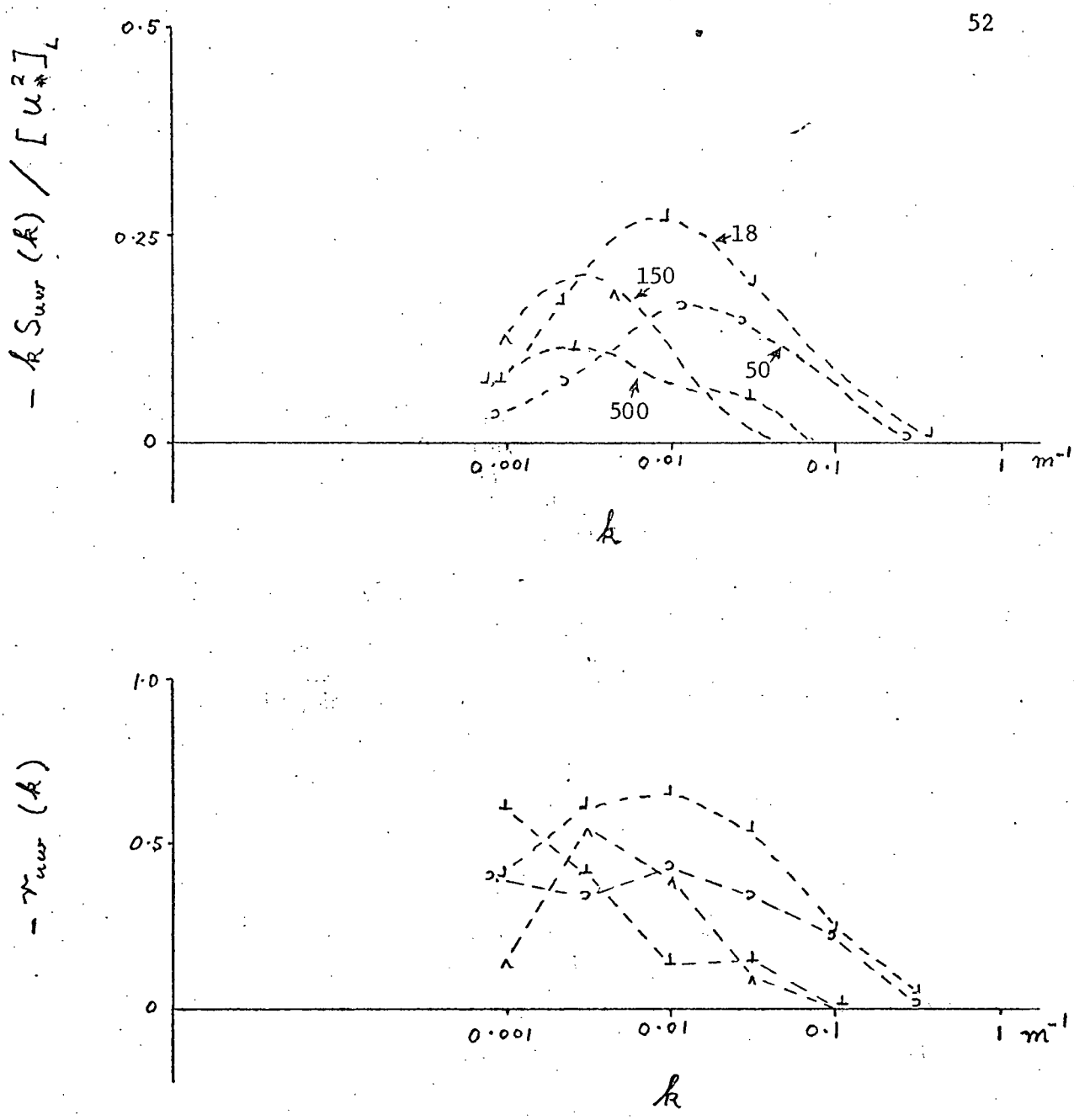

FIGURE 25. MOMENTUM COSPECTRA (UPWIND)
Flight # 3.

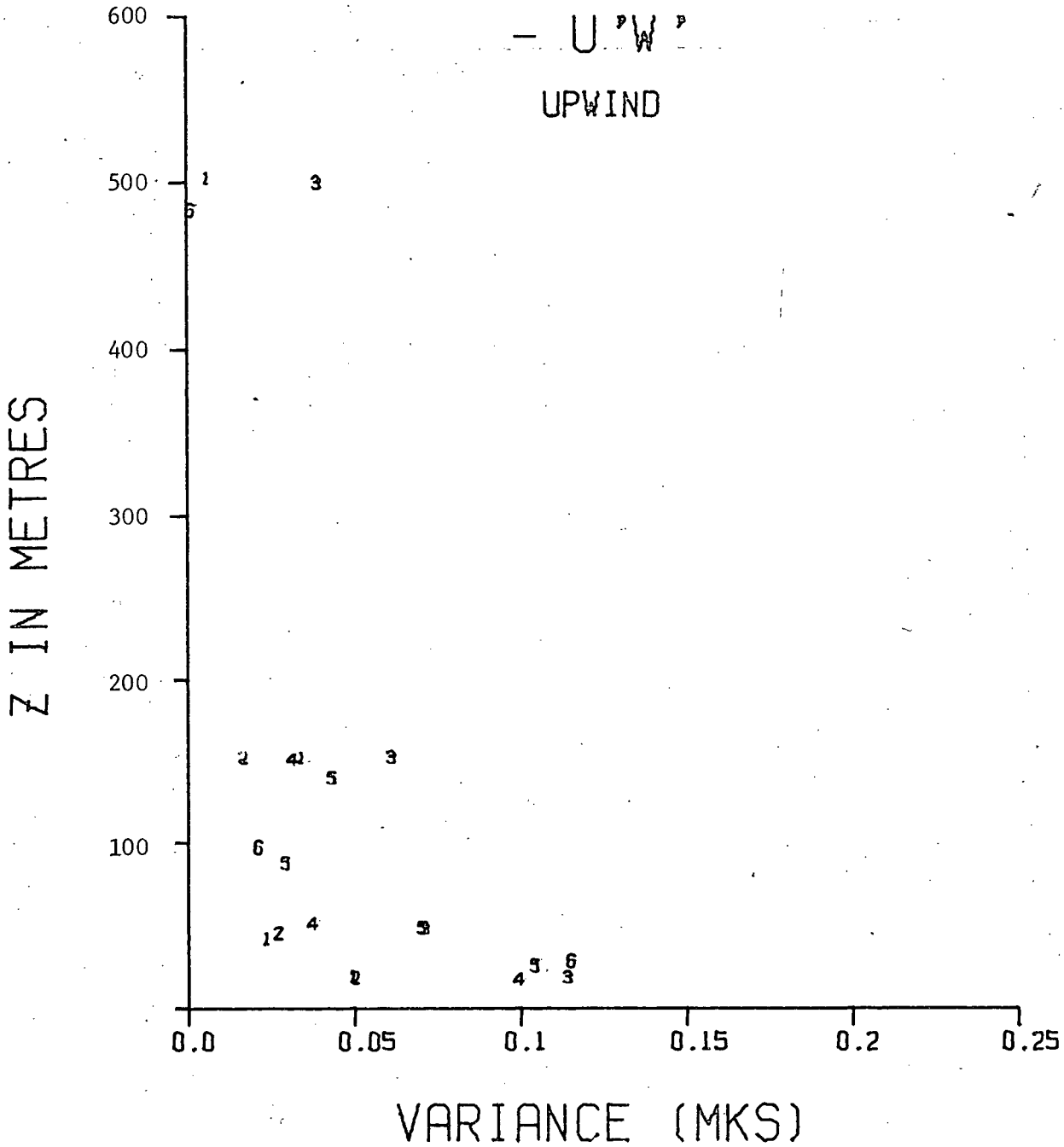

FIGURE 26. u_*^2 VS. Z

balance the stress gradient at say, 50 m: the mean wind speed would have to decrease at the rate of 2 m/sec/hour or increase towards the east by 4 cm/sec/km ; on the other hand, either a zonal pressure gradient of 10 μ bars/km or temperature gradient of 0.2C°/km would alone be adequate to counter balance the observed stress gradient at 50 m. Although it is possible that in any one case these terms were of the correct size and sign to balance the stress gradient ($\doteq 10^{-2}$ dynes/cm^2/m), it is extremely unlikely that this unusual coincidence occurred during the five daytime flights and the single flight at night. Hence, it seems likely that at 50 m and above some of the momentum flux was carried by scales larger than 20 km.

Both the momentum k-cospectra and the associated spectral correlation coefficients $r_{uw}(k) = S_{uw}(k) . [S_{uu}(k) . S_{ww}(k)]^{-1/2}$ are displayed in semi-logarithmic coordinates against the wave number k in Figure 25. and the overall correlation coefficient $-r_{uw}=-\overline{u'w'} . [\sigma_u . \sigma_w]^{-1}$ is plotted against Z for all the flights in Figure 27.

The k-cospectra (Figure 25) at 18 m are like those obtained under similar conditions in the surface layer, and the value (0.4) of the average of the correlation coefficients $-r_{uw}$ at this level (Figure 27) is also typical of the surface layer. However, with increasing height $-r_{uw}$ decreases rapidly, especially its contribution from the smaller eddies (see Figure 25). In other words, as successively larger eddies become less anisotropic (see Figures 8 and 14) they lose their ability to transport momentum.

Previous workers have remarked on the intermittency of the instantaneous momentum transfer, and have concluded that most of the momentum transfer near the surface takes place in short intense bursts separated by long quiet areas. Figure 24 does not agree with this observation at low levels; although there are areas of unusually high intensity, they cannot be said to dominate the overall transfer. Higher up, however, the product does become

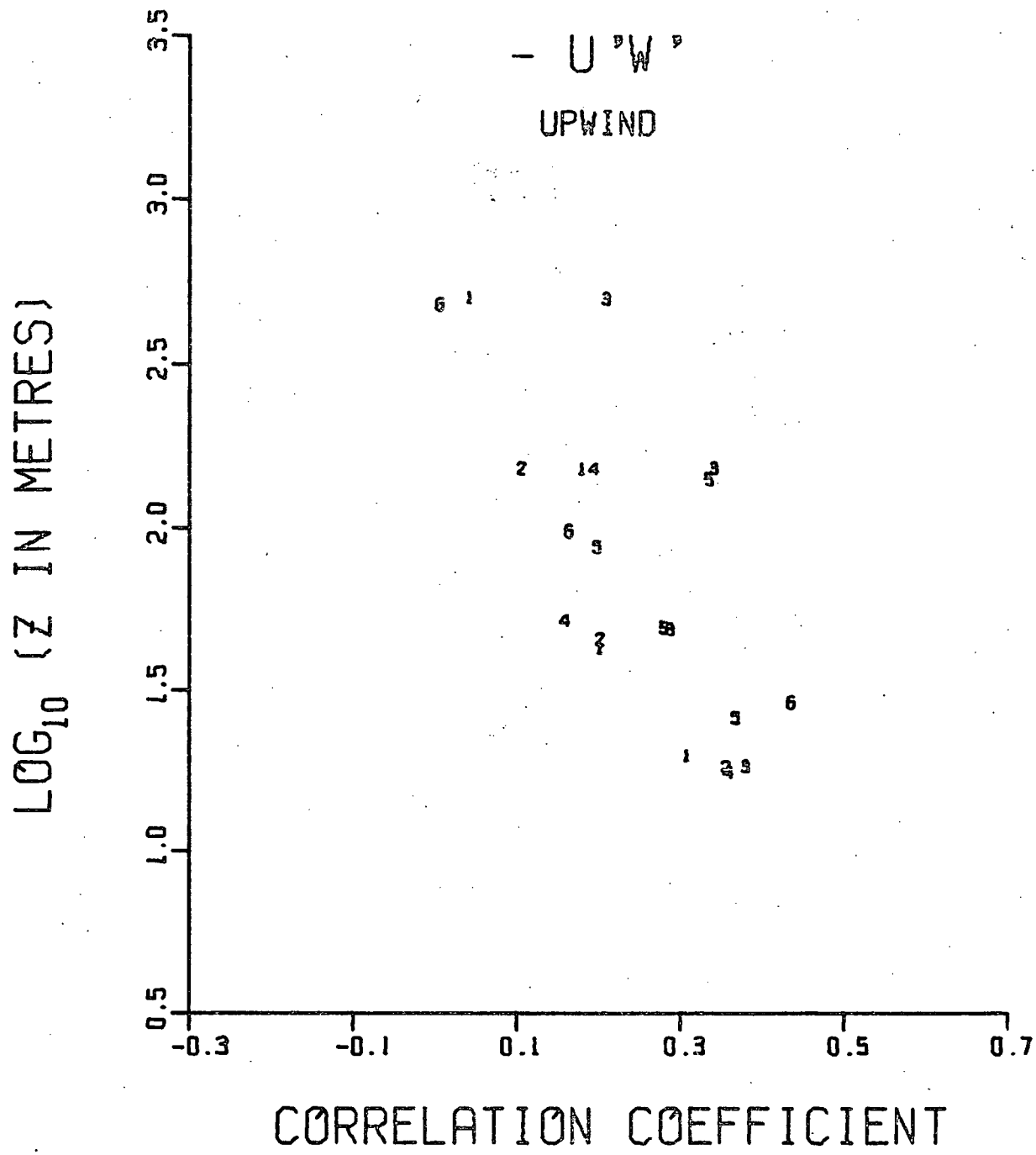

FIGURE 27. $-r_{uw}$ VS.Z

spotty (see run # 1/7 of Figure 24). It seems reasonable that this effect could be due to the action of convection; in which case the momentum flux and density flux should become more similar in appearance with increasing height. The two components of the density flux w'T' and w'Q' are plotted in Figures 30 and 33 on scales such that equal ordinate steps of both w'T' and w'Q' contribute about equally to $w'\rho'$; positive values of w'T' imply downward flux of air molecules, but positive values of w'Q' imply upward flux of water molecules. From these figures (see, for example, runs 1/7 and 1/12) it seems that the momentum flux is carried by the larger scales associated with the moisture flux rather than by those responsible for the transport of sensible heat.

Figure 28 indicates that the momentum carrying eddies tend to be larger with height at least up to a height of about 150 m. The initial increase of L_M reflects the tendency for the energy peak of $kS_{ww}(k)$ to shift to larger scales with height; the possibly less rapid increase of L_M at greater height may be indicative of the effects of buoyancy. That is to say: lighter air rising in a velocity shear probably contributes more to the momentum flux than heavier rising air since it will on average rise higher and faster; with the result that the momentum flux is enhanced at scales where buoyancy is important. These scales tend not to be height dependent.

The natural logarithmic bandwidth B (Figure 29) does not appear to be particularly height dependent.

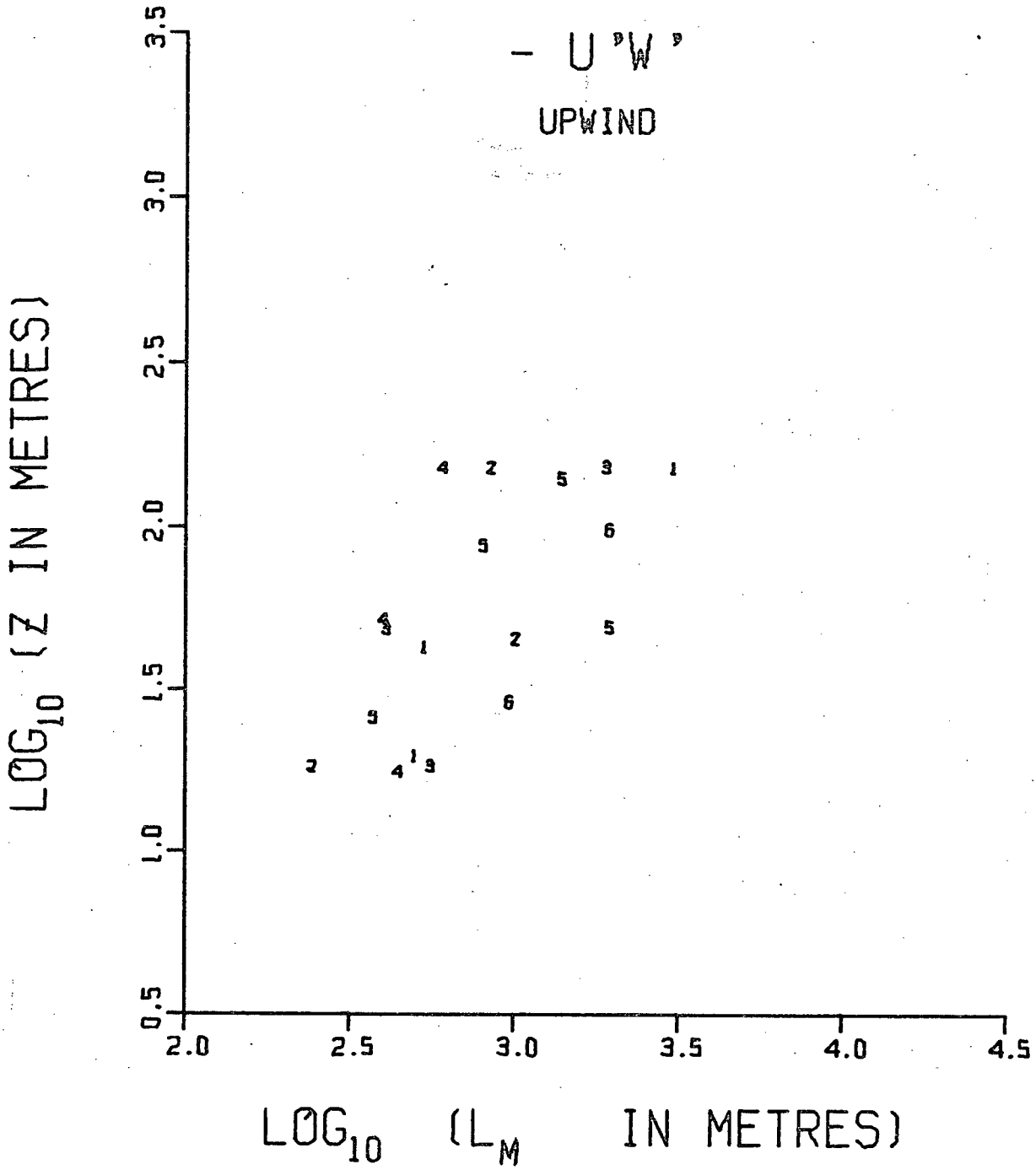

FIGURE 28. $(L_M)_{uw}$ VS. Z

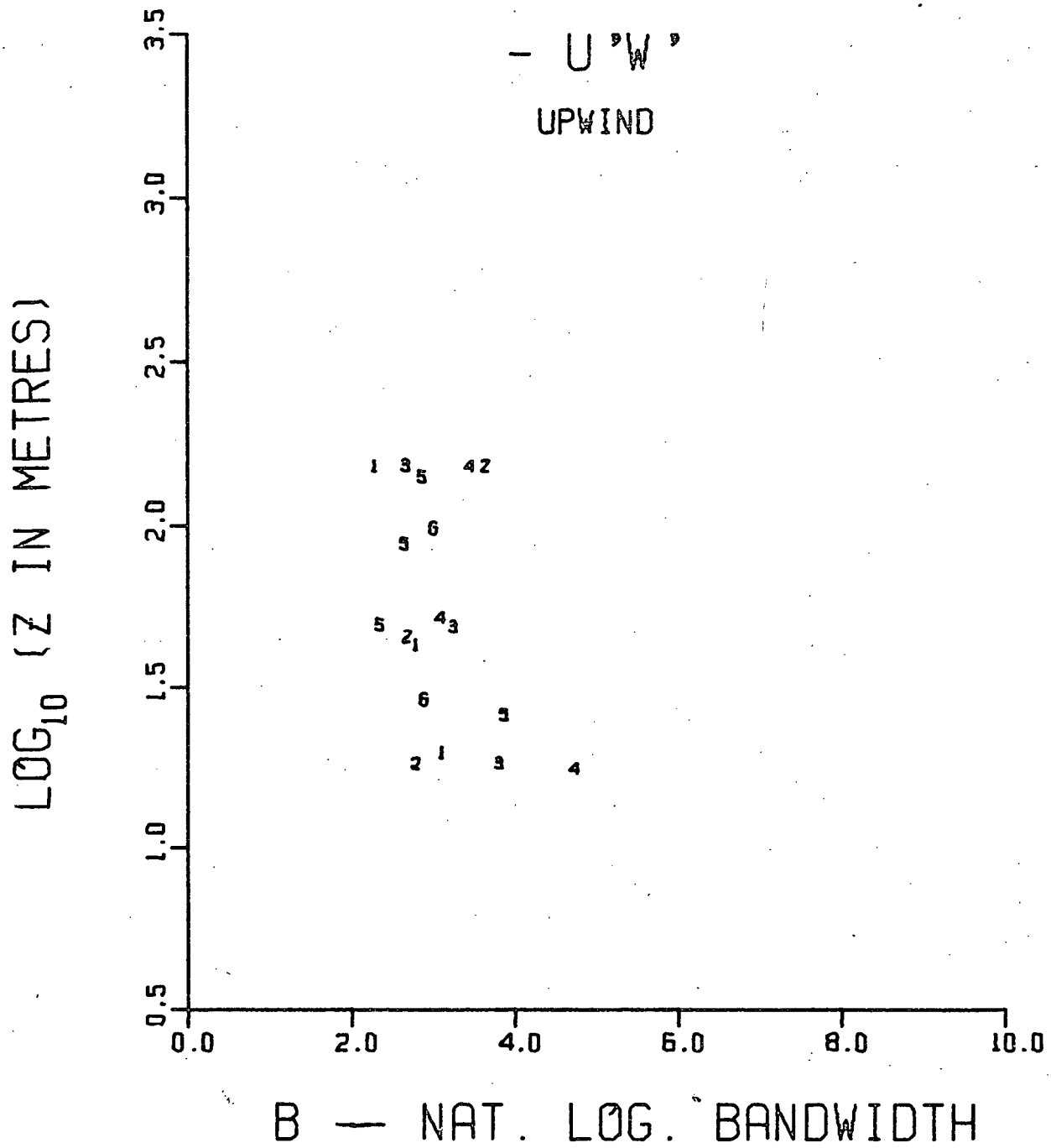

FIGURE 29. B_{uw} VS. Z

3.2.6 Heat Flux

Here the discussion is handled in terms of $\overline{w'T'} = F_H/\rho C_p$ where F_H is the heat flux, C_p the specific heat at constant pressure of the air and ρ its density.

The most striking feature of these traces (Figure 30) is the preponderence of small scale energy at the lowest levels; which is not surprising in view of the character of the temperature trace (Figure 20). Like momentum, there is a general decrease of intensity with height, and a tendency towards spottiness. Like temperature, the heat flux acquires renewed strength at the highest level in the large scale sizes, but the heat flux at these scales is generally directed downwards. It seems, then, that the higher altitude source of large scale temperature fluctuations is often associated with a negative heat flux.

Some peaks of Figure 30 have been designated 'U' or 'D' depending on whether the vertical velocity was upward or downward; it appears that, although the updrafts carry positive heat flux, the downdrafts may be associated with flux of either sign. Lumley and Panofsky (1964) reported that inspection of some temperature records of E.K. Webb's (unpublished) revealed that rising air tended to coincide with energetic temperature fluctuations and subsiding air with a smooth temperature trace - the small scale vertical velocity being equally energetic throughout. This phenomenon is frequently observed under convective conditions; for example Katz (1970), in which it is shown that the humidity trace behaves in a similar fashion. Close inspection of Figures 9, 20 and 23, however, indicates that large scale updrafts and downdrafts are about equally endowed with smaller scale fluctuations of temperature and humidity. The fact that the updrafts are associated

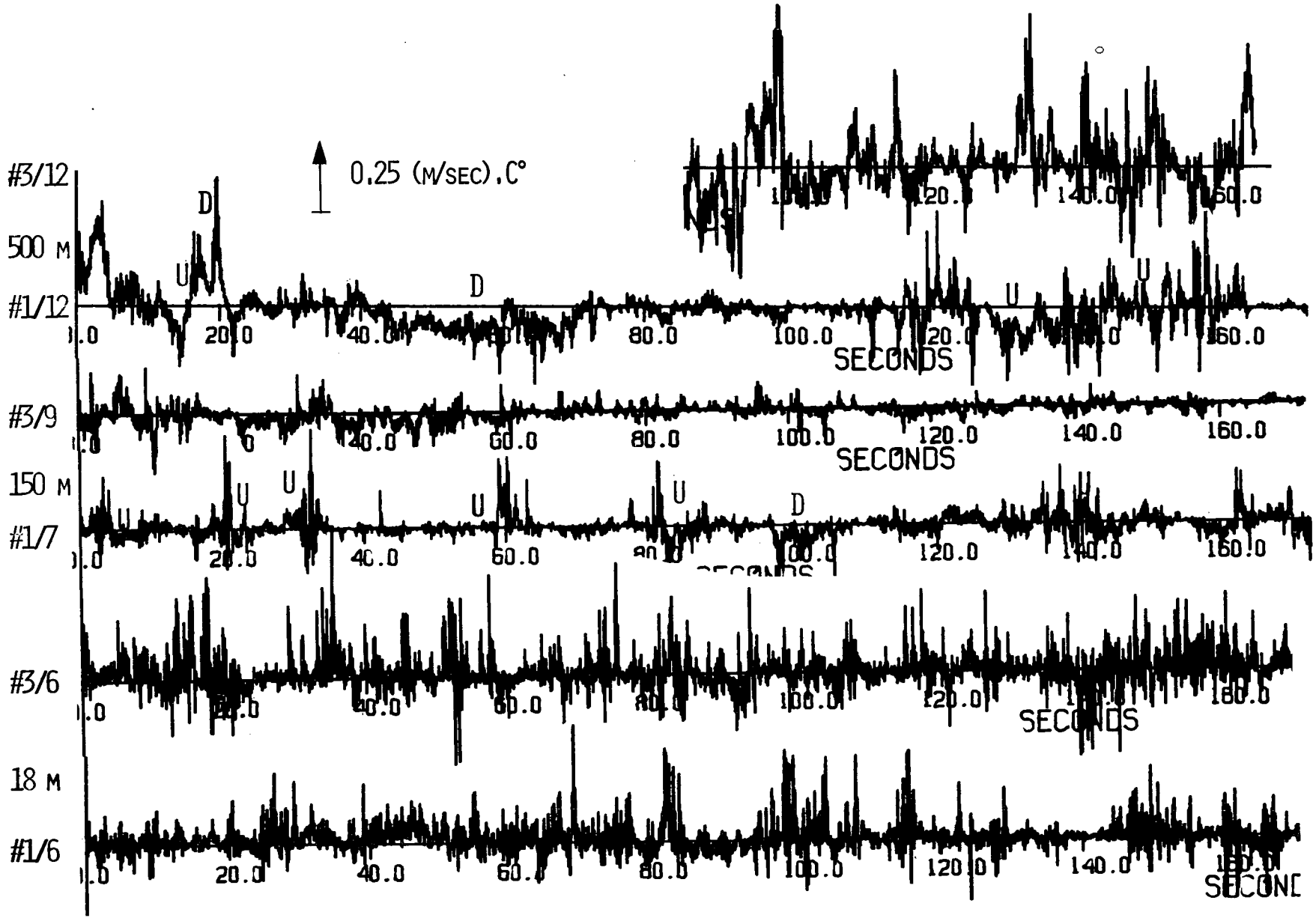

FIGURE 30. HEAT FLUX TRACES (UPWIND)

with a more energetic w'T' product (Figure 30) indicates that the small scales of vertical velocity tend to be coherent with small scale temperature fluctuations in the updrafts but not in the downdrafts.

The k-cospectra and correlation coefficients of Figure 31 reveal some interesting features of the heat flux and its height dependence during the experiment. It appears that the total sensible heat flux is comprised of a balance between the large scale negative flux and a comparable positive portion carried by much smaller eddies. The transition eddy size between the fluxes of opposite sign does not seem to be very height dependent but appears at smaller scales in the higher wind speed case. Cospectra of temperature and vertical velocity have been computed in the past; often in the surface layer over land and water (e.g. Panofsky and Mares, 1968; Miyake et al 1970c ; Miyake and McBean, 1970); and infrequently in the planetary boundary layer over land (Kukharets and Tsvang, 1969). Gurvich and Tsvang (reported by Monin, 1962) and Robinson (1959) presented data which suggested that the heat flux near the surface is associated with slightly larger eddies than is the momentum flux; whereas those of Panofsky and Mares (1968) and Miyake, Stewart and Burling (1970) show no difference while data described by Miyake and McBean (1970) indicate the reverse. Generally, it is found that the cospectra of the heat and momentum fluxes are quite similar. Thus, the outstanding dissimilarity of the k-cospectra of Figures 25 and 31 suggests an important difference in the structure of the atmospheric boundary layer from that previously observed. However, the airborne measurements of Kukharets and Tsvang (1969) provide an interesting comparison. In their Figure 3 the non-normalized heat flux n-cospectra are displayed in the same fashion as Figure 31; their k-cospectra have a single peak near $k = 0.008 m^{-1}$ and extend over the wave number range $0.001 < k < 0.1\ m^{-1}$. The Bomex k-cospectra have

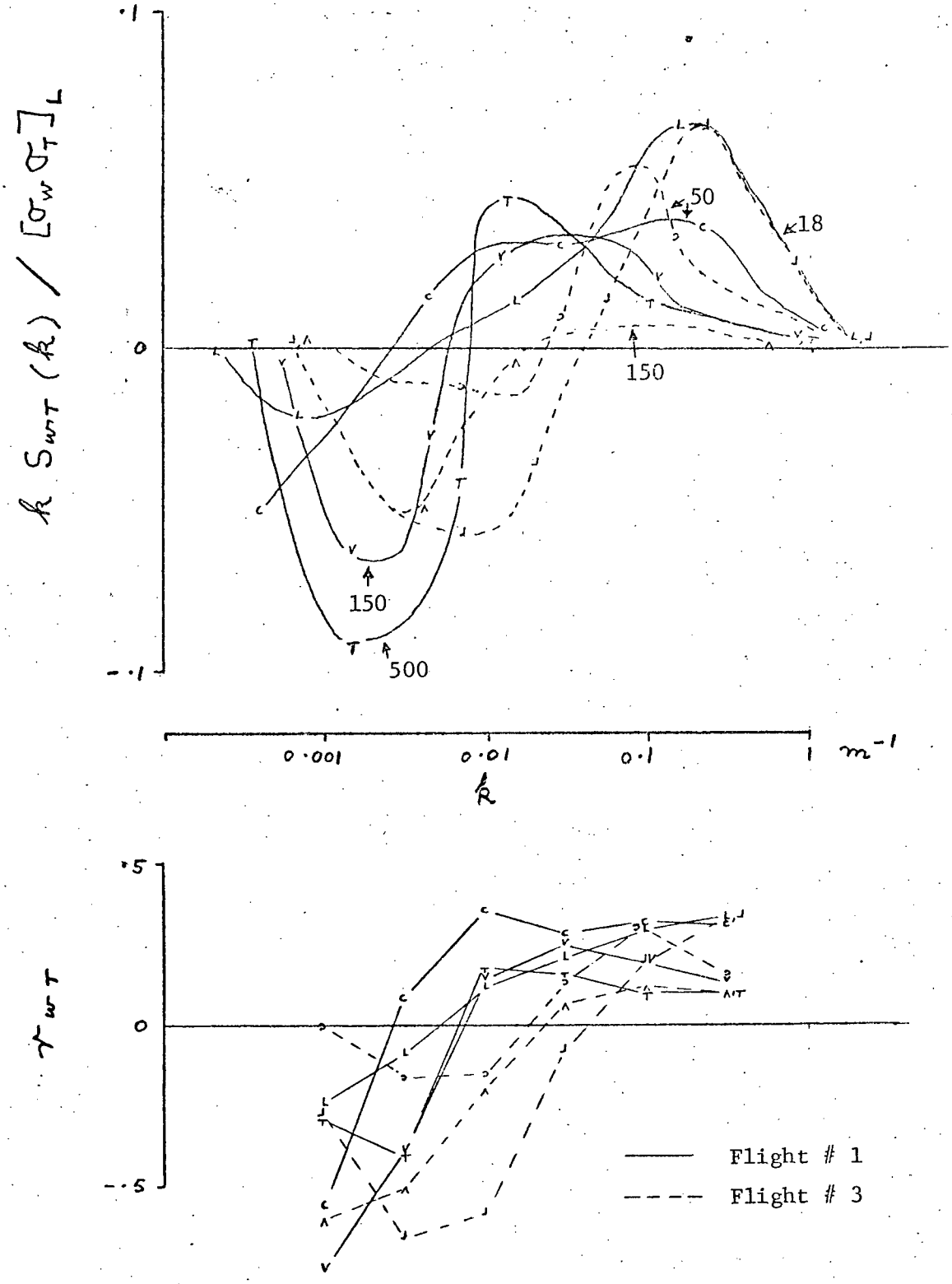

FIGURE 31. HEAT FLUX COSPECTRA (UPWIND)

two distinct peaks of opposite sign. Both the Russian k-cospectra and the positive hump of the Bomex k-cospectra show a tendency to decrease in amplitude with increasing height. Furthermore, Kukharets and Tsvang remark that at altitudes > 500 m the k-cospectra often develop a negative hump at large scales. They speculate that this may be caused by a mechanism proposed by Vul'fson (1961), in which the downward heat flux at large scales is due to displaced colder air masses which descend slowly around the smaller blobs of rising warm air. This mechanism requires the presence of a layer of air above in which the potential temperature gradient is negative.

The height dependence of the sensible heat flux is displayed in Figure 32. It is seen that there is a general tendency for the flux to decrease with increasing altitude. The average value of the heat flux near the surface is about 1.0 mW/cm^2 (see Figure 32 and Table 3).

In summary: the total sensible heat flux, during these aircraft observations in Bomex, is due to a large scale negative contribution and a smaller scale positive contribution. At the surface the heat flux is about 1.0 mW/cm^2 on average, but with increasing altitude the negative contribution due to large scales increases in importance and consequently the heat flux is reduced. The systematic appearance of the negative 'hump' in the k-cospectra has not previously been noticed at such low altitudes. Both the wave number and the amplitude of the positive k-cospectral peak decrease with increasing height. The effect of increasing wind speed appears to be simply to shift the k-cospectra bodily to higher wave numbers, and the cospectral transition from negative to positive does not seem to be very sensitive to altitude.

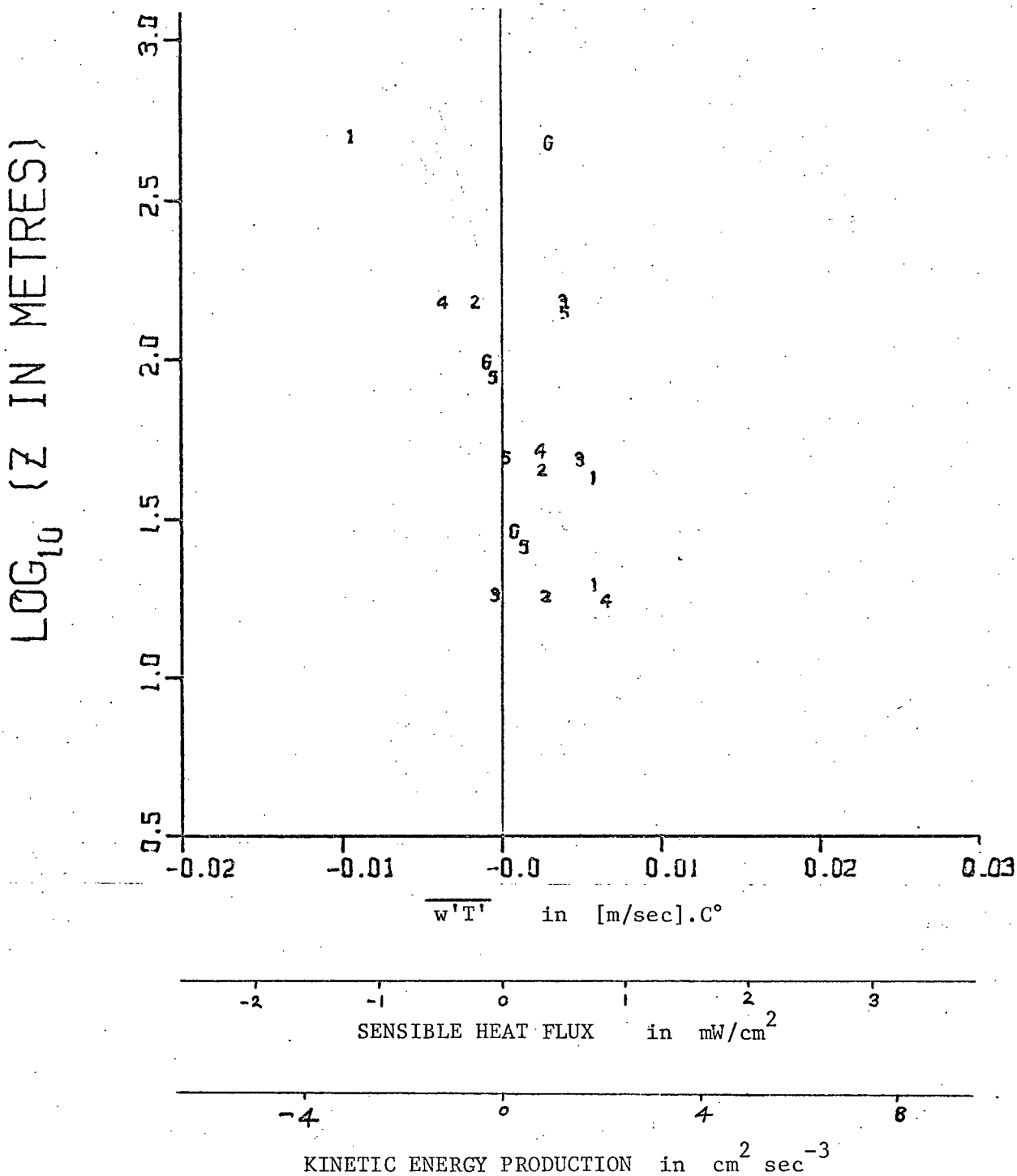

FIGURE 32. HEAT FLUX VS. Z (UPWIND)

3.2.7 Moisture Flux

$\overline{w'Q'}$, which when multiplied by ρL yields the flux of latent heat, is now considered. (L is the latent heat of vapourization of water).

The similarity of these traces (Figure 33) with those of momentum flux (Figure 24) is striking, as is the contrast with the heat flux traces (Figure 30). W'T' and W'Q' become spotty with increasing height; but, while the heat flux changes sign frequently, the moisture flux is positive nearly everywhere. Here again the direction of the vertical velocity at some peaks of W'Q' is indicated, and it is seen that the updrafts tend to produce slightly more intense moisture fluxes than the downdrafts, although, as in the case of temperature, the moisture fluctuations are no more energetic in the updrafts than in the subsidence areas.

A comparison of Figures 25 and 34 reveals the similarity of the fluxes of momentum and moisture at low levels, the main difference being the relatively larger energy in the moisture flux at wave numbers in excess of 0.1 m^{-1}. Both k-cospectra become narrower and shift to lower frequencies with height, but while the momentum transfer diminishes rapidly the moisture flux does not.

As mentioned before, it has often been noticed that under weakly convective conditions, the momentum and sensible heat flux are very similar. However, in such cases the boundary layer convective process is dominated by temperature variations; whereas over the tropical ocean the moisture fluctuations contribute at least as much to the buoyancy as do those of temperature. It seems that the humidity fluctuations are more closely correlated with the vertical velocity and retain their correlation at larger heights than the temperature fluctuations. Nonetheless, since the boundary layer between heights of 50 m and 500 m during this experiment was character-

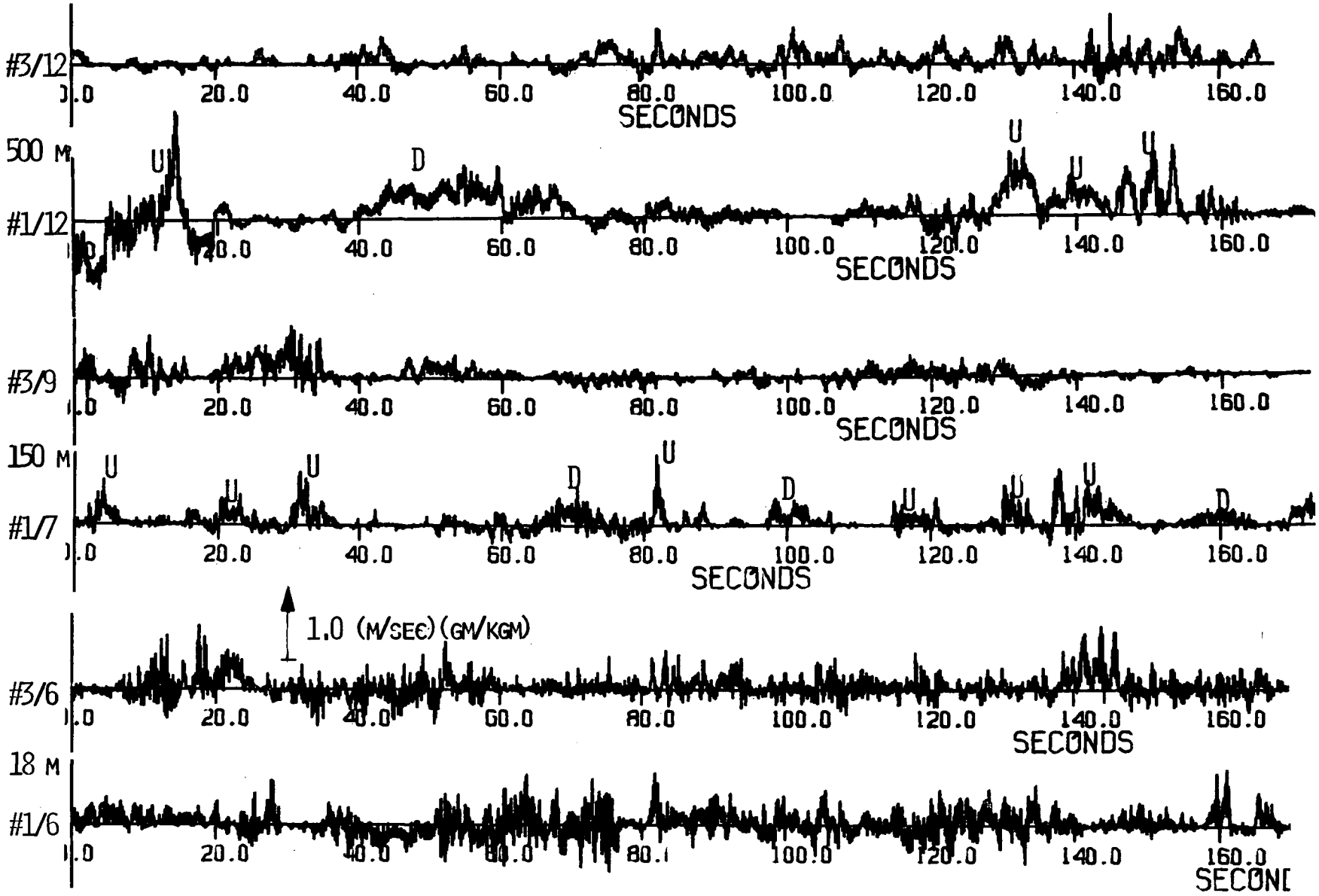

FIGURE 33. MOISTURE FLUX TRACES (UPWIND)

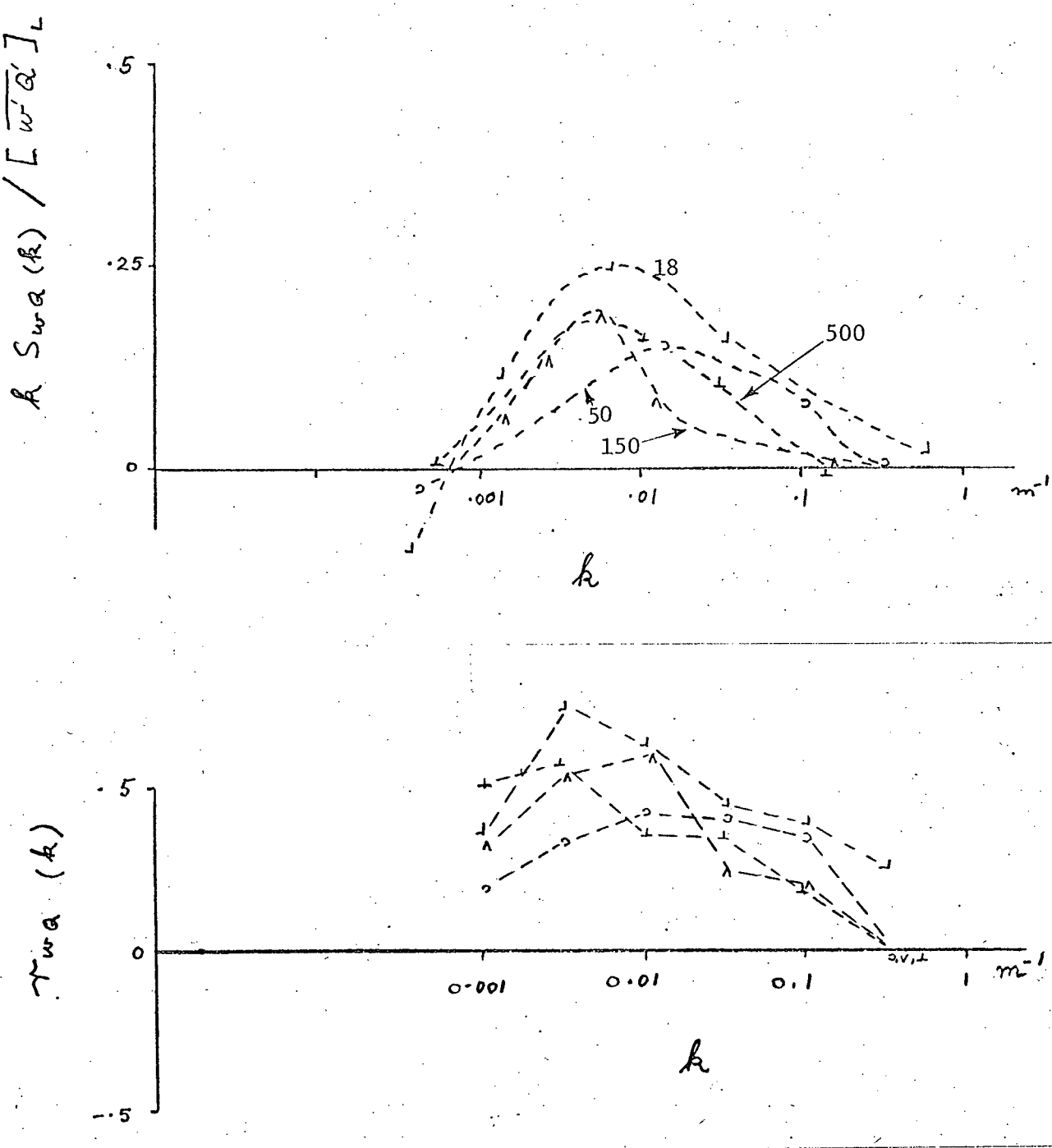

FIGURE 34. MOISTURE FLUX COSPECTRA (UPWIND)

Flight # 3.

ized by a very small gradient of potential virtual temperature (see Figure 5), most large scale updrafts were both warm and wet (Figures 9, 20 and 23). It is therefore appropriate to adopt Ball's (1960) coinage, and to refer to such updrafts as warm 'moistals'. The large scale subsidence zones, on the other hand, are generally drier but not necessarily colder than the average. Since the density fluctuations due to temperature are about as large as those due to moisture, the similarity of moisture and momentum fluxes and the dissimilarity of heat and momentum fluxes must be attributed to the more efficient momentum transfer properties of the large scales associated with the fluctuations of humidity relative to those associated with temperature variations. From this it can be inferred that under unstable conditions the similarity of the mass and momentum transfer depends on the spectral distribution of buoyancy variations. That is, if the most energetic scale sizes of the buoyancy variations are those capable of the most efficient transfer of momentum the fluxes of mass and momentum will have similar spectral distributions; otherwise the peak of the k-cospectrum of the momentum flux will be shifted, relative to that of the mass flux, towards the scale sizes which transport momentum most efficiently.

The correlation coefficients $r_{wQ}(k)$ and $-r_{uw}(k)$ (Figures 25 and 34) are quite similar at low levels, and their overall values (Figures 27 and 36) diminish with increasing altitude: $-r_{uw}$ very rapidly at first and then more slowly; r_{wQ} decreases quite slowly from a surface value of about 0.4 to about 0.3 on high. The reduction of r_{wQ} with height, even though the effects of convection become more pronounced, as the mechanical turbulence diminishes, is probably due to the counter effects of temperature fluctuations and those of humidity to control the buoyancy (see Section 3.5).

The height dependence of the latent heat flux is displayed in Figure 37.

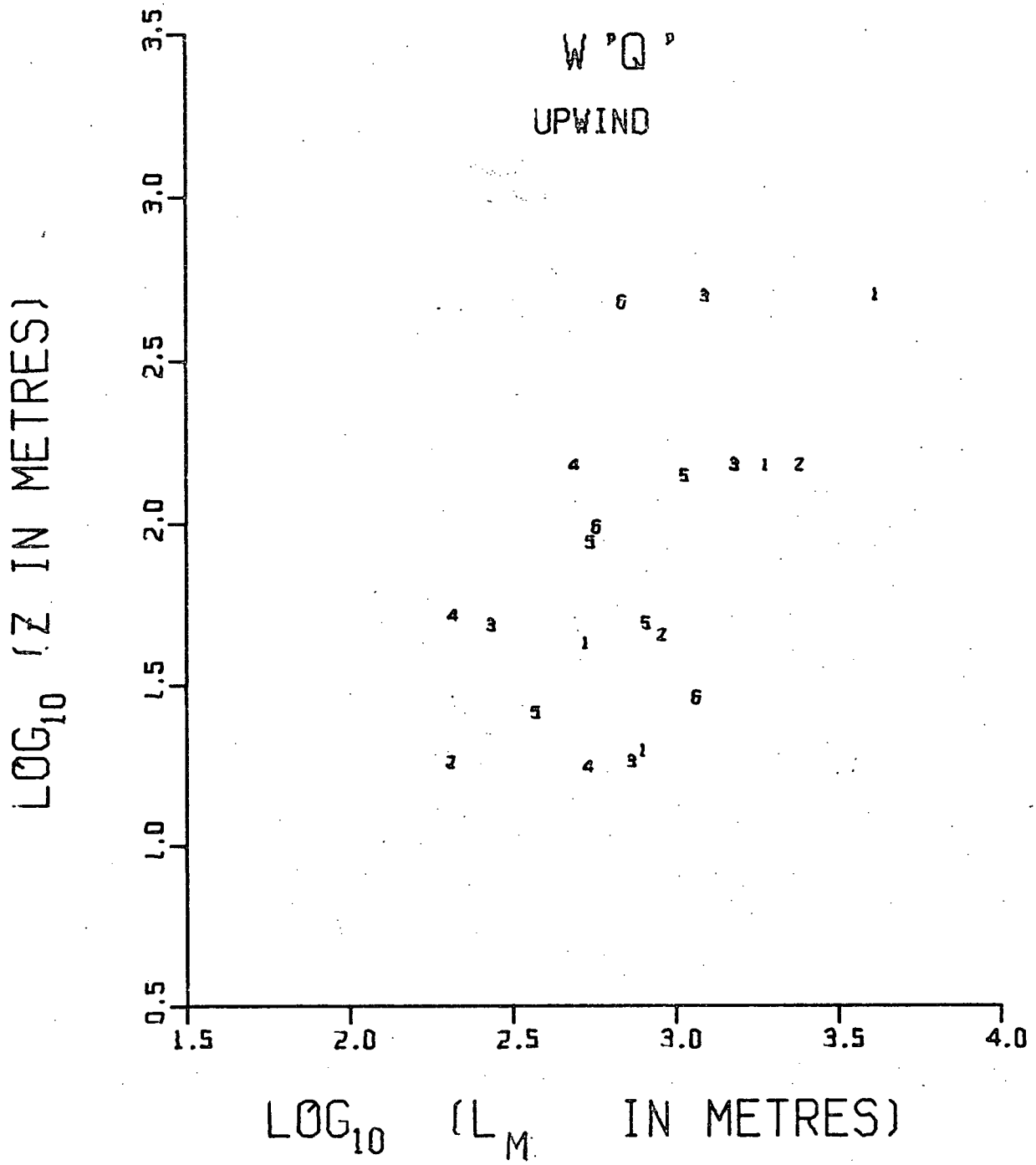

FIGURE 35. $(L_M)_{wQ}$ VS. Z (UPWIND)

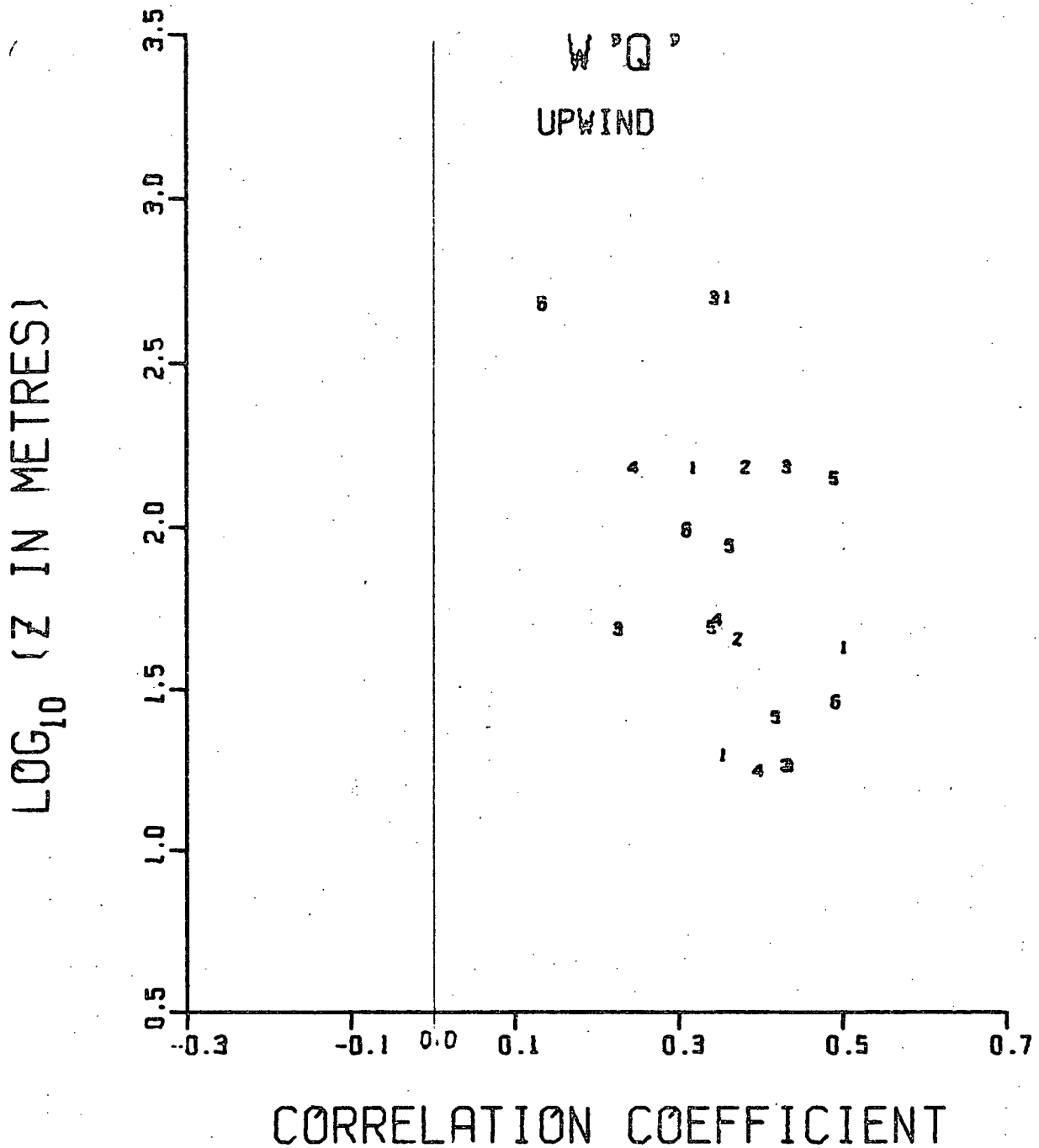

FIGURE 36. r_{wQ} VS. Z (UPWIND)

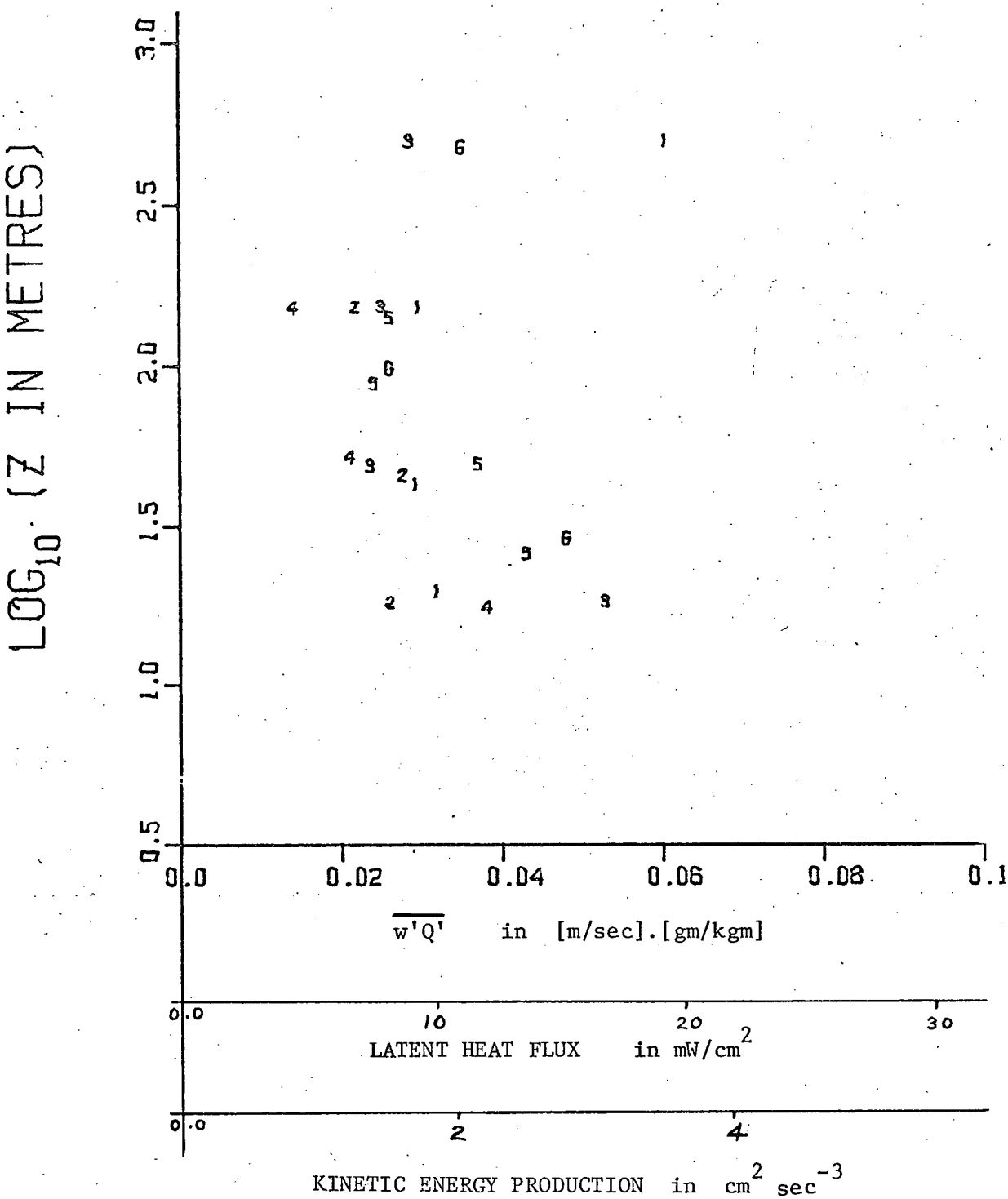

FIGURE 37. MOISTURE FLUX VS. Z (UPWIND)

The flux decreases from an average value near the surface of about 12 mW/cm^2 to a minimum of about 8 mW/cm^2 at an altitude of about 150 m; above this level there appears to be a general increase in the latent heat flux; but this tendency may have been more clearly revealed had there been data from at least one more level between 150 m and 500 m.

3.3 Comparison of crosswind measurements with measurements along the wind

3.3.1 Introduction

One of the important features of these airborne turbulence measurements is the difference obtained from flight paths along and perpendicular to the wind. The flights (1, 2, 3 and 4) which were flown in a rectangular pattern (flight pattern 1; see Figure 4) were designed to investigate this difference. However, in order that the aircraft remain in the vicinity of the surface platform, which would later act as a 'ground truth' station, the crosswind flights were much shorter than the upwind cases discussed. This limitation proved to be not very serious because the largest scale sizes were somewhat smaller across than along the wind.

In this section many of the results of measurements in the wind direction (Section 3.2) are compared and contrasted with their cross-wind counterparts and various inferences are drawn from their similarities and differences.

3.3.2 Vertical Velocity

The traces of vertical velocity measured in flights along (Figure 9) and perpendicular to (Figure 38) the wind present some interesting contrasts, the most striking of which is the increased regularity and sharpness of the large scale updrafts sampled at 150 m and 500 m in crosswind flight over those discussed previously.

Radar photographs of low level clear-air convection, in which the convective cells are aligned in rows analogous to cloud streets but an order of magnitude smaller in horizontal scale, indicate that the convective areas are generally circular in horizontal cross-section and vary in diameter by about a factor 3 between the smallest and largest (Konrad, 1970). A crosswind traverse through such a buoyant field would encounter updrafts of various durations. Crosswind runs # 1/8 at 150 m and # 1/11 at 500 m provide estimates of the average crosswind width and separation of the updrafts as approximately 500 m and 800 m respectively. Windwise traverses on the other hand, may encounter many, few or no updrafts, according as the flight path is directly through, on the edge of, or far from an aligned convective strip. The character of # 1/7 (Figure 9) suggests that it may have been directly through a convective strip. Assuming, for the moment, that this is the case, it is a simple matter to deduce from run # 1/7 that the width and separation of these updrafts in the wind direction are approximately 500 m and 800 m respectively. There is a pronounced difference between the appearance of the updrafts of run # 1/7 and those of # 1/11; the difference implies that the transition between and updraft and subsidence is sharper on the crosswind sides of an updraft than on its downwind or upwind sides.

The k-spectra of the vertical velocity component are displayed in Figure 39 (crosswind traverses) and in Figure 8 (along wind traverses).

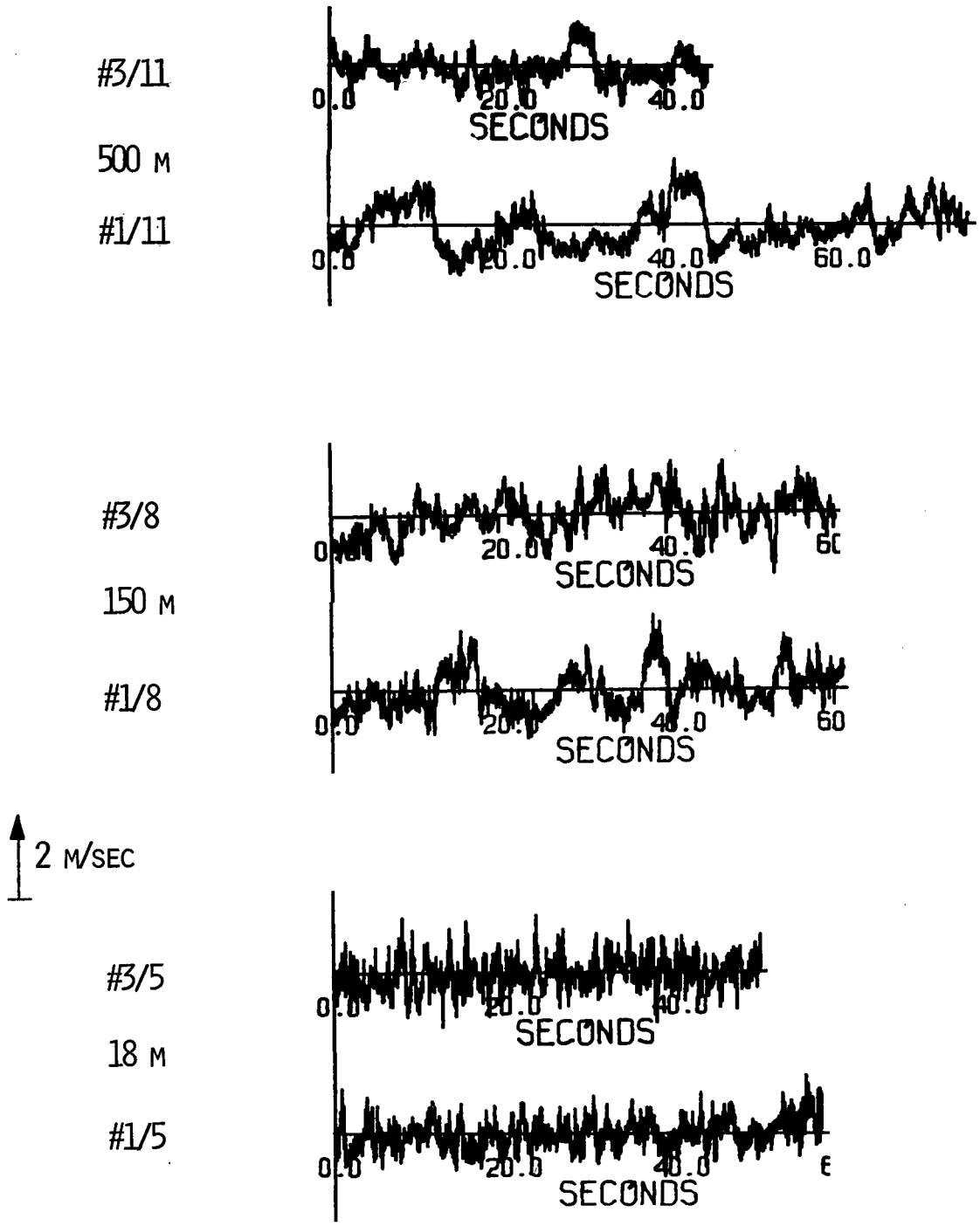

FIGURE 38. VERTICAL VELOCITY TRACES (CROSSWIND)

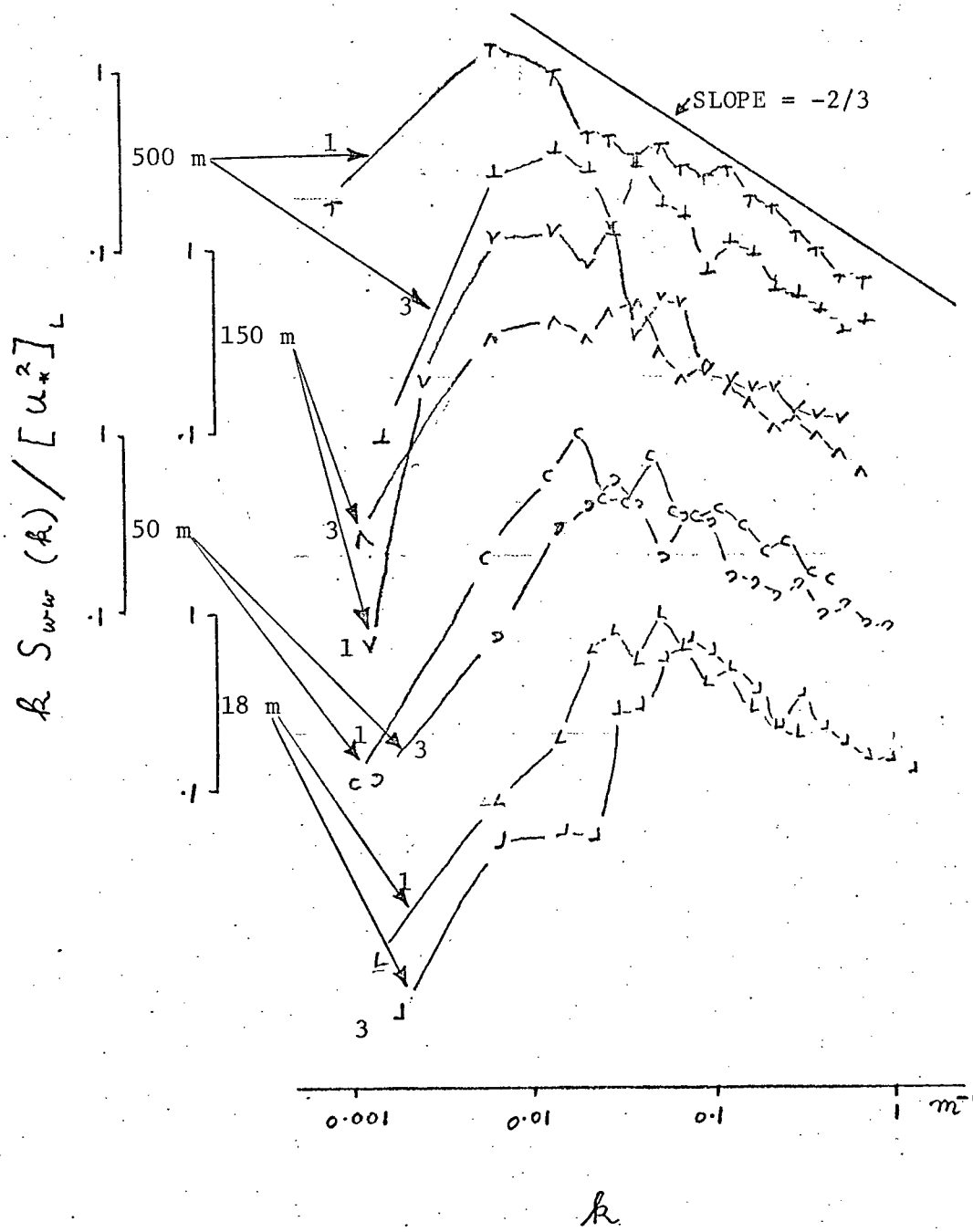

FIGURE 39. VERTICAL VELOCITY SPECTRA (CROSSWIND)

Evidently the shape of the k-spectra are quite similar; the main difference being that the k-spectra of the along wind measurements (Figure 8) are slightly broader than those measured across the wind. The k-spectral peak occurs at about the same wave length L_M in both along wind (Figure 8) and crosswind (Figure 39) measurements, and L_M increases with increasing altitude in much the same manner in both cases.

Priestly (1959) has found that in convective situations over land the scale of vertical velocity fluctuations is smaller across than along the wind. He attributes this effect to the stretching of plumes in the direction of the wind shear and to the merging of the stretched plumes in that direction. Perhaps the reason for the absence of this effect here is that over water with such uniform surface temperatures the convective areas are not tied to the surface, whereas over land they frequently are. The appearance of the time traces (Figures 9 and 38) suggests that the plumes do not develop until heights of 50 m or more, where the wind shear is far too weak to produce any appreciable plume elongation.

One of the striking features of Figure 8 was the enormous disparity of the normalized k-spectra at 150 m between flights 1 and 3 when the k-spectra at other levels were quite comparable. The effect is not nearly so pronounced in Figure 39 and this suggests that the turbulent field either contains important inhomogeneities of several kilometers in extent or is sufficiently well organized that the measured statistics depend on the choice of flight path. The latter possibility is the more palatable since it is difficult to imagine a mechanism capable of producing important vertical velocity differences of such large extent at these altitudes.

3.3.3 Horizontal Velocity

Measurements over land (Lumley and Panofsky, 1964) reveal a great deal of low frequency energy in the spectrum of lateral velocity under unstable conditions; while the inshore over water measurements of Miyake, Stewart and Burling (1970) reveal a lateral velocity spectrum having considerably more low frequency energy than that of the vertical velocity but slightly less than the longitudinal velocity spectrum. A comparison of Figures 8, 14 and 40 indicates that the lateral velocity fluctuations contain less large scale energy than those of the longitudinal velocity component and more than those of the vertical; lying, in fact, close to the median of these two. This is what one would expect as, having to extract its energy from the mean flow, the lateral velocity component is likely to be less energetic at large scales than the component in the direction of the mean flow itself; on the other hand, not being directly restricted by the presence of boundary, the lateral velocity component's large scale fluctuations develop more easily than those of the vertical velocity. Perhaps topographic features were instrumental in increasing the large scale lateral velocity fluctuations in the inshore and over land measurements. Certainly the constancy of direction of the trade winds off Barbados would not obtain over or near a land mass.

It is interesting to note that the wave length of the k-spectral peak (Figure 40) does not vary appreciably with height. This underlines the unimportance of the boundary in limiting the scale sizes of the lateral velocity component.

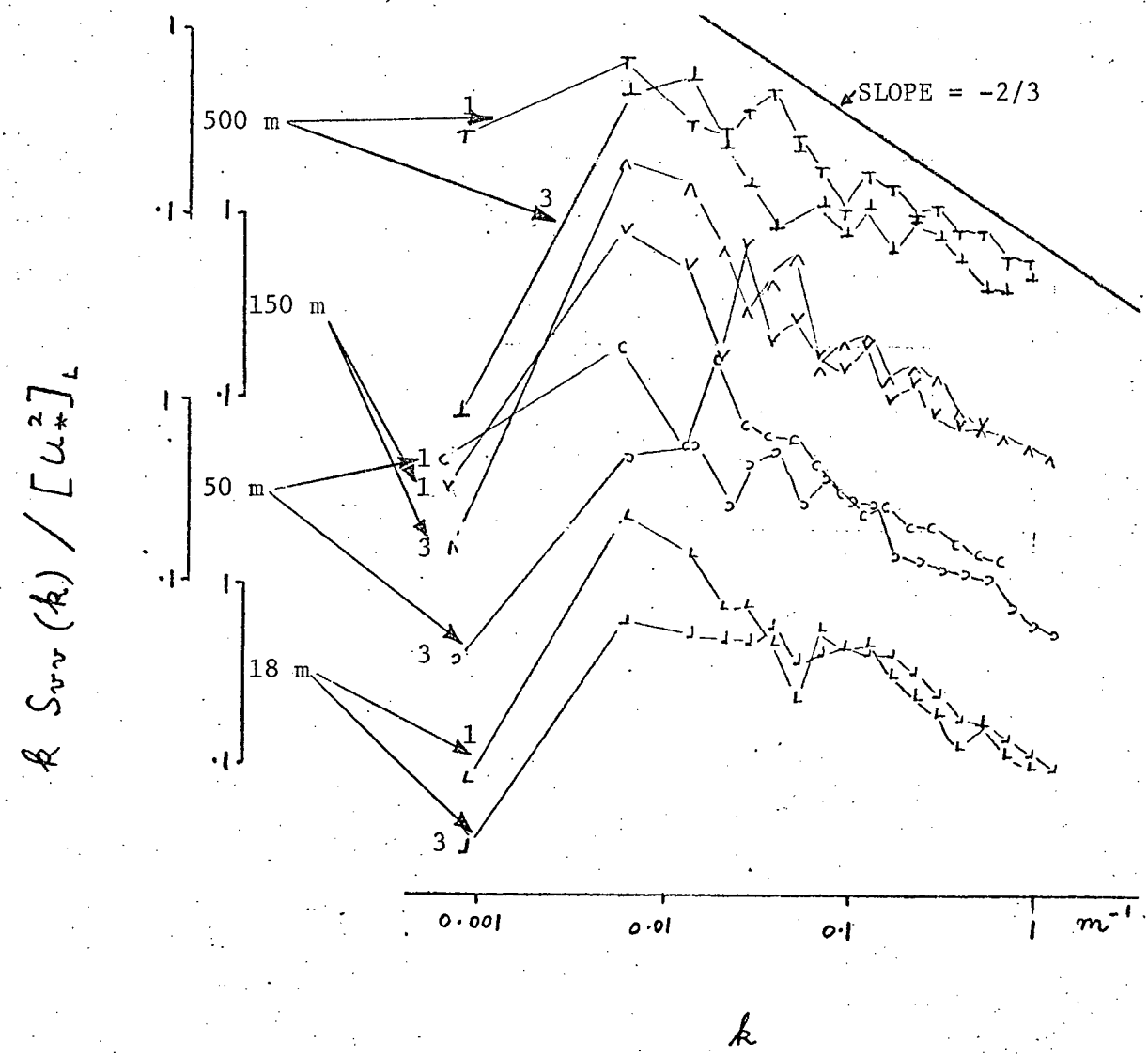

FIGURE 40. LATERAL VELOCITY SPECTRA

3.3.4 Temperature and Humidity

The standard deviations of the temperature fluctuations σ_T and those of humidity σ_q are plotted versus $\log_{10}Z$ in Figures 41 and 42 respectively. Here, as in the corresponding figures in the section on measurements in the wind direction (Figures 18 and 22), it seems that both the temperature and humidity fluctuations are least energetic at some altitude between 50 m and 500 m.

In the data gathered along the wind (Section 3.2) the peak of $kS_{TT}(k)$ (Figure 19) displayed a systematic shift to lower wave numbers with increasing altitude: the peak of $kS_{QQ}(k)$ did not. In contrast the crosswind measurements show no systematic height dependence of the wave length of the peak of $kS_{TT}(k)$, but they do indicate (Figure 43) that there is a definite shift of the wave length L_M of the peak of $kS_{QQ}(k)$ to larger scales with increasing altitude.

$$L_M \doteqdot 185 \ (Z/10)^{0.45} \text{ metres}$$

representing the line shown in Figure 43.

3.3.5 Heat Flux

One of the striking features of the k-cospectra of the heat flux measured along the wind (Figure 31) was their double peak: upward flux at small scales and downward flux at large scales. In the k-cospectra measured across the wind (Figure 44) this duality is evident in the runs at 150 m, but the negative peak is absent or much reduced in amplitude at the other levels.

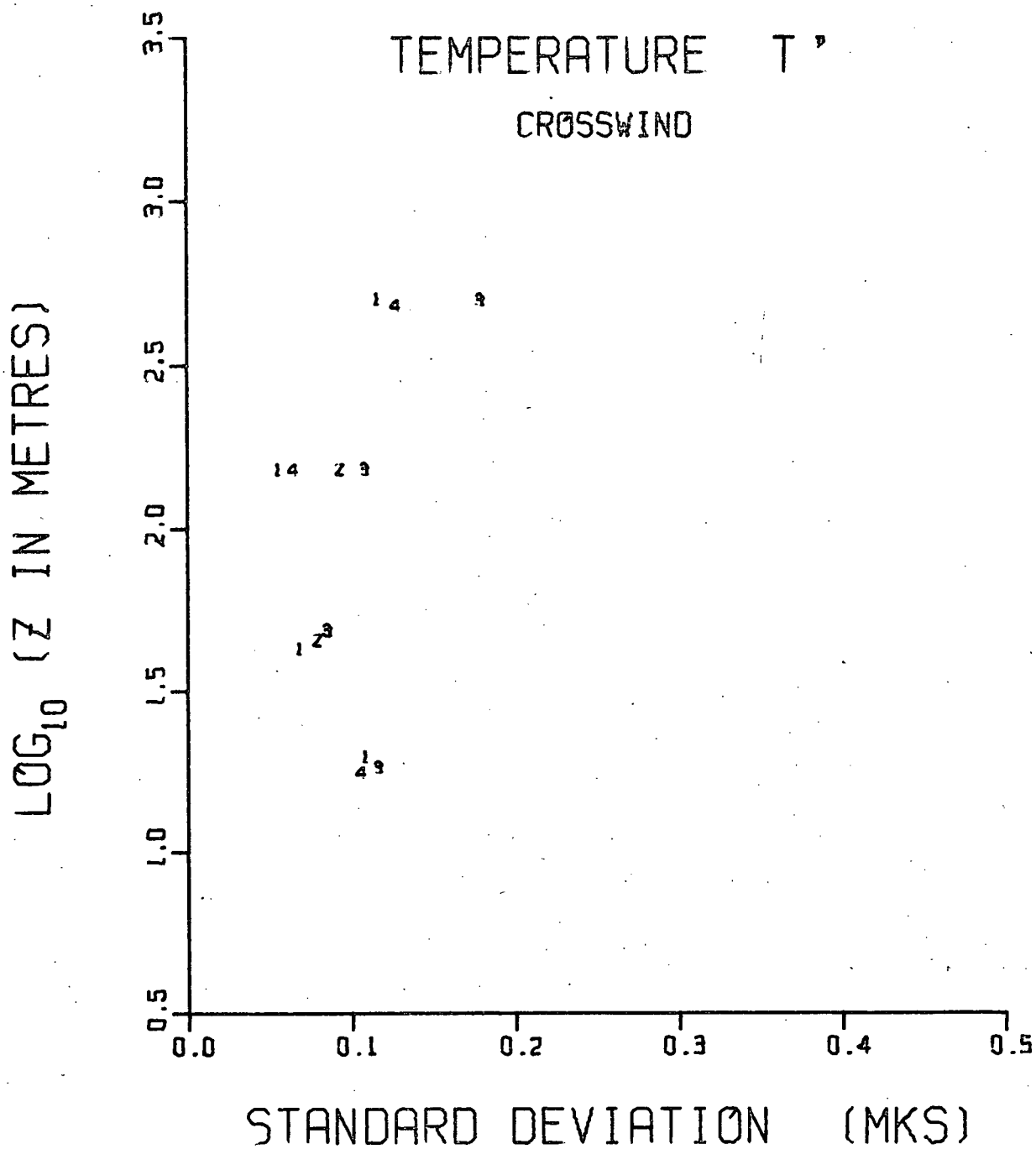

FIGURE 41. σ_T VS. Z (CROSSWIND)

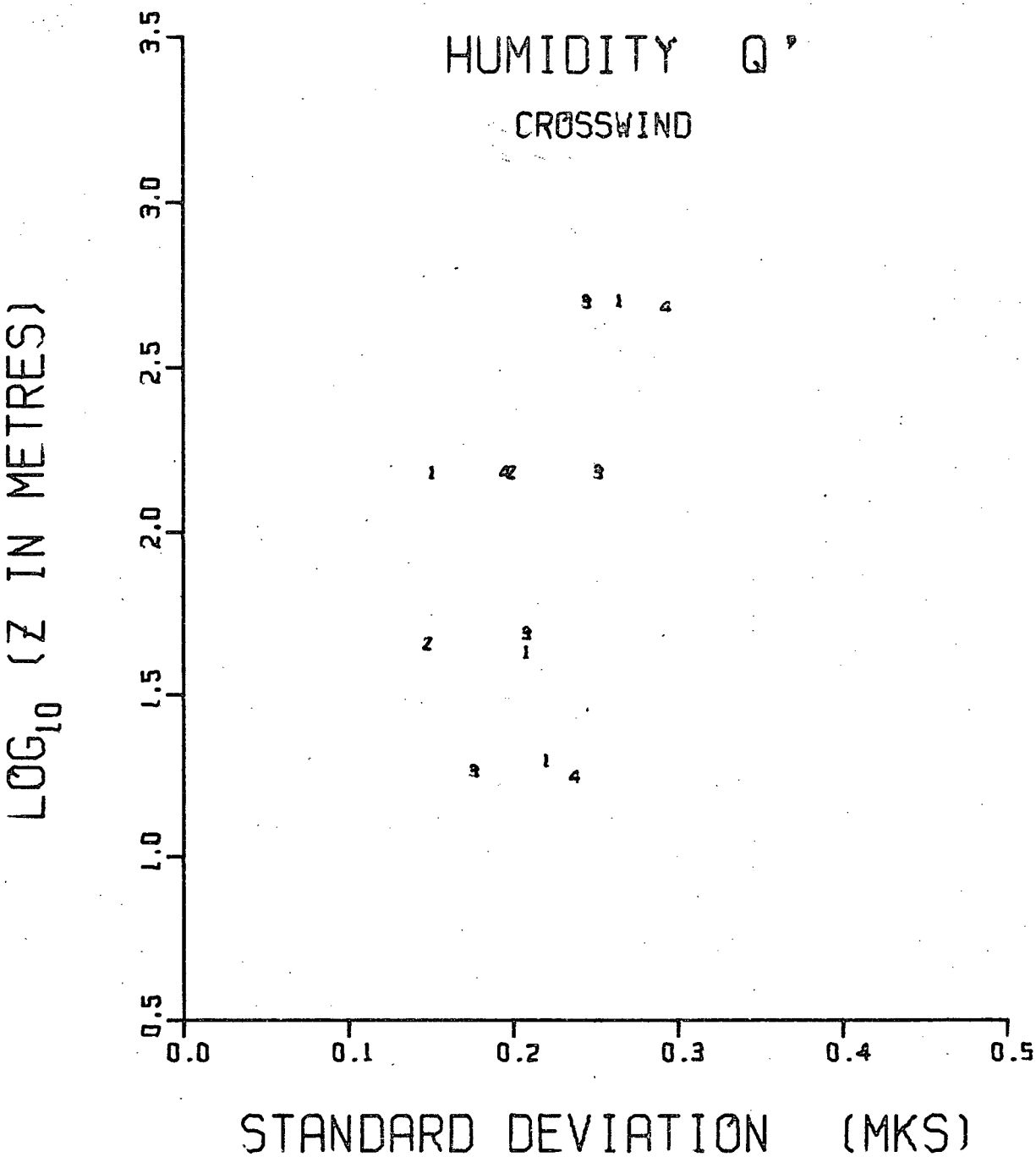

FIGURE 42. σ_Q VS. Z (CROSSWIND)

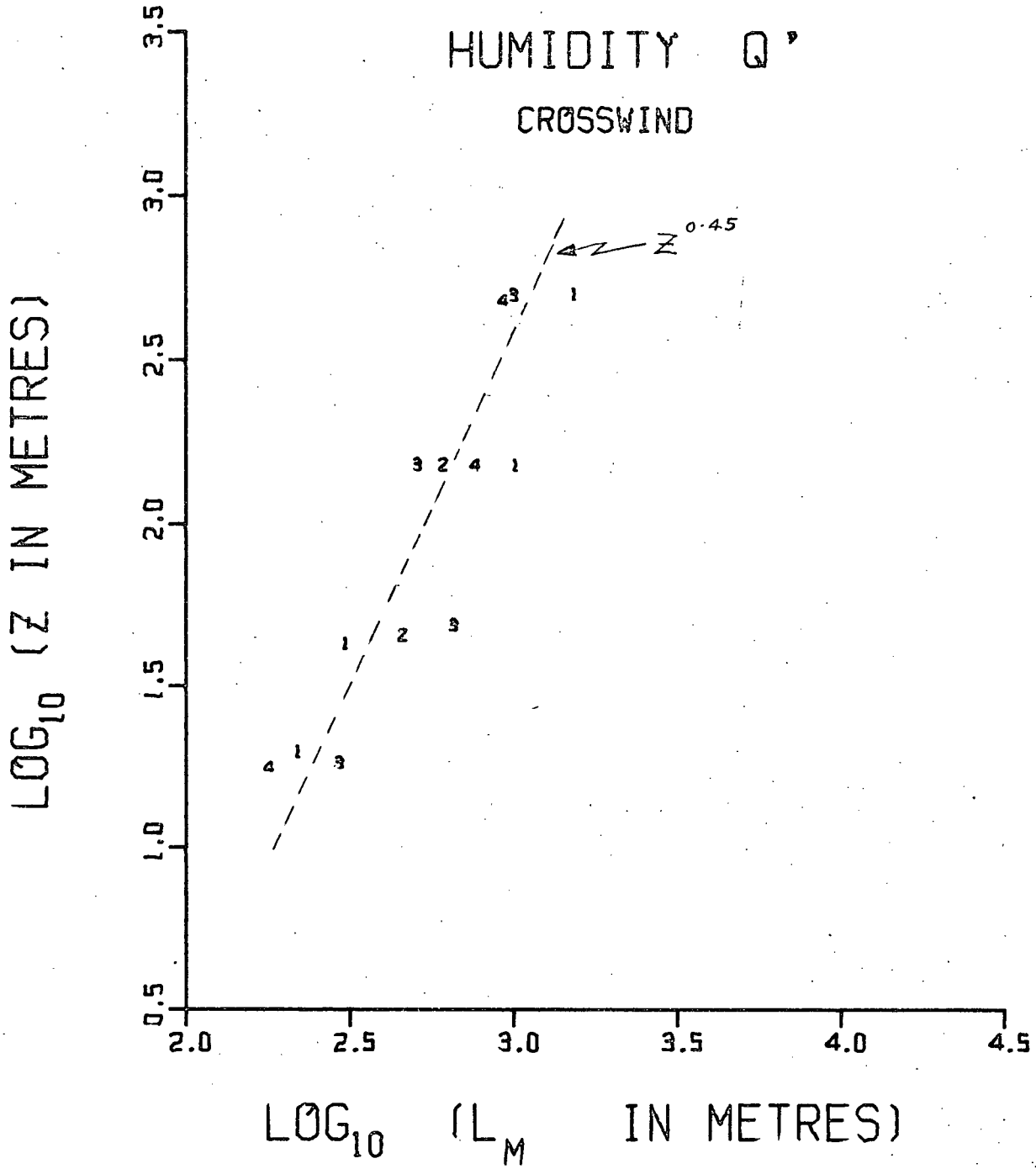

FIGURE 43. $(L_M)_Q$ VS. Z (CROSSWIND)

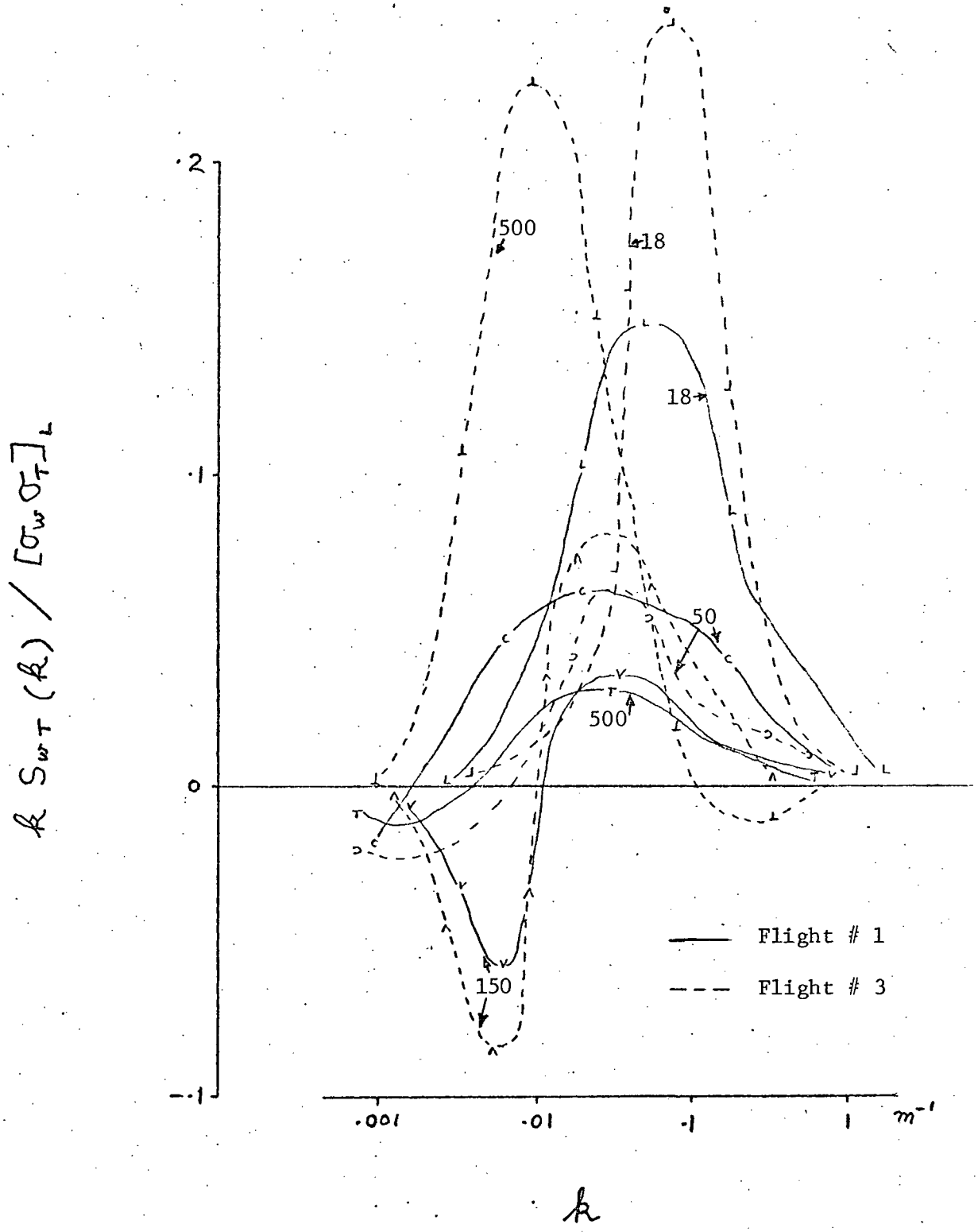

FIGURE 44. HEAT FLUX COSPECTRA (CROSSWIND)

3.3.6 Moisture Flux

The traces of Figures 33 and 45 are quite similar in general character, except that the bursts of positive moisture flux have sharper sides in the crosswind sample. The same pattern was noticed in the vertical velocity traces (Figures 9 and 38), and it is not difficult to see that the effect of a mechanism tending to align convective cells in one direction, while imposing no restrictions on their spacings in the other, would be to sharpen the transition from updraft to downdraft across the alignment direction.

A comparison of Figures 35 and 46 reveals that the wave length of the peak of $kS_{wQ}(k)$ is considerably more height dependent in the measurements across the wind (Figure 46) than in those obtained from traverses in the wind direction (Figure 35). The line drawn on Figure 46, as a convenient representation of the behaviour of L_M versus height, can be expressed as:

$$L_M \doteqdot 80 \ (Z/10)^{0.7} \text{ metres}$$

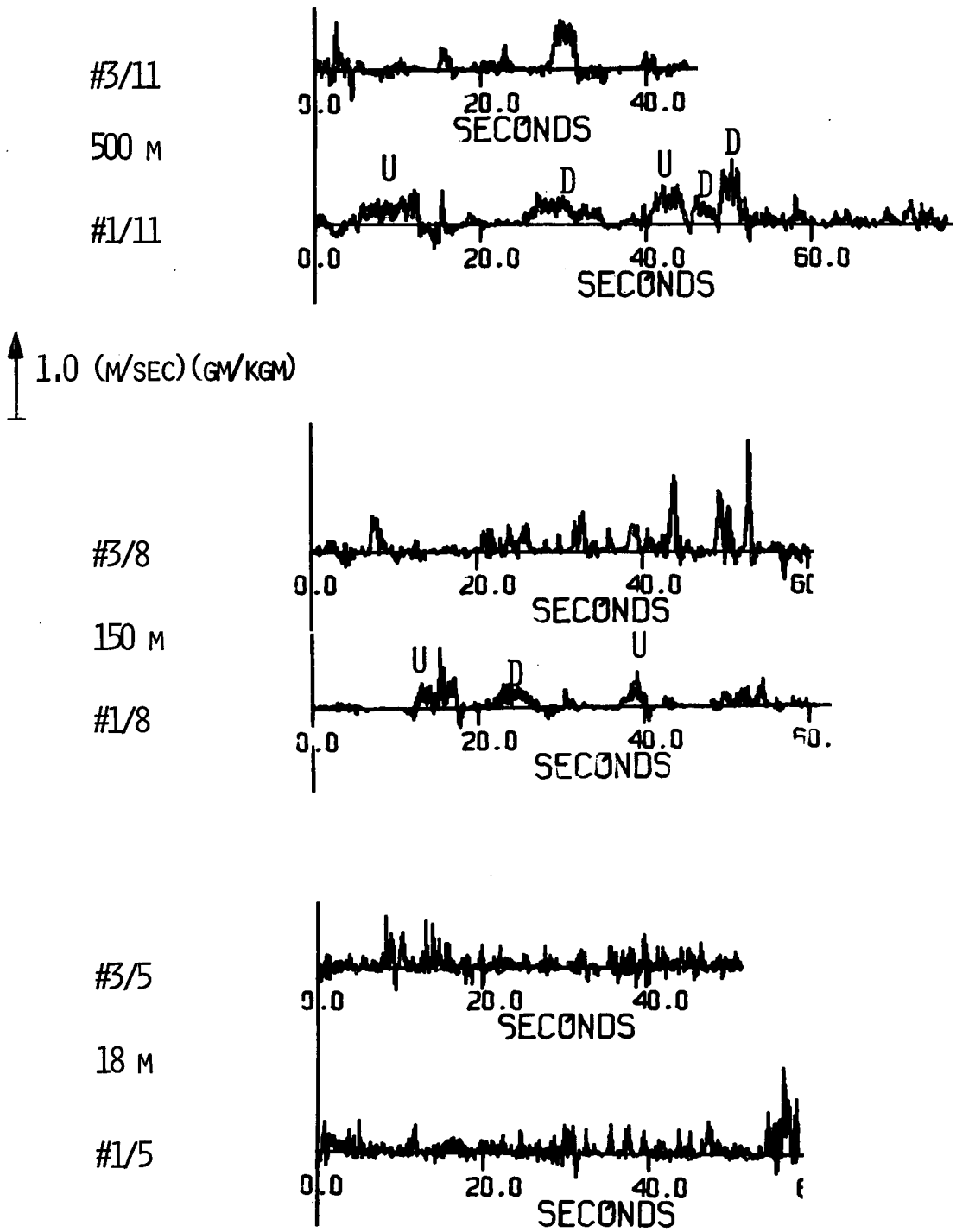

FIGURE 45. MOISTURE FLUX TRACES (CROSSWIND)

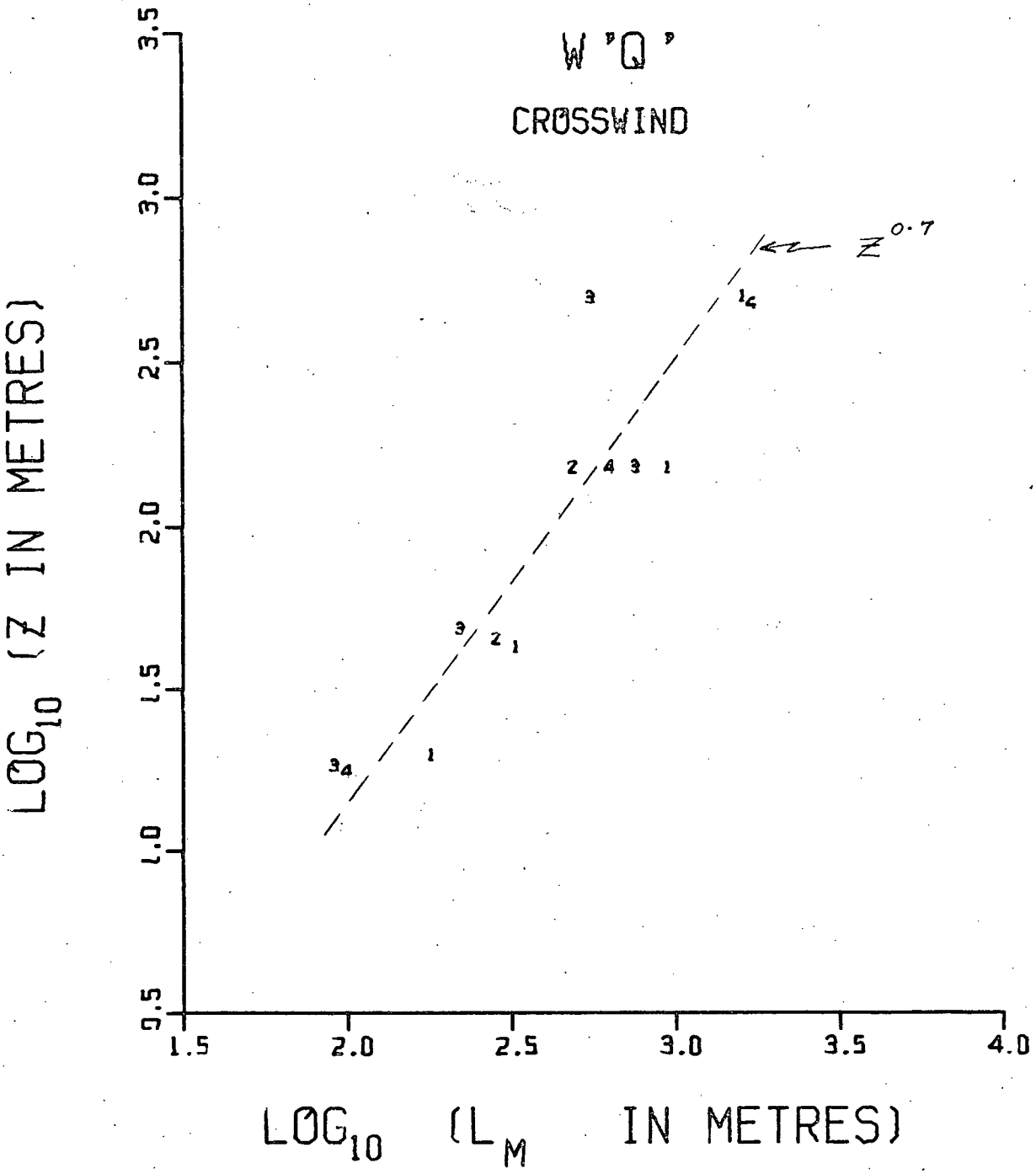

FIGURE 46. $(L_M)_{wQ}$ VS. Z (CROSSWIND)

3.4 The Turbulent Kinetic Energy Budget

3.4.1 Introduction

The turbulent kinetic energy budget of horizontally homogeneous turbulence with a mean wind shear in the vertical (from Lumley and Panofsky, 1964, p. 120) modified for the effect of moist convection can be given by:

$$\frac{\partial e}{\partial t} + \epsilon = - \overline{u'w'} \frac{\partial \bar{u}}{\partial Z} - \overline{v'w'} \frac{\partial \bar{v}}{\partial Z} + (g/\bar{T}) \overline{w'T'}$$

$$+ 0.61\ g\ \overline{w'Q'} - \frac{\partial \overline{w'e}}{\partial Z} - \frac{1}{\rho} \frac{\partial \overline{w'p'}}{\partial Z} \qquad (3.4.1)$$

The measurements made during this experiment do not provide estimates of every term in the kinetic energy budget. Some of the terms are measured directly; others are inferred from the data coupled with certain previously obtained relations; yet others, which are generally believed to be small, are ignored.

The second term on the left hand side of Equation 3.4.1 is the rate of dissipation of the kinetic energy ϵ . It is estimated from the spectral density of the longitudinal velocity component at high wave numbers as discussed in Section 3.2.2.

Since the mean wind gradient cannot be accurately determined from the aircraft's Doppler radar measurements, the first two terms on the right hand side of 3.4.1 are not directly accessible. The second of these $- \overline{v'w'} \frac{\partial \bar{v}}{\partial Z}$ is neglected on the grounds that at low levels where there may be an appreciable wind gradient $\overline{v'w'}$ is negligible. The first production term $- \overline{u'w'} \frac{\partial \bar{u}}{\partial Z}$ is estimated by u_*^3/kZ, a relation which, strictly speaking, is only valid under neutral conditions.

The term $(g/\bar{T})\ \overline{w'T'}$ is the buoyant production due to the sensible heat

flux, while 0.61 g $\overline{w'Q'}$ is the moisture flux's contribution to the buoyant production. Both of these are directly measured.

The term $-\frac{1}{\rho}\frac{\partial \overline{w'p'}}{\partial Z}$ has recently been carefully measured over water (Elliott, 1970) and found to be about 10% of the shear production term at levels between 1 m and 4 m. Elliott also measured the energy divergence term $+\frac{\partial \overline{w'e}}{\partial Z}$. His results indicate that at those levels the divergence and pressure terms have about the same magnitudes and opposite signs. At the levels being considered here it is probable that these terms are more important either jointly or singly. However, as the aircraft measurements cannot provide any direct estimate of them it is convenient to treat them, together with any other terms omitted through the initial assumptions, as a collective residual term, D.

At some distance from land with a steady wind blowing over effectively infinite fetch, if the turbulent field is reasonably horizontally homogeneous, the local rate of change of energy may be neglected. Generally under these conditions it is two orders of magnitude less than the production and dissipation terms (Lumley and Panofsky, 1964).

In this section the turbulent kinetic energy budget is investigated in two ways: 1) The height dependence of each term for all the flights analysed (Section 3.4.2); 2) The budget for flights 1 and 3 taken separately (Section 3.4.3).

3.4.2 Height dependence of terms in Kinetic Energy Budget

3.4.2.1 Mechanical production estimated by $\frac{u_*^3}{\kappa z}$

Figure 47 illustrates the rapid decrease of shear production with increasing altitude. This arises from two factors: the measured stress (Section 3.2.5) decreases with height; and the wind gradient, inferred from the ratio of friction velocity to altitude, rapidly decreases. Evidently the importance of mechanical production is restricted to the first 100 metres only. The various terms of equation (3.4.1) are tabulated in Appendix D.

3.4.2.2 Buoyancy Production $(g/\bar{T})\ \overline{w'T'}$ and $0.61\ g\ \overline{w'Q'}$

The buoyancy production terms are summarized for all the flights in Figures 32 and 37, in which the third scale on the abscissa is in kinematic units of energy production $(cm^2\ sec^{-3})$.

At the lowest level these terms are, in most cases, an order of magnitude smaller than the shear production term, but while the latter decreases rapidly with height the buoyancy production terms change little. Thus at higher levels (above 100 m) most of the kinetic energy is produced by the action of buoyancy. At intermediate and higher levels the overall heat flux may be negative, but in these cases the buoyancy production due to the moisture flux exceeds the negative contribution due to the heat flux. Thus the total buoyancy production was everywhere positive between 18 m and 500 m during this experiment.

3.4.2.3 Dissipation

Figure 48 illustrates the dependence of the rate of dissipation on height. Apparently the rate of decrease of ϵ is very much more rapid at low levels than at the higher levels. Figure 48 also indicates that the reduction of ϵ between the 18 m level and the 50 m level is less pronounced in the 'low' wind speed flights than it is in the others. This behaviour at

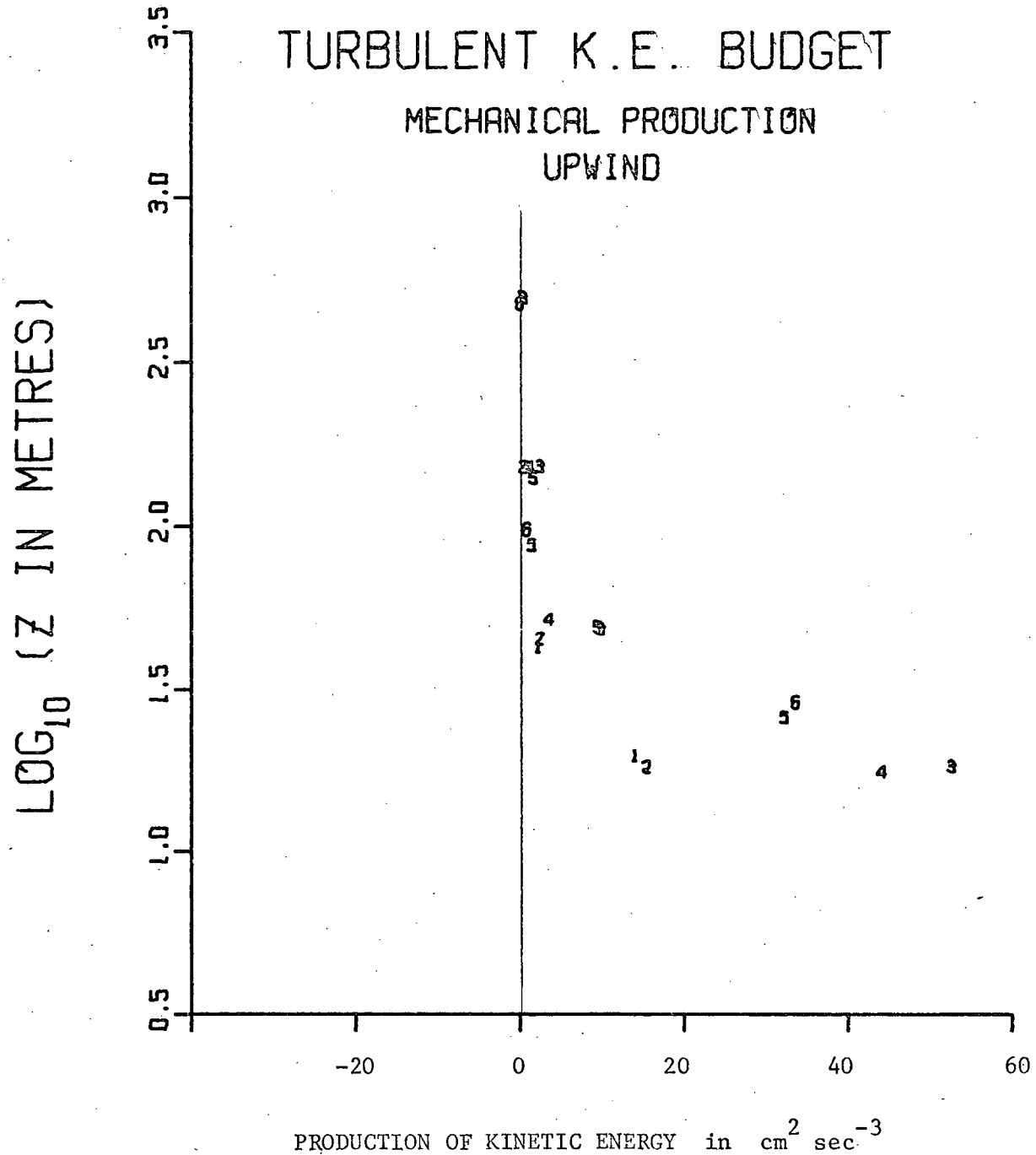

FIGURE 47. MECHANICAL PRODUCTION VS. Z

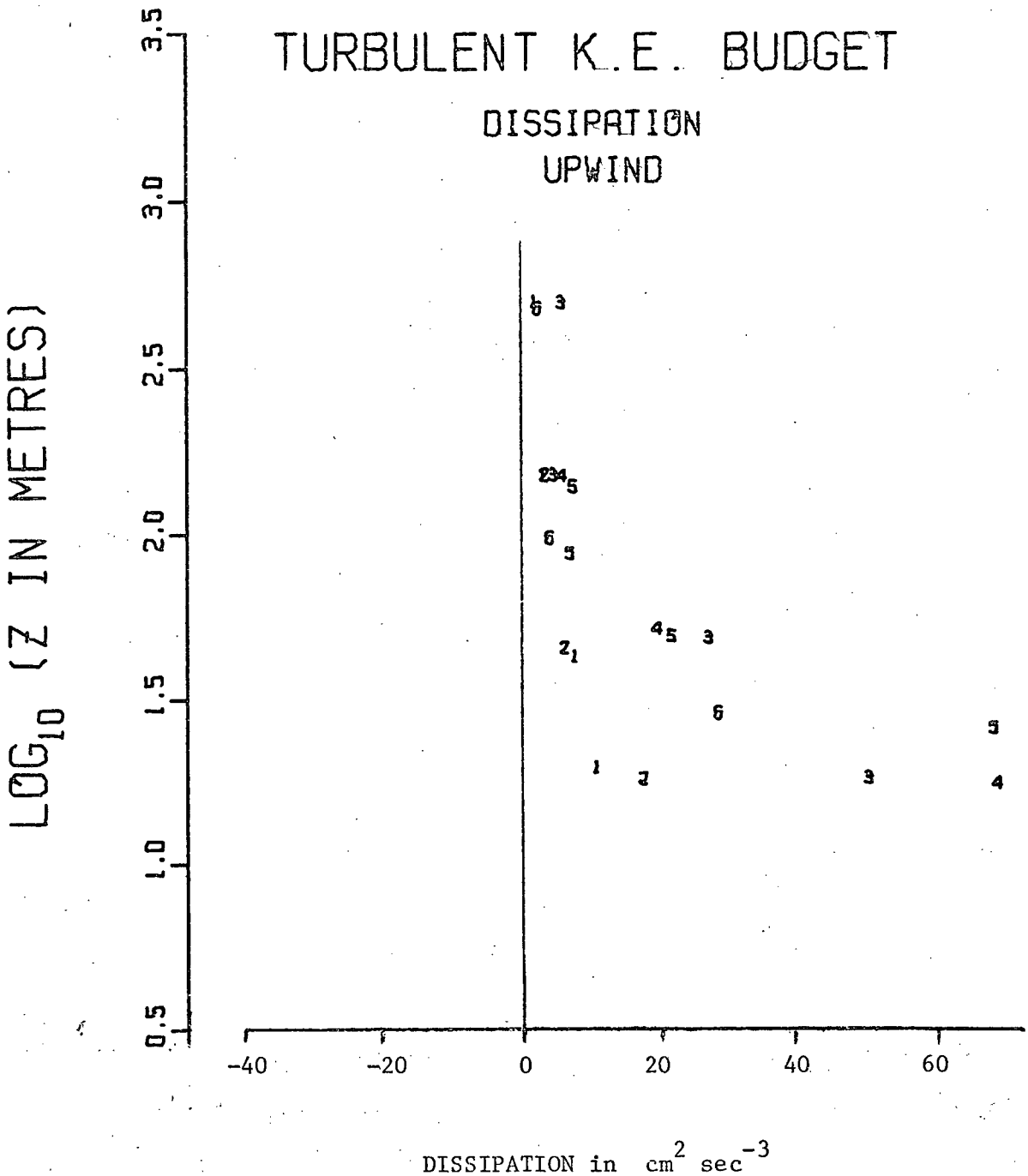

FIGURE 48. DISSIPATION VS. Z

low levels reflects that of the shear production term (Figure 47); i.e. where kinetic energy is being produced by shear turbulence it is also being dissipated. The question of whether or not all the shear produced energy is dissipated locally will be approached through the magnitude and height dependence of the residual term D.

3.4.2.4 The residual term: $D = -\frac{\partial}{\partial Z}\left(\overline{w'e} + 1/\rho\ \overline{w'p'}\right)$

There is some conceptual difficulty in discussing this term without knowing whether it is dominated by the divergence of energy ($+\frac{\partial\ \overline{w'e}}{\partial\ Z}$) or by the working of the pressure forces. It is evident however (Figure 49) that it is considerably larger at low levels than at high, and it is generally positive below the 150 m level. This means either that energy is being exported upwards to be dissipated at levels above the layer of intense shear production or that the rate of working of the pressure forces decreases rapidly with height. In any case it appears that shear production is not balanced locally by viscous dissipation.

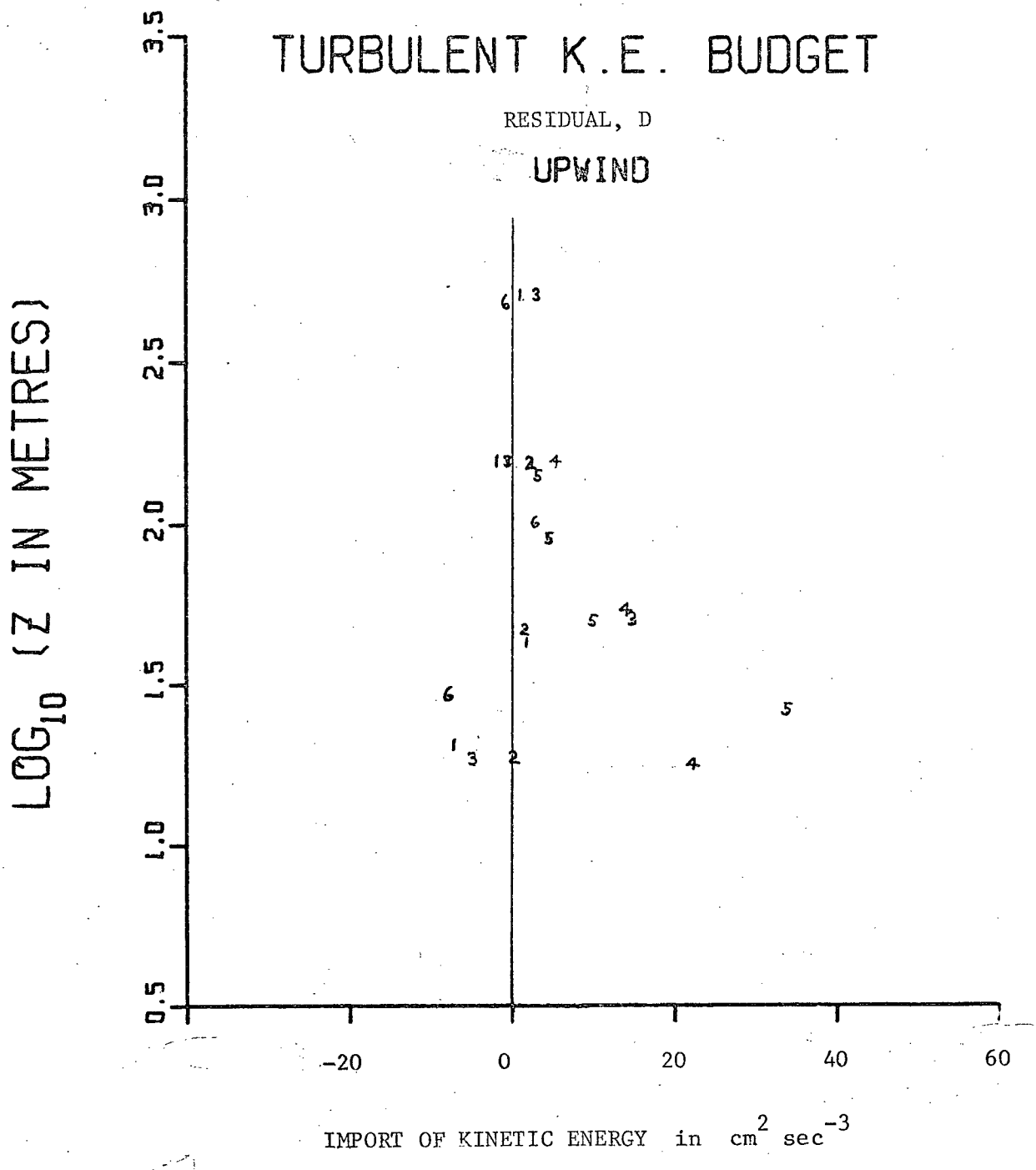

FIGURE 49. DIVERGENCE VS. Z

3.4.3 The budget for flights 1 and 3

The five terms discussed in the previous section are plotted versus height in Figure 50 (flight # 1) and Figure 51 (flight # 3). The height dependence of the separate terms having just been treated at some length, the relevance of these figures lies in their illustration of the relative importance of the five terms for a particular flight. At low levels the balance is essentially between shear production dissipation and the residual term; at higher levels the shear production term is negligible and the four other terms are comparable in magnitude.

It seems then that the surface layer shear generated turbulence is not completely dissipated locally, but some of it is exported to higher levels and dissipated with reduced intensity until, at about 200 m in these data, the process is virtually complete. If the value of the Kolmogoroff constant is 0.55 rather than the value used ($K = 0.48$), then the dissipation estimates obtained here are 18% too large. A reduction of 18% in ϵ will decrease but not remove the difference between dissipation and shear production.

It appears that the over estimate of the drag coefficient obtained from the estimated dissipation (Section 3.2.2 and Table 4) may be due, in part, to the assumption that energy is produced and dissipated at the same rate.

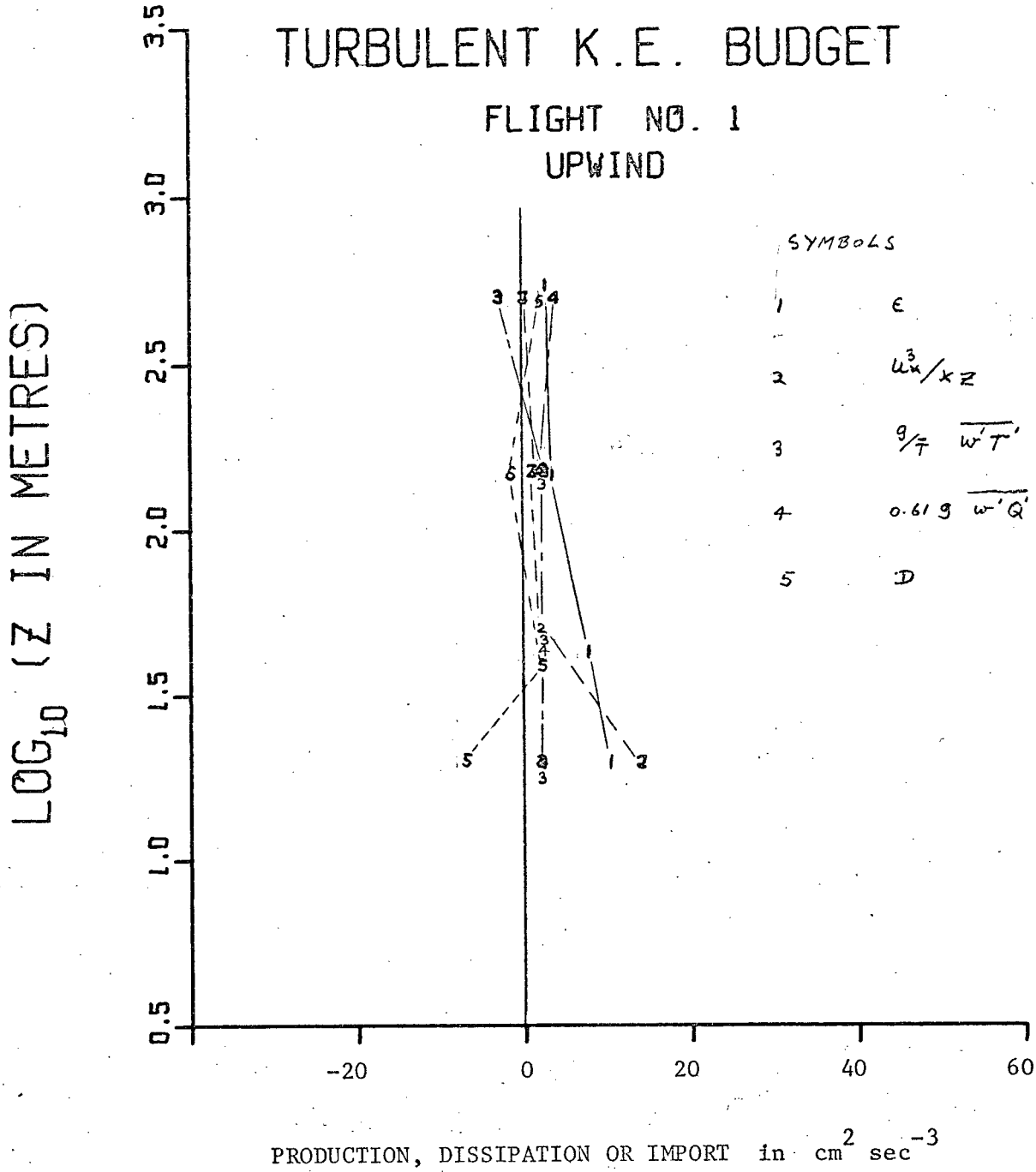

FIGURE 50. KINETIC ENERGY BUDGET FOR FLIGHT # 1

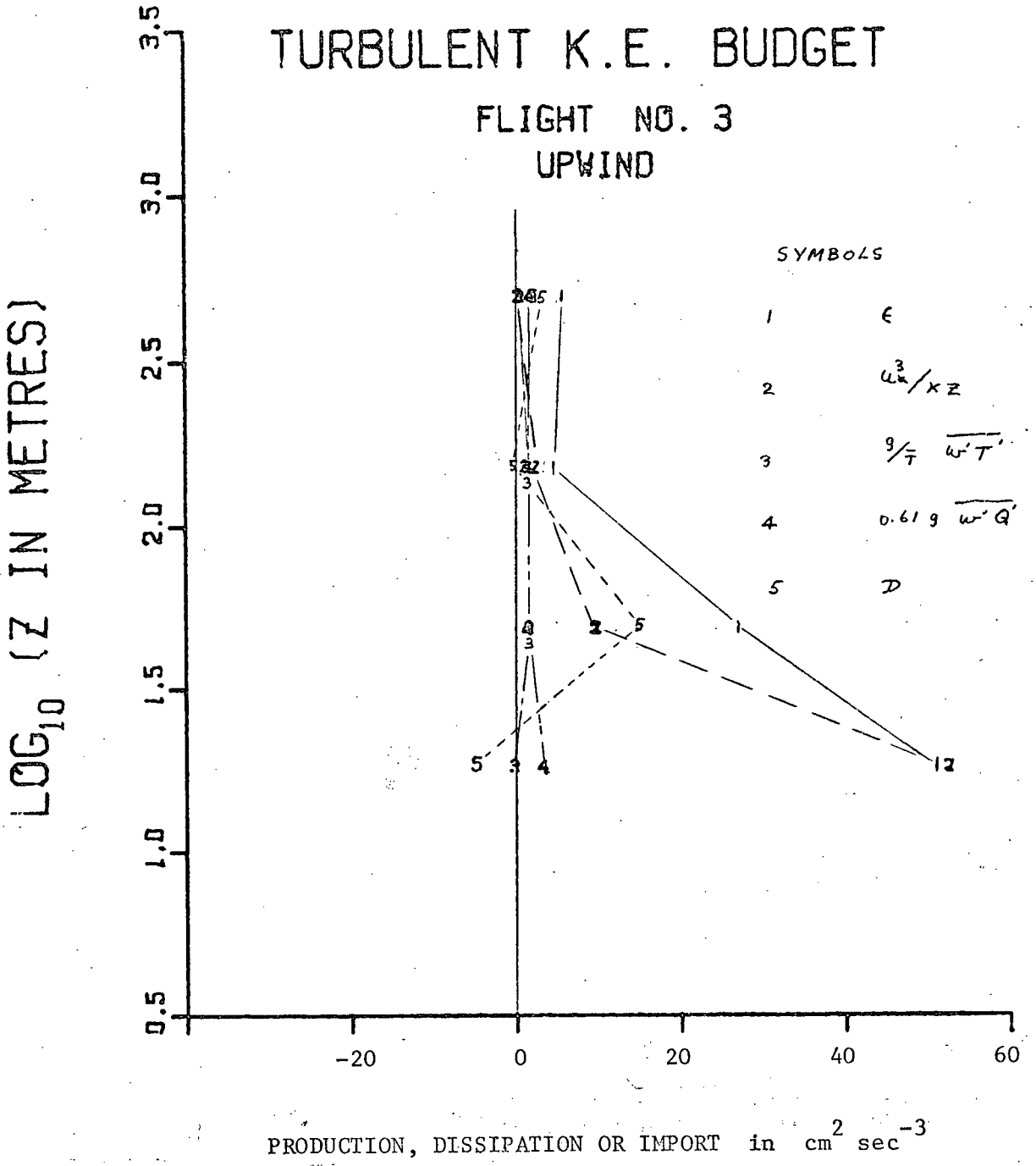

FIGURE 51. KINETIC ENERGY BUDGET FOR FLIGHT # 3

3.5 The Temperature-Humidity Correspondence

One of the most striking aspects of the data presented was the dissimilarity of the cospectral shapes of the fluxes of heat and water-vapour. It may be that the correspondence between fluctuations of temperature and humidity will throw some light on the matter.

The instantaneous product of the fluctuations of temperature and humidity is displayed in Figures 52 and 53. From an energetic and positive (at all but the largest scales) value near the surface, the T'Q' product decreases to a small and intermittent value at intermediate levels. When it reappears strongly again it does so at relative large scale sizes, and it may be either positive or negative. It is of interest, here, to examine the sign of the correlation in the different areas depicted in Figures 52 and 53. For this purpose the more pronounced updrafts and downdrafts have been, as before, designated 'U' and 'D'. In general it seems that the updrafts are associated with a positive temperature-humidity correlation r_{TQ}, while the correlation is usually negative in the downdrafts.

The time series of Figure 52 and the correlation coefficients r_{TQ} of Figure 54 are very similar to the corresponding W'T' time series (Figure 30) and correlation coefficients (Figure 31). In Figure 54 it is seen that temperature and humidity are positively correlated at the small scale sizes and negatively correlated at the large scale sizes. This observation is consistent with the observation that the updrafts carry a positive value of r_{TQ} and the downdrafts, a negative value; i.e. the updrafts, containing air from close to the surface, are well endowed with the small scale fluctuations generated by shear turbulence; the downdrafts, on the other hand, consist of air whose velocity fluctuations are characteristic of the larger scales associated with buoyancy. Flights 1 and 3 (Figure 54) show no definite height

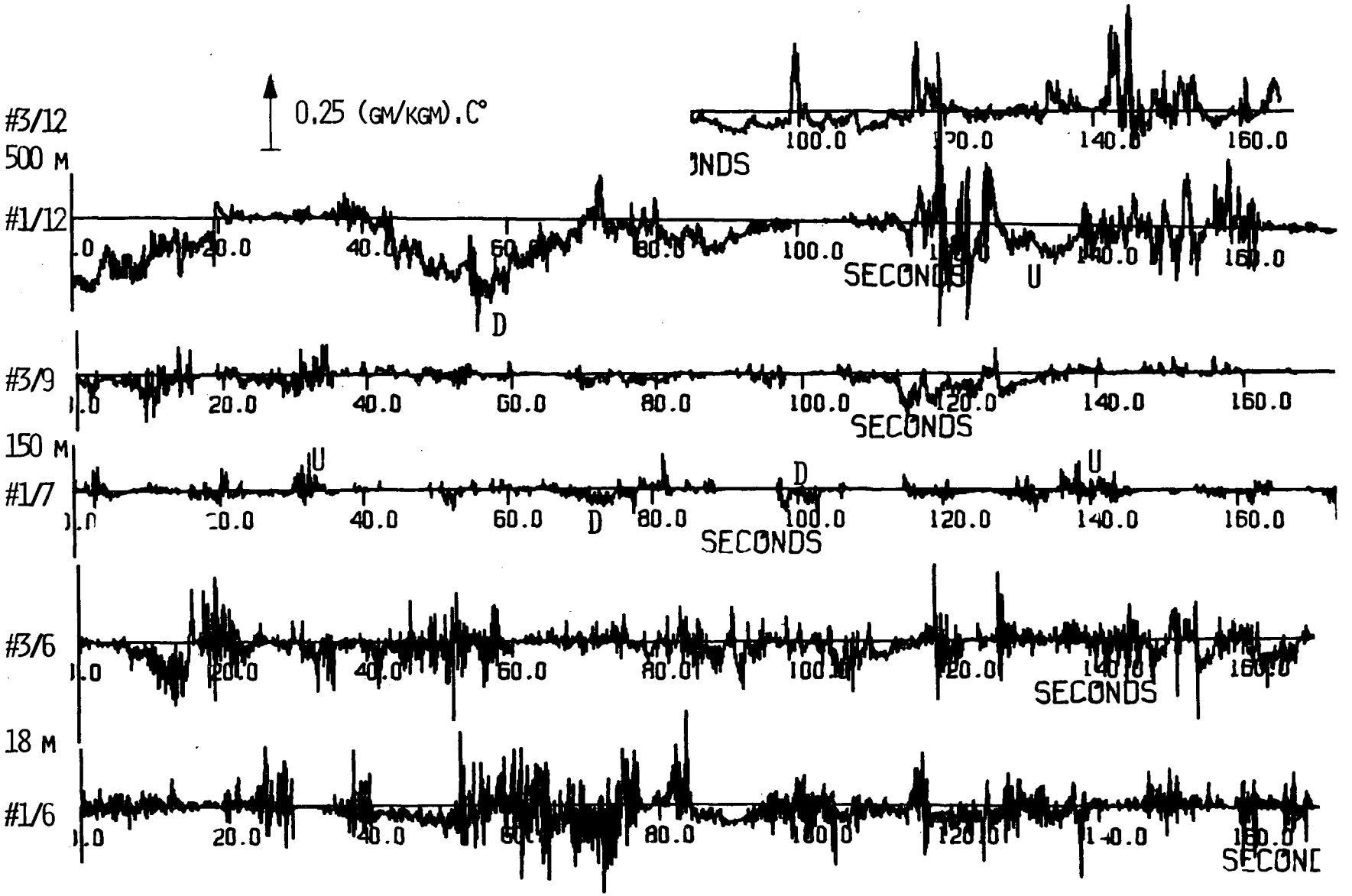

FIGURE 52. T'Q' (t) (UPWIND)

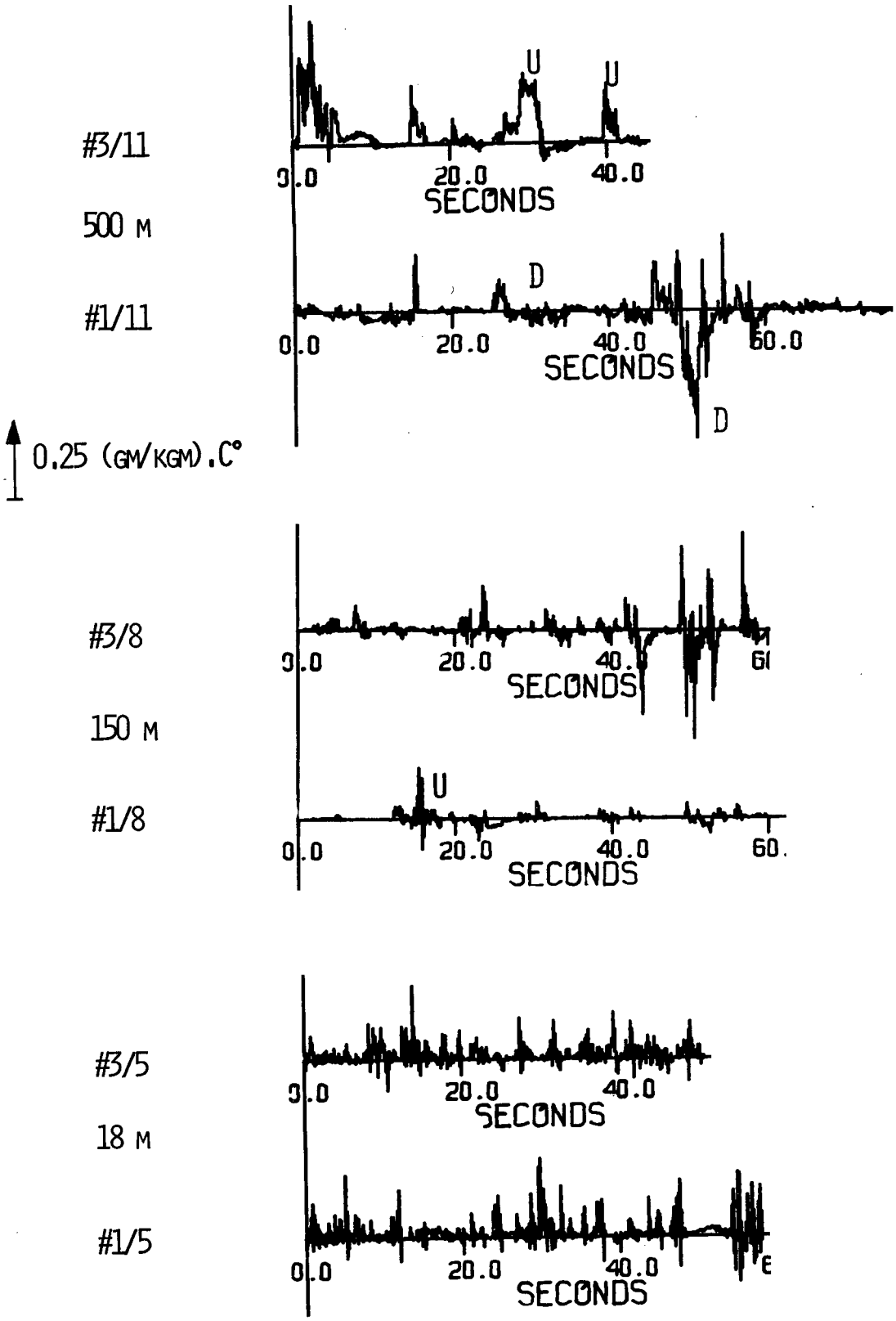

FIGURE 53. T'Q' (t) (CROSSWIND)

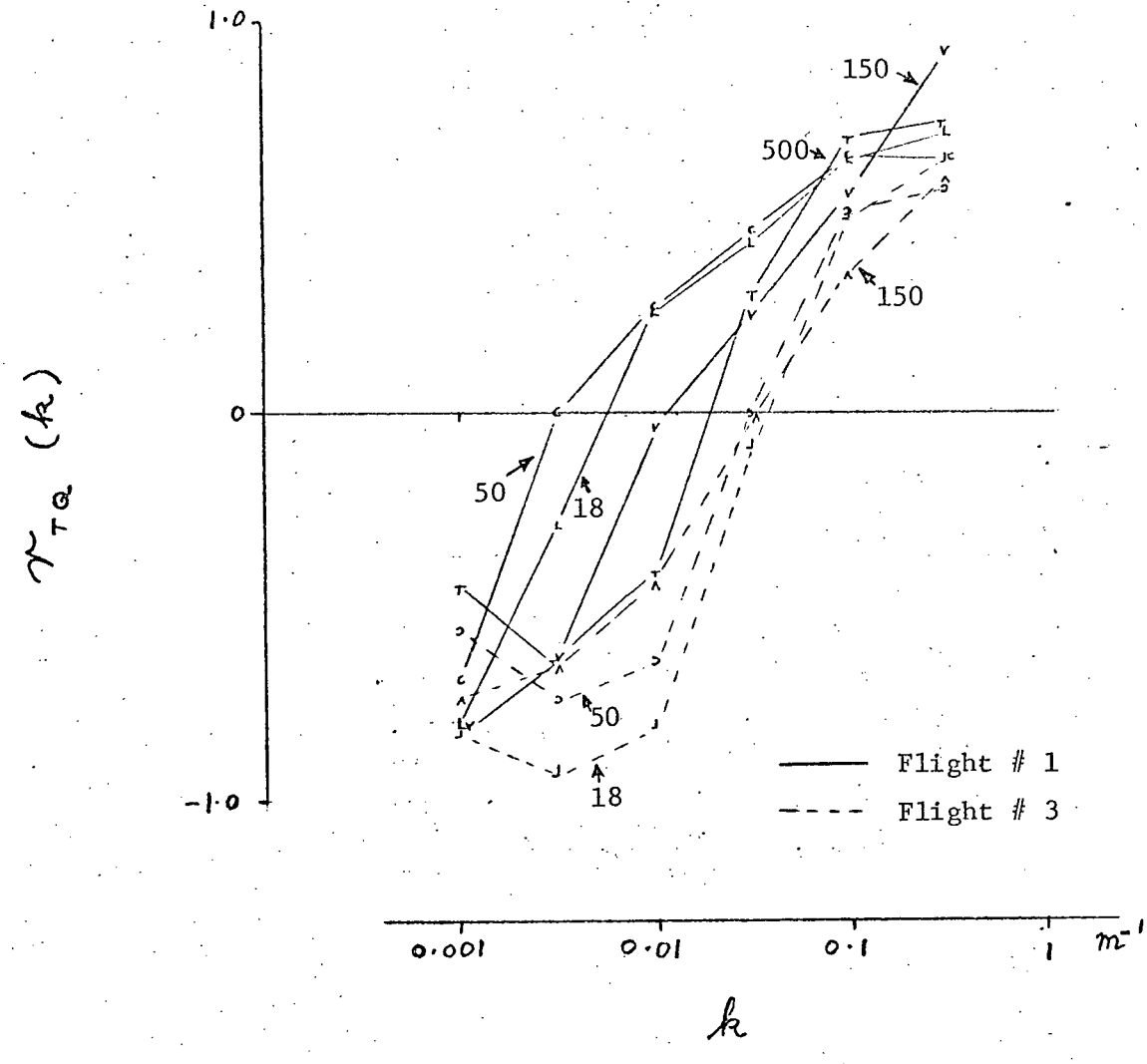

FIGURE 54. $r_{TQ}(k)$ (UPWIND)

dependence of the wave length L_+ associated with the change of sign of $r_{TQ}(k)$ from negative to positive values. Whereas the corresponding L_+ values from crosswind traverses (Figure 55) indicate that L_+ decreases with increasing altitude. To clarify this point the values of L_+ for all the flights are plotted versus height in Figure 56 (upwind) and Figure 57 (crosswind). In the upwind case L_+ shows no definite height dependence (the value indicated by 'F' was obtained from Flip during flight 4). The crosswind case, on the other hand, behaves in the same way above 150 m but is both altitude and wind speed dependent below that height. In general the low wind speed case is the more height dependent; in both cases L_+ decreases with height.

Temperature profiles obtained from Flip showed that the near surface layer was unstable with regard to the temperature gradient; and the humidity gradient is, of course, negative. Therefore blobs of rising air near the surface are warmer and moister than their surroundings. At higher levels (500 m) the time domain traces clearly reveal a large scale negative temperature-humidity correlation, which, as we have seen, is due to descending air which is relatively warm (r_{WT} is negative, Figure 31) and dry (r_{WQ} is positive, Figure 34). As the warm, dry air descends it mixes with ascending warm moist air. Somewhere between the surface and 500 m this mixing process is most complete and the instantaneous T'Q' product is a minimum (see the 150 m level in Figures 52 and 53). There is no corresponding minimum in the correlation coefficient $r_{TQ}(k)$ at the 150 m level. This implies that the amplitudes of the fluctuations of temperature or humidity or both are smallest at this level. Such minima in $\sigma_T(Z)$ and $\sigma_Q(Z)$ have already been noticed (Sections 3.2.3 and 3.2.4) but, due to the paucity of data points at the 500 m level, the evidence was not overwhelming. The product of temperature and humidity is, of course, doubly sensitive to such

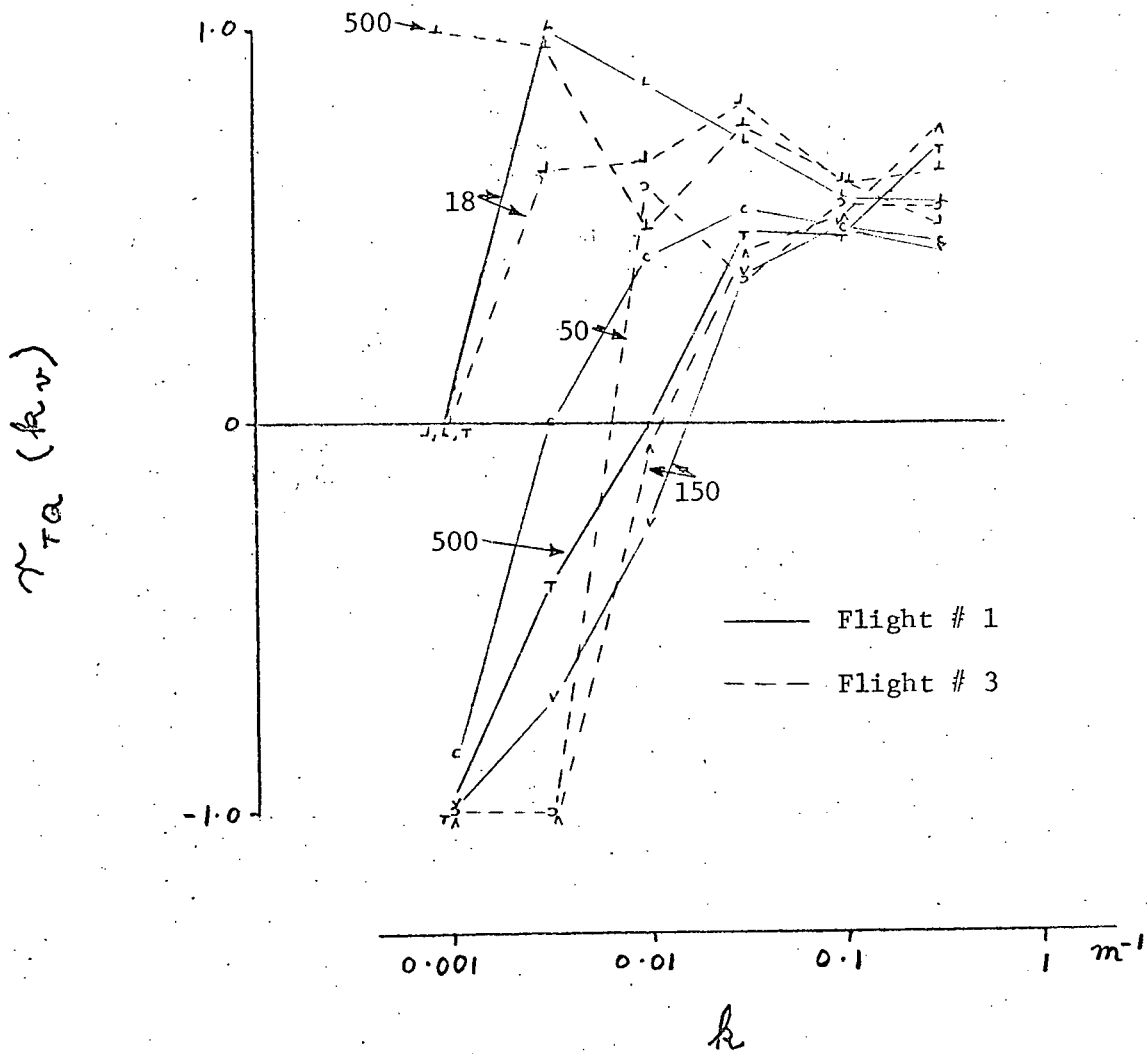

FIGURE 55. $r_{TQ}(k_v)$ (CROSSWIND)

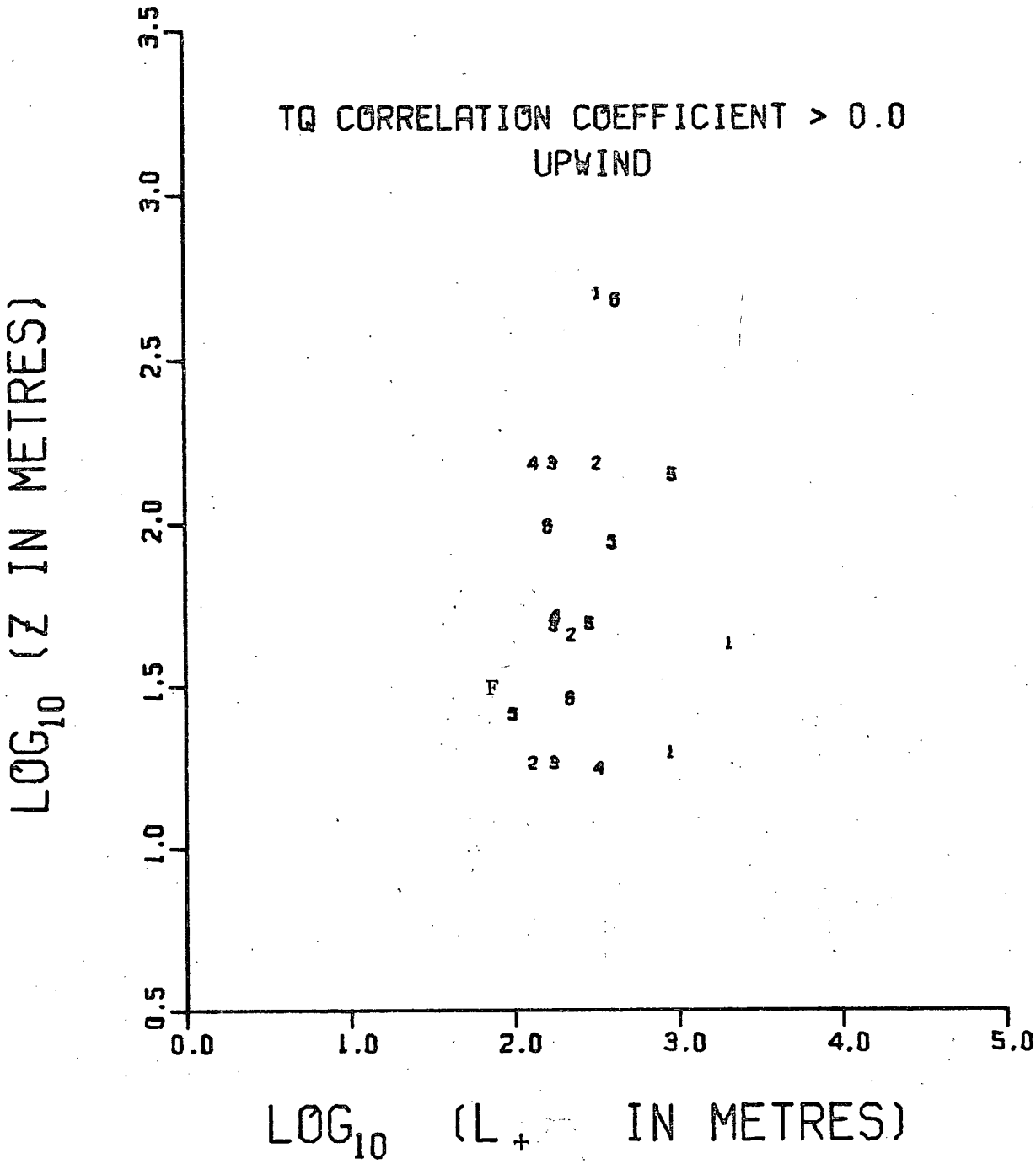

FIGURE 56. $(L_+)_{TQ}$ VS. Z (UPWIND)

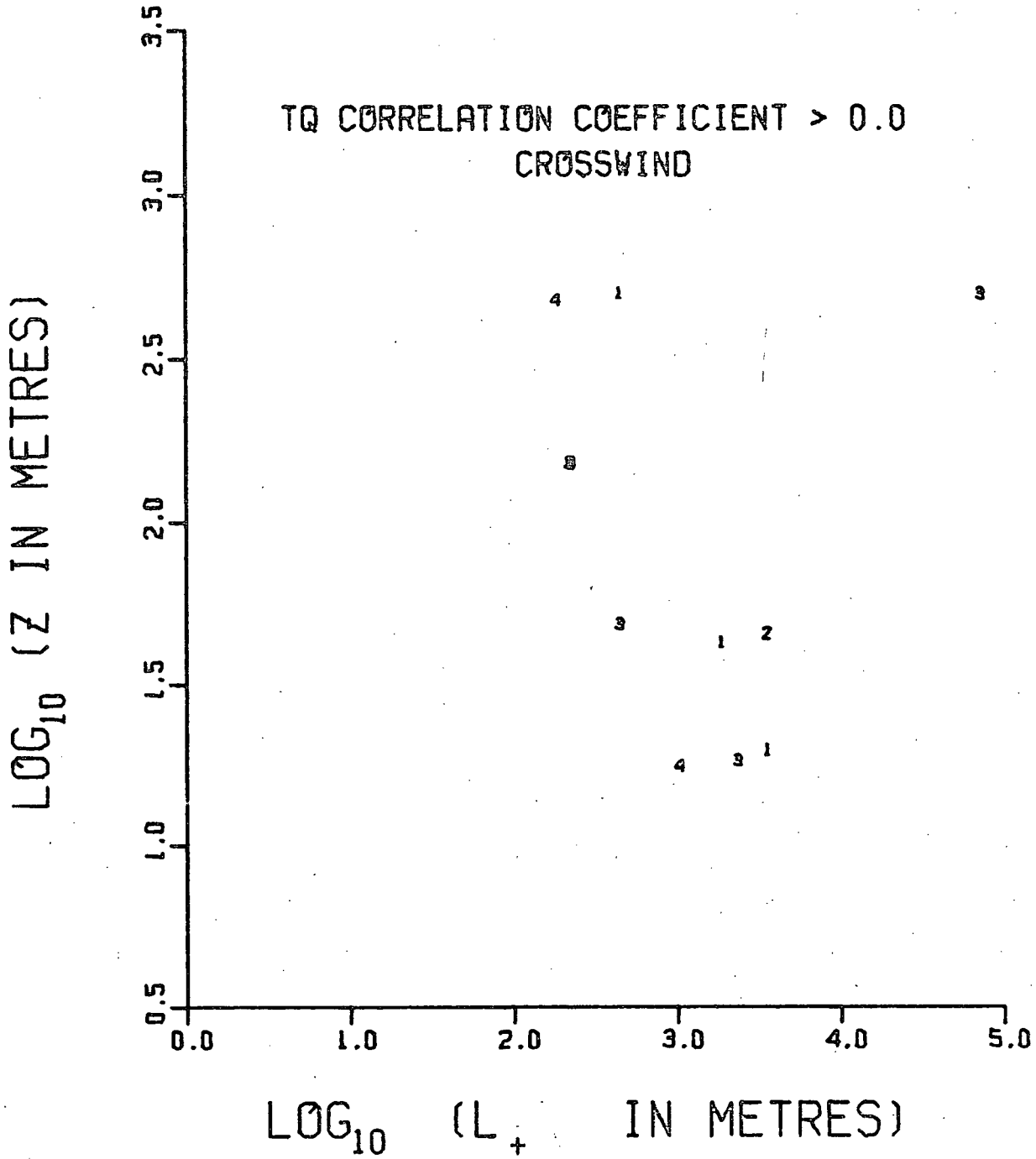

FIGURE 57. $(L_+)_{TQ}$ VS. Z (CROSSWIND)

minima in the amplitudes of the fluctuations of both T' and Q'; the traces of Figures 52 and 53 exhibit this clearly (see also Figure 58).

The minimum in the amplitude of the T'Q' product but not in the value of $r_{TQ}(k)$ at the 150 m level suggests that, during the mixing process, parcels of air retain their moisture and temperature signatures. This, of course, is the expected result, since the opposite result would imply that the molecular diffusivity of either water-vapour or heat is comparable to its eddy diffusivity.

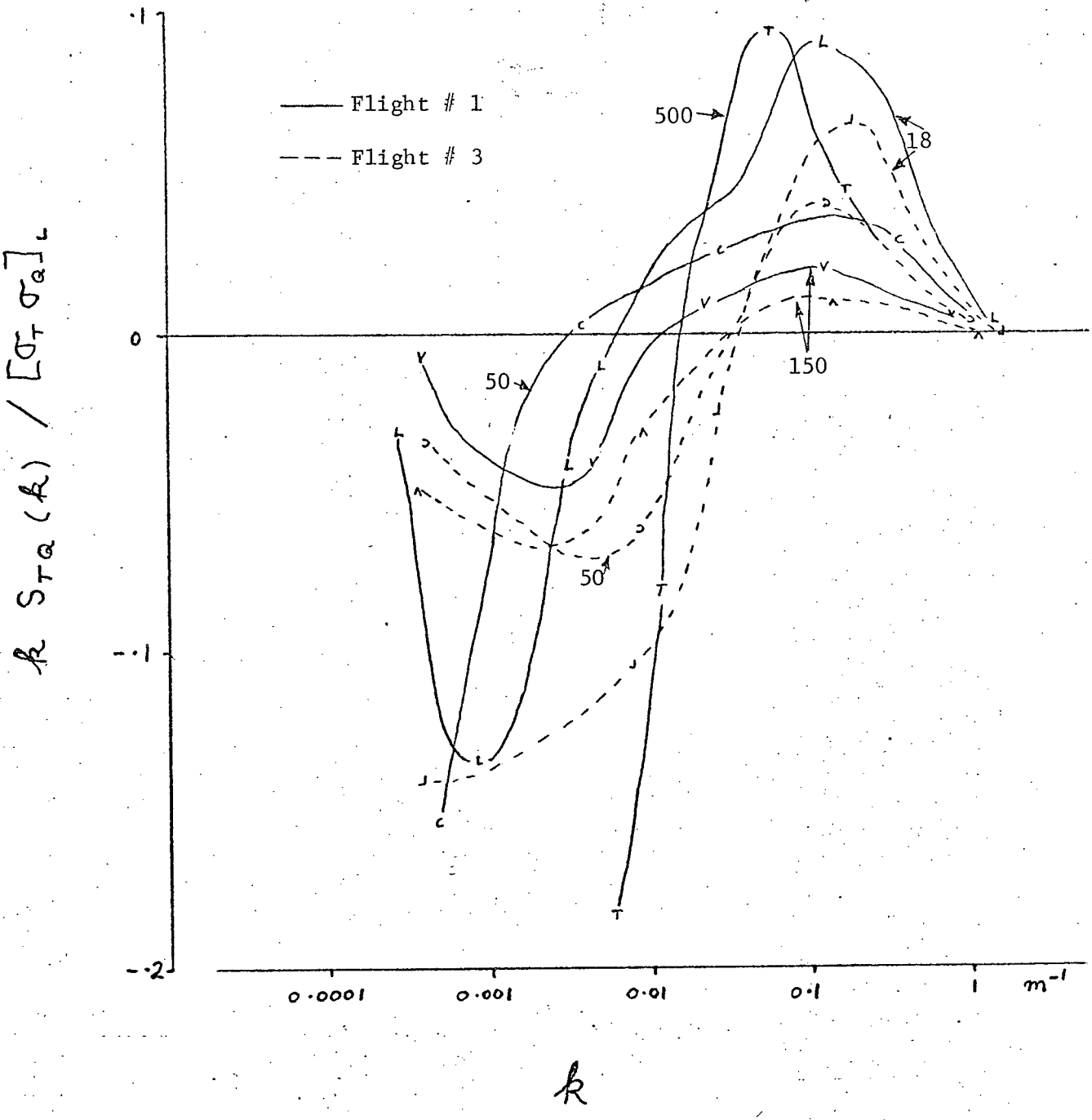

FIGURE 58. CROSS-SPECTRA OF T' AND Q' (UPWIND)

3.6 Discussion of a possible pattern of convective organization

In the last section it was shown that a number of curious results, such as the minima of $\sigma_T(Z)$ and $\sigma_Q(Z)$, were clarified somewhat by an examination of the temperature-humidity correspondence. However some of the results of the measurements along the wind (Section 3.2) and of the comparison of them with measurements across the wind (Section 3.3) indicated that there were differences between the measurements made in the wind direction and those made in the crosswind direction. This implies that the turbulent field was organized to some degree.

In order to tie together the observations which have no ready explanation a particular pattern of convective organization is suggested. Before describing the pattern it may be useful to summarize the observations discussed before, which pertain directly to the question of convective organization:

a) At every level and in both flight directions the products W'T' and T'Q' are much alike. One particularly important aspect of their behaviour is the occurrence of a large scale negative k-cospectral peak in all cases along the wind, but not in runs at 18 m across the wind.

b) Although the wave length at which r_{TQ} first becomes positive L_+ is insensitive to height along the wind, it is not across the wind, except above 150 m. Across the wind the low wind speed cases are associated with L_+ values larger and more height dependent than the high wind speed cases in such a way that the L_+ values decrease and converge to a common value at and above 150 m.

c) The wave length of the k-spectral peak of humidity fluctuations and the moisture flux display no definite height dependence in the wind direction, but do so across the wind: the wave length of the k-spectral peak of the moisture flux increases with height like that of the vertical velocity, but more

quickly than that of the humidity fluctuations.

If it is assumed that above 500 m, but still some distance beneath cloud base, the air is quite dry and the temperature gradient is very slightly stable (Roll, 1965, p.292), then a warm moistal rising to this level will displace dry air, which descending will be slightly warmer than its surroundings. If it is further supposed that the subsidence is not evenly distributed around the updraft but tends to be more pronounced on its upwind and downwind sides, then, using the estimated updraft dimensions obtained from the traces of vertical velocity (Section 3.3.2), a possible pattern of convective organization emerges. Figure 59 depicts this pattern by means of isotachs of vertical velocity. The directions of the large scale fluxes of sensible heat and moisture are indicated in the updrafts and subsidence zones, as is the sign of temperature-humidity correlation at large scales.

In the along wind subsidence areas the downdrafts are strong enough to impress on the fully turbulent region below the negative temperature-humidity correlation; however, in the crosswind subsidence areas the downdrafts are frequently too weak to influence the turbulence much below the convective layer. As a result; along wind runs alternately encounter regions of positive heat and moisture fluxes and r_{TQ} (updrafts) and regions of positive moisture flux and negative heat flux and r_{TQ} (downdrafts). The crosswind runs, on the other hand, show basically the same pattern in the convective layer, but often fail to encounter regions of negative heat flux and r_{TQ} in the turbulent layer.

In the wind direction the fact that the wave length of sign change of r_{TQ} is invariant suggests that the descending warm, dry air always succeeds in seeping down into the turbulent surface layer. Whereas in the crosswind direction the success of the weaker downdrafts in affecting the turbulent

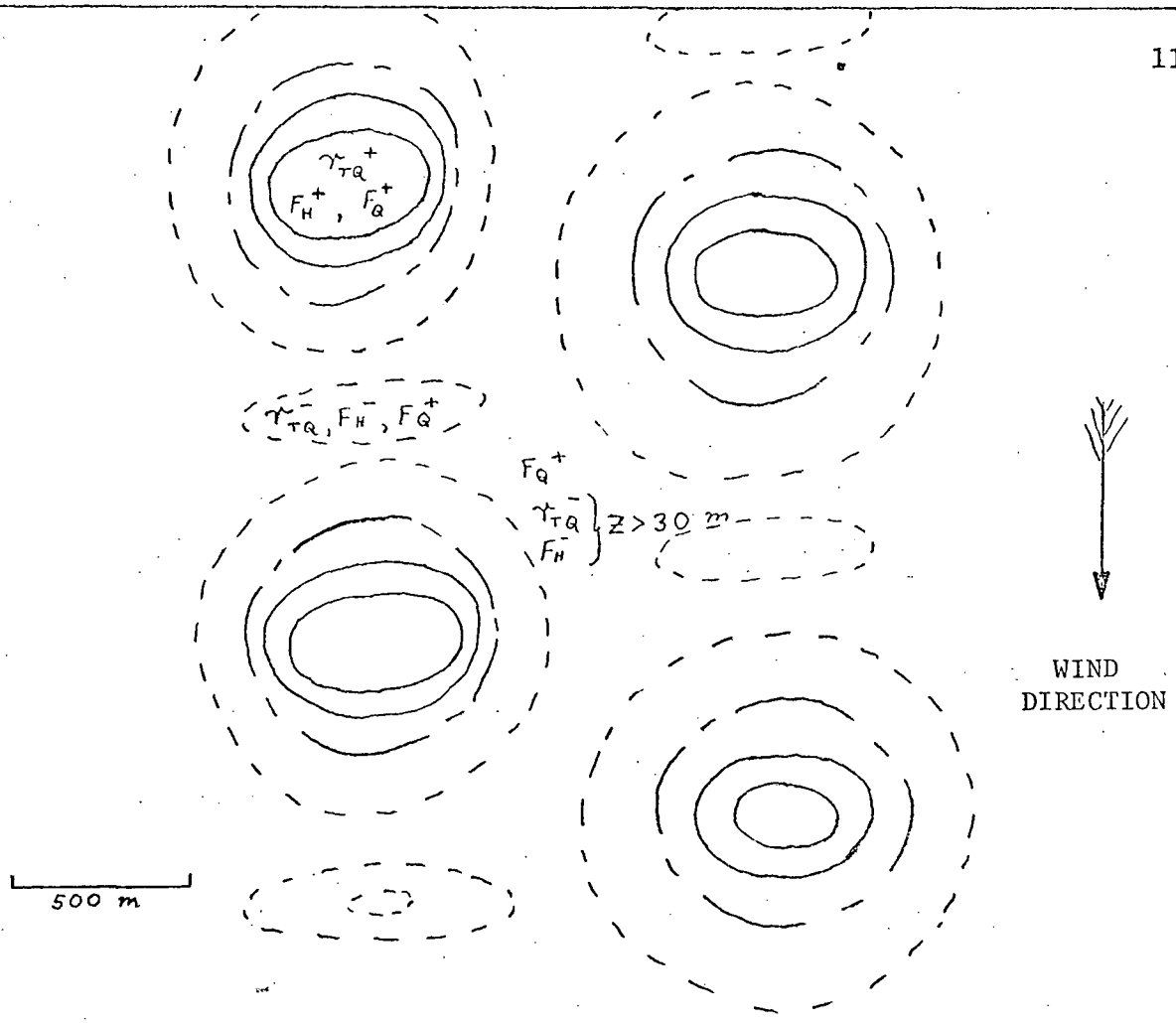

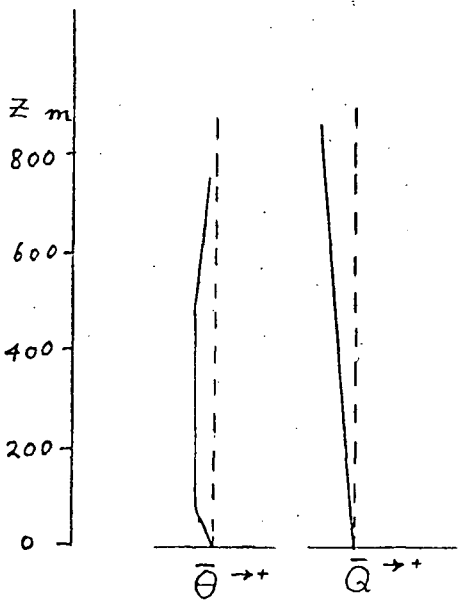

ISOTACHS - ARBITRARY UNITS

- ---- w < 0
- — - — w = 0
- ——— w > 0

Plan view of suggested convective field; showing isotachs of large scale vertical velocity and the sign of the correlations of w with T and with Q and of T with Q. The profiles of potential temperature and specific humidity are also shown.

FIGURE 59. A POSSIBLE PATTERN OF CONVECTIVE ORGANIZATION

layer is less frequent, and, of course, the fewer the penetrations the longer the measured wave length of r_{TQ} sign change. Thus, from Figure 57, it may be tentatively concluded that increasing the wind speed increases the effectiveness of the downdrafts in impressing a negative r_{TQ} value on the turbulent layer. Although this is a paradoxical result, as increased turbulence would be expected to reduce the effects of convection on the turbulence, it can be explained in terms of the observed increase of organization of the convection with wind speed (e.g. Woodcock, 1942).

The height dependence of the wave length of the k-spectral peak of the humidity fluctuations and the moisture flux is quite pronounced across the wind but not in the wind direction. This can be attributed to the relative intensity of the moisture fluxes in the various downdrafts; i.e. in the downdrafts between successive updrafts along the wind the moisture flux is as strong as it is in the updrafts, whereas in the downdrafts separating updrafts across the wind direction it is not. Thus, in runs along the wind, the k-cospectrum of moisture flux and the humidity k-spectrum are quite flat, making the determination of a peak wave length rather uncertain. Whereas the weaker flux encountered in crosswind downdrafts serves to reduce the spectral values at large scales and hence produce a k-spectral peak whose wave length is related to the size and spacing of the large updrafts.

The convective pattern postulated above was used to explain a number of curious features of the data presented. It is not suggested this pattern is typical of the trade wind zone or even that it did occur during this experiment; but it is suggested that some similar pattern could have been associated with a turbulent field of the kind described herein.

CHAPTER 4

SUMMARY OF CONCLUSIONS

The purpose of this study was the experimental investigation of the turbulent atmospheric boundary layer in the atlantic trade wind zone.

The data were collected on five consecutive days using a light aircraft which was instrumented to measure the fluctuations of temperature, humidity and two components of air velocity; the vertical component and the component in the direction of the aircraft's velocity relative to the air. During each of the six flights data were collected at several altitudes between 18 m and 500 m. Spectra of and cross-spectra between the fluctuations of the four measured parameters (w', u', T' and Q') were computed. The following is a summary of the results obtained.

The fluxes of momentum, heat and moisture

The fluxes of moisture and momentum have similar single-peaked k-cospectral distributions below 50 m and the most predominant of the scales responsible for the transfers have about the same wave length in both fluxes at all altitudes. These wave lengths seem to show a general increase with height in both cases, but there is a great deal of scatter. The similarity of these fluxes is also evident from the time domain traces of their instantaneous values.

By contrast, the k-cospectra of the sensible heat flux often contain two peaks of opposite sign. The positive peak is at smaller scales than are the peaks of the other fluxes, while the negative peak occurs at

larger scales.

Apparently buoyancy influences the cospectral distribution of the momentum flux, but, although fluctuations of temperature and humidity produce density variations which are comparable, the momentum flux appears to have a greater affinity for the relatively large scales of the humidity variations compared to those of temperature. It is suggested that the momentum flux seeks the 'path of least resistance'; i.e. if the density fluctuations are associated with the scales which transport momentum most efficiently, then the fluxes of mass and momentum will have similar cospectral distributions; otherwise the peak of the k-cospectrum of the momentum flux will be shifted, relative to that of the mass flux, towards the scale sizes which transport momentum most efficiently.

The latent heat flux measured at 18 m was 12 mW/cm^2 on average, while the average sensible heat flux at that level was only 1.0 mW/cm^2, i.e. less than 10% of the total turbulent heat transfer. Both fluxes decreased with height between 18 m and 100 m, but, while the sensible heat flux showed a weak tendency to continue this trend, the moisture flux increased slightly again about 150 m. In some cases the heat flux was zero or even negative (downward flux) above 100 m; whereas the minimum moisture flux, averaged at any level, was about 8 mW/cm^2 (at the 150 m level).

The fluctuations of temperature, humidity and the vertical and longitudinal velocity components

The spectra of temperature, humidity and each of the velocity components invariably displayed a -5/3 slope at high wave numbers. However, consideration

of the available evidence indicated that the flow was not locally isotropic.

The value of the drag coefficient estimated from $nS_{uu}(n)$ was $(2.68 \pm 1.03) \times 10^{-3}$; the limits given are one standard deviation on either side of the mean. This method overestimated the drag coefficient computed by the 'eddy correlation technique' $(1.45 \pm 0.08) \times 10^{-3}$ by about 85%. The drag coefficients given were estimated for 4 runs of mean wind speed between 7 m/sec and 10 m/sec.

There appeared to be no definite height dependence of the variance of vertical velocity; on the other hand, the variance of the longitudinal velocity component showed a general decrease with height, but the ratio of the standard deviation of this component to the friction velocity was more or less independent of height; with some scatter the mean value of this ratio was about 2.3. The variances of the fluctuations of both temperature and humidity decreased by about 40% with height up to about 100 m and increased by roughly the same amount between 100 m and 500 m.

The wave lengths of the scales containing the most energy showed a different height dependence for each parameter; those of the vertical velocity component increased as $Z^{0.75}$ approximately, and there was no essential difference between measurements across and along the wind; those of the horizontal velocity component were not height dependent for either the along wind or the crosswind component; those of the temperature fluctuations increased as $Z^{0.75}$ in the wind direction, but were not consistently height dependent across the wind; those of the fluctuations of humidity were not height dependent along the wind, but increased about as $Z^{.45}$ across the wind.

Throughout the layer between 18 m and 500 m the spectra of the fluctuations of humidity and those of the horizontal velocity component were very similar in shape in the measurements made along the wind. The spectra

of the lateral velocity component contained more low frequency energy than those of the vertical velocity component but less than those of the longitudinal velocity component. The spectra of the temperature fluctuations were unique: at low levels the small scales (those having wave numbers larger than that of the peak of the vertical velocity k-spectrum) contained most of the energy; higher up a low frequency peak appeared and, in general, grew with height, so that at intermediate levels (about 50 m to 150 m) the two peaks were about equal and at the top level (500 m) the low frequency peak was the larger.

The kinetic energy budget

The buoyancy production terms were directly measured; the dissipation was inferred from the spectral energy density in the '-2/3 region' of the k-spectrum of the longitudinal velocity component; shear production was estimated using the measured friction velocity and an assumed logarithmic wind profile; the other terms of the energy budget were lumped together as a 'residual' term.

At the lower levels (18 m and 50 m) the balance was between shear production, dissipation and the residual term; at higher levels the shear production term was negligible and the buoyancy terms were comparable to the dissipation and residual terms.

It was concluded that the kinetic energy generated by the velocity shear near the surface is probably not all dissipated locally.

Convective organization

Measurements made during flights in the wind direction of the fluctuations of temperature and humidity at all levels yielded a positive correlation between them at small scales and a negative one at large (in excess of 100 m) scales. It was suggested that this is due to a positive

gradient of potential temperature and a negative specific humidity gradient above the highest (500 m) level. Measurements made across the wind, on the other hand, indicated a similar pattern except at the lowest level, where a negative temperature-humidity correlation coefficient occurred only at the largest scales investigated. The correlation coefficient between vertical velocity and temperature behaved in a similar fashion.

It was speculated that there may have been a certain amount of organization of the convective elements. The available evidence suggested that the convective cells tended to line up in the direction of the mean wind, which, as far as could be determined from the Doppler radar measurements, did not change direction appreciably between 18 m and 500 m.

LIST OF REFERENCES

Ball, F.K. (1960). Control of inversion height by surface heating. Quart. J. Roy. Meteorol. Soc., 86, p.483.

Blackman, R.B. and J.W. Tukey (1958). The Measurement of Power Spectra. Dover, New York.

BOMEX Project Office, (1969). Bomex bulletin No. 3. U.S. Dept. of Commerce, Environ. Sci. Services Admin., Rockville, Md.

Bunker, A.F., (1955). Turbulence and Shearing Stresses Measured Over the North Atlantic by an Airplane Acceleration Technique, J. Meteor. 12, 445.

Bunker, A.F., (1957). Aircraft (PBY-6A) Fluctuation and Flux Data - Woods Hole Oceanographic Institution, Sec. 5.3 in Exploring the Atmosphere's First Mile, (H. Lettau and B. Davidson, eds.) Pergamon Press, London and New York.

Bunker, A.F., (1960). Heat and Water Vapor Fluxes in Air Flowing Southward Over the Western North Atlantic Ocean, J. Meteor., 17, 52.

Dascher, A.J., (1966). NCAR Aircraft Research Instrumentation System (ARIS). Internal report, Facilities Division, National Centre for Atmospheric Research, Boulder, Colorado.

Davidson, B., (1968). The Barbados Oceanographic and Meteorological Experiment, Bull. Amer. Meteorol. Soc., 49, 928-934.

Dutton, J.A. and D.H. Lenschow, (1962). An airborne measuring system for micrometeorological studies, Annual Report, Contract No. DA-36-039-SC-80282, Dept. of Meteor., Univ. of Wis., Madison, Wis.

Elliott, J.A., (1970). Microscale pressure fluctuations measured within the lower atmospheric boundary layer. Ph.D. Dissertation, University of British Columbia.

Garrett, J.F., (1970). Field observations of frequency domain statistics and nonlinear effects in wind-generated ocean waves. Ph.D. Dissertation, University of British Columbia.

Grant, H.L., R.W. Stewart and A. Moilliet, (1962). Turbulence spectra from a tidal channel. J. Fluid Mech., 12, Pt. 2, p.241.

Hinze, J.O., (1959). Turbulence. McGraw-Hill, New York.

Katz, I., (1970). A comparison of remote and in-situ measurement in convection. To be presented at the 14th Weather Radar Conference, Tucson, Arizona in November.

Kolmogorov, A.N., (1941). The local structure of turbulence in incompressible viscous fluid for very large Reynolds numbers. Doklady ANSSSR, 30, p.301.

Konrad, T.G., (1970). The dynamics of the convective process in the clear air as seen by radar. To be presented at the 14th Weather Radar Conference, Tucson, Arizona in November.

Kuettner, J.P., and J. Holland, (1969). The BOMEX Project, Bull. Amer. Meteorol. Soc., 50, 394-402.

Kukharets, V.P., and L.R. Tsvang, (1969). Spectra of the turbulent heat flux in the atmospheric boundary layer. Izv., Atmospheric and Oceanic Physics, Vol. 5, No. 11, 1969, pp. 1132-1142, translated by Allen B. Kaufman.

Kuprov, B.M. and L.R. Tsvang, (1965). Direct measurements of the turbulent heat flux from an aircraft, Bull. (Izv.) Acad. Sci. USSR, Atmospheric and Oceanic Physics, 1, No. 6.

Lappe, U.O., B. Davidson and C.B. Notess, (1959). Analysis of atmospheric turbulence spectra obtained from concurrent airplane and tower measurements. Inst. Aero. Sci. Rep., No. 59-44.

Lumley, J.L. and H.A. Panofsky, (1964). The Structure of Atmospheric Turbulence. Interscience Publishers, New York.

McBean, G.A., (1970). The turbulent transfer mechanisms in the atmospheric surface layer. Ph.D. Dissertation, University of British Columbia.

Miyake, M., M. Donelan, G. McBean, C. Paulson, F. Badgley, and E. Leavitt, (1970a). Comparison of turbulent fluxes over water determined by profile and eddy correlation techniques, Quart. J. Roy. Meteor. Soc., 96, pp. 132-137.

Miyake, M., M. Donelan, and Y. Mitsuta, (1970). Airborne measurement of turbulent fluxes, J. Geophys. Research, 75, No. 24, pp. 4506-4518

Miyake, M., R.W. Stewart, and R.W. Burling, (1970c). Spectra and cospectra of turbulence over water, Quart. J. Roy. Meteor. Soc., 96, pp. 138-143.

Miyake, M., and G. McBean, (1970). On the measurement of humidity transport over land, Boundary Layer Meteorology, 1, pp. 88-101.

Monin, A.S., (1962). Empirical data on turbulence in the surface layer of the atmosphere. J. Geophys. Research, 67, p.3103.

Monin, A.S., and A.M. Obukhov, (1954). Basic regularity in turbulent mixing in the surface layer of the atmosphere. Trudy Geophys. Inst. ANSSSR, No. 24, p.163.

Myrup, L.O., (1965). The Structure of Thermal Convection in the Lower Atmosphere Under Conditions of Light Winds and Strong Surface Heating. Ph.D. Thesis, Univ. of Cal. at Los Angeles, Los Angeles, Cal.

Obukhov, A.M., (1951). Investigations of the microstructure of the wind in the atmosphere near the surface. Izv., ANSSSR Geophys. Ser., No. 3, p.49.

Panofsky, H.A., and E. Mares, (1968). Recent measurements of cospectra of heat-flux and stress. Quart. J. Roy. Meteorol. Soc., 94, 402, p.581.

Payne, F.R., and J.L. Lumley, (1966). 1-D spectra derived from an airborne hot-wire anemometer. Quart. J. Roy. Meteorol. Soc., 92, 393, p.397.

Pond, S., R.W. Stewart and R.W. Burling, (1963). Turbulence spectra in wind over waves. J. Atmosph. Sci., 20, p.319.

Priestley, C.H.B., (1959). Turbulent transfer in the lower atmosphere. University of Chicago Press, Chicago.

Robinson, G.D., (1959). Vertical motion and the transfer of heat and momentum near the ground. Advances in Geophysics, 6, p.259.

Roll, H.U., (1965). Physics of the Marine Atmosphere. Academic Press, New York.

Rudnick, P., (1964). FLIP: an oceanographic buoy. Science, 146, pp. 1268-1273.

Sheih, C., (1969). Airborne hot-wire measurements of the small-scale structure of atmospheric turbulence. Ph.D. Dissertation, Pennsylvania State University.

Smith, S., (1967). Thrust anemometer measurements of wind-velocity spectra and of Reynolds stress over a tidal inlet. J. Mar. Res., 25 (3). pp. 239-262.

Taylor, G.I., (1954) The Dispersion of Matter in Turbulent Flow Through a Pipe. Proc. Roy. Soc. Series A, Vol .ccxxiii, pp. 446-468

Telford, J.W., and J. Warner, (1962). On the measurement from an aircraft of buoyancy and vertical air velocity in cloud. J. Atmos. Sci., 19, pp. 415-423.

von Mises, R., (1945). Theory of Flight. 629 pp., Dover Publications Inc., New York.

Vul'fson, N.I., (1961). A Study of Convective Motions in a Free Atmosphere, Acad. Sci. USSR Publishing House.

Weiler, H.S., and R.W. Burling, (1967). Direct measurements of stress and spectra of turbulence in the boundary layer over the sea. J. Atmos. Sci., 24, (6) pp. 653-664.

Woodcock, A.H., (1942). Soaring over the open sea. Sci. Monthly, 55, pp.226-232.

APPENDIX A

THE INSTRUMENTS

A.1 Introduction

The instrumentation and method of correction for the aircraft's motion are described by Miyake et al (1970b). However, their concern was largely with the determination of the velocity components and the momentum flux. Inasmuch as several of the results of this thesis hinge on the measurement of the fluxes of sensible and latent heat, it is advisable to attempt to assess the accuracy, resolution and frequency response of the temperature and humidity sensors.

A.2 The temperature sensor

This device, constructed in this laboratory, consisted of a thermistor bead in a DC Wheatstone bridge. The primary basis for choice of bead was its small thermal lag; Victory Engineering Company's thermistor model 41 A 401C was found to be quite suitable. It has a nominal diameter of 127 μ and resistance and resistance change per C^{o} at 25 degrees centigrade of 10 KΩ and 360 Ω respectively.

The probe current of 5 μ amps was selected by wind tunnel testing to ensure adequate sensitivity to temperature and insignificant response to velocity fluctuations (the'anemometer effect').

The current was provided by an alkaline battery (9.7 volts) and limited by fixed bridge arms of 2.2 MΩ so that for temperature fluctuations of 6 C^{o} the probe current varied less than 0.01%. Mean temperature offset was achieved by means of a ten turn potentiometer in the fourth bridge arm. The bridge output was buffered by a high impedence unity gain stage (voltage follower) and then amplified in two stages,

the second of which was adjustable to give an overall sensitivity of either 1.4 or 3.2 C^{o}/volt approximately. The noise level was about 0.5 mv, which is equivalent to a signal level of about 0.001 C^{o}.

The thermistor was calibrated in the laboratory; also the 'in situ' resistance versus temperature response was determined by comparing the traces of the thermistor and a standard airborne thermometer during a sounding; both calibrations produced essentially the same result. Although the mean response is non linear, the device is essentially linear for small ($< 3\ C^{o}$) fluctuations.

The response of the instrument was measured directly in three ways: two in the wind tunnel and one in the field. The first wind tunnel method was to superimpose a step voltage decrease on the bridge voltage and record the cooling response on chart paper; the time constant was deduced from the exponential decay trace. In the second method the thermistor and a thin wire resistance thermometer (response flat to 20 kHz) were placed in the wake of a heated soldering iron; the cut-off of a low pass RC filter in the output of the resistance thermometer was adjusted until the outputs of both instruments produced the most similar chart records. Both tests indicated a cut-off frequency (-3 db point) near 30 Hz.

The field test relies on a comparison of a measured temperature spectrum with its well established form in the inertial sub-range (Figure 60) which is known to extend well beyond 30 Hz. If the frequency response inferred from the wind tunnel tests is used to correct the measured spectrum, the result, shown in Figure 60, lends credence to the representation of the thermistor's response as similar to that of a simple low pass filter with a frequency cut-off of 30 Hz.

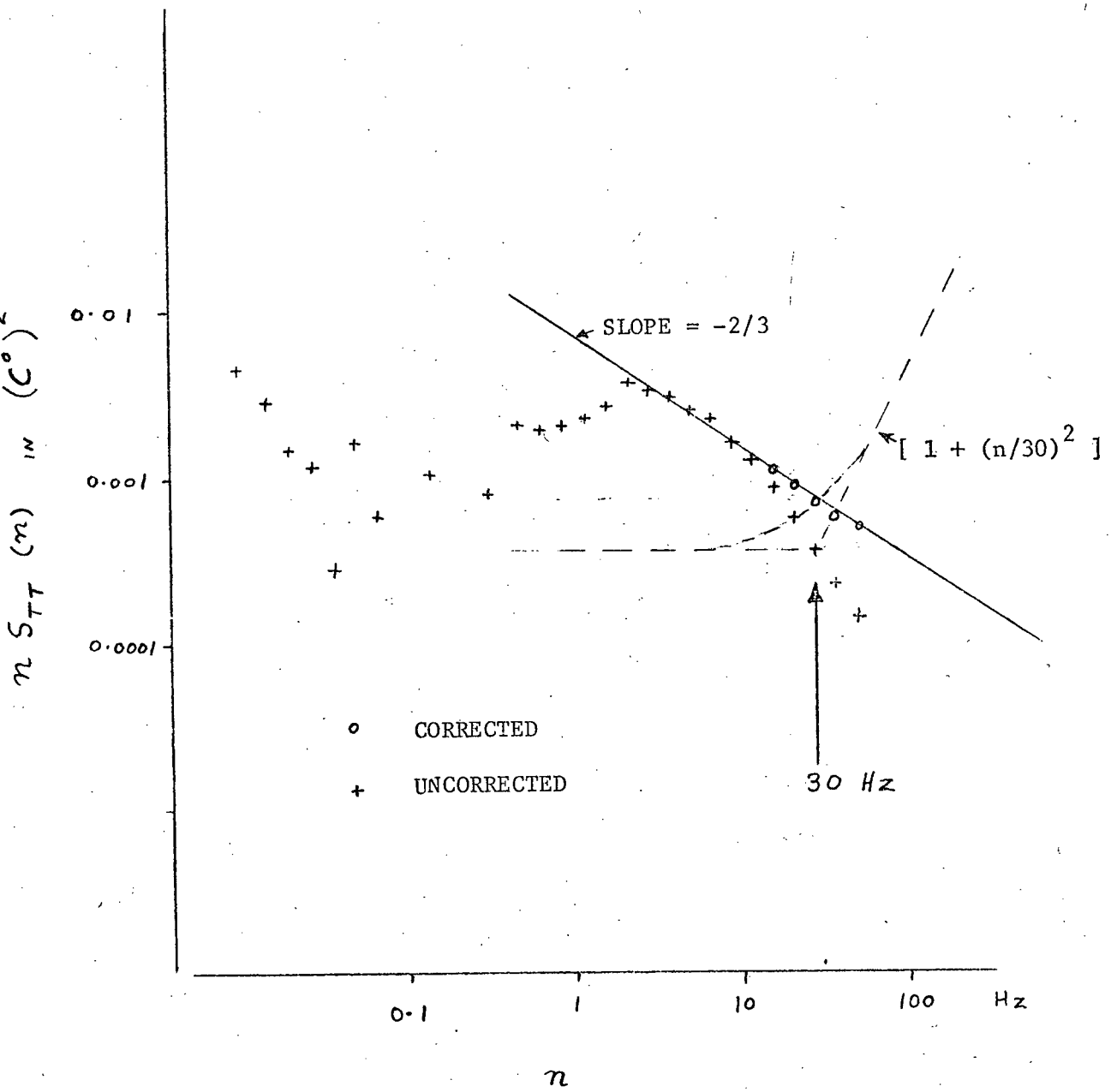

FIGURE 60. THE FREQUENCY RESPONSE OF THE THERMISTOR

There are two further problems associated with the use on aircraft of an exposed, slightly heated sensor for the measurement of temperature: one is frictional-compressional heating and the other is the 'anemometer effect'. Fortunately these act in opposition; an increase in air speed increases the frictional-compressional heating and at the same time reduces the self heating by improving the ventilation; thus this circumstance can be employed in the design to make an exposed bead thermometer quite indifferent to velocity fluctuations. However in this case the approach taken was a cautious one: the anemometer effect was made negligible with the intention of correcting for the frictional-compressional heating in the analysis if this proved necessary. It is of interest to examine the importance of these two effects.

The widely used hot-wire anemometer equations (Hinze, 1959, p. 78) provide an estimate of 6.6×10^{-4} C^{o} for the self heating at the aircraft's speed (70 m/sec), and indicate that the apparent temperature sensitivity to velocity changes is only -4.5×10^{-6} C^{o} $(m/sec)^{-1}$ and is proportional to the square of the probe current. Evidently the latter effect is negligible, and the in-flight excess temperature is therefore due to frictional-compressional heating.

At light aircraft speeds, as a rough approximation, the actual sensor overheat T_f, due to frictional-compressional heating, is assumed to be proportional to the square of the air speed. Since T_f was observed to be 1.9 C^{o} at 70 m/sec, the constant of proportionality is 3.9×10^{-4} C^{o} $(m/sec)^{-2}$. Thus the temperature sensitivity to velocity changes is 5.4×10^{-2} C^{o} $(m/sec)^{-1}$ at the same aircraft speed. Obviously the velocity contamination due to frictional-compressional heating is not negligible, and, with typical maximum velocity changes of

2m/sec occurring with temperature fluctuations of about $1\,C^{o}$, it reduces the equivalent signal to noise ratio to ten (20 db).

Although it is a relatively simple matter to remove the effect of frictional-compressional heating in the digital analysis, it was regarded as unnecessary. It is interesting to note that, merely by increasing the probe current one hundred-fold, the two velocity effects would counter-balance each other and, of course, the bridge sensitivity would increase with the probe current. Such an increase of the probe current would produce an overheat of $6.6\ C^{o}$.

A.3 The humidiometer

The Lyman-Alpha humidiometer used in this experiment is described by Miyake et al (1970b). As stated by them the primary factor which limited the response to small scale humidity fluctuations was the mixing of air in the inlet tubing and instrument housing. Because of the 'S' bend in the tygon inlet tube, it is difficult to determine theoretically the exact transfer function of the air passage. However Taylor (1954) has shown that in turbulent flow in a straight pipe the impulse response of the pipe is gaussian. In terms of the spectral amplitude transfer function $H_{(n)} = e^{-(Bn)^2}$, where B was estimated to be about 0.01. However, this transfer function produces a cut-off which is far sharper than that observed. It is presumed that the many sharp bends in the tube are the cause of this.

It was found, by comparison of the measured spectra with the expected -2/3 slope, that the transfer function of the tube could be reasonably well represented by:

$$H_T(n) = \begin{cases} [\,1 - An\,] & , \ An \leqslant 1 \\ [\,o\,] & , \ An \geqslant 1 \end{cases}$$

Where the value of A represents the degree of turbulent diffusion over the length of the tube and depends on the flow rate through it. Turbulent diffusion, therefore, acts to smooth rapid changes in moisture content symmetrically in both directions along the axis of the tube with respect to the frame of reference moving with the mean flow. Thus, there is ideally no phase shift associated with the amplitude reduction. In Figure 61 a measured humidity spectrum $nS_{QQ}(n)$ and a corrected spectrum are displayed. The value of A (0.023) was selected from all the spectra so that the transfer function would be significantly different from unity at the point where the measured spectrum falls beneath the -2/3 line. It is seen that the corrected spectrum follows the commonly observed -2/3 law in the same region as the downwind velocity component (Figure 14) lending credence to the postulated approximate inlet tube transfer function.

As with the other turbulence sensors, the practice of 'in situ' calibration was observed whenever possible. In this case the standard of comparison was the spectrum obtained from a laboratory calibrated Bendix Dew Point Hygrometer. Neither the calibrations of these two instruments nor the relation between them is linear, but for small excursions about a mean value the effect of non-linearity is unimportant. Dr. S. Pond of Oregon State University has computed spectra, from a record obtained by the Lyman Alpha Humidiometer, using first a calibration constant and then the actual logarithmic dependence of the detector current on the moisture content: he reports (personal communication) that there is no significant difference for fluctuations of one or two gm/Kgm about a mean value ten times as great. Consequently no attempt has been made to linearize the humidiometer records used herein. The non-linearity of the

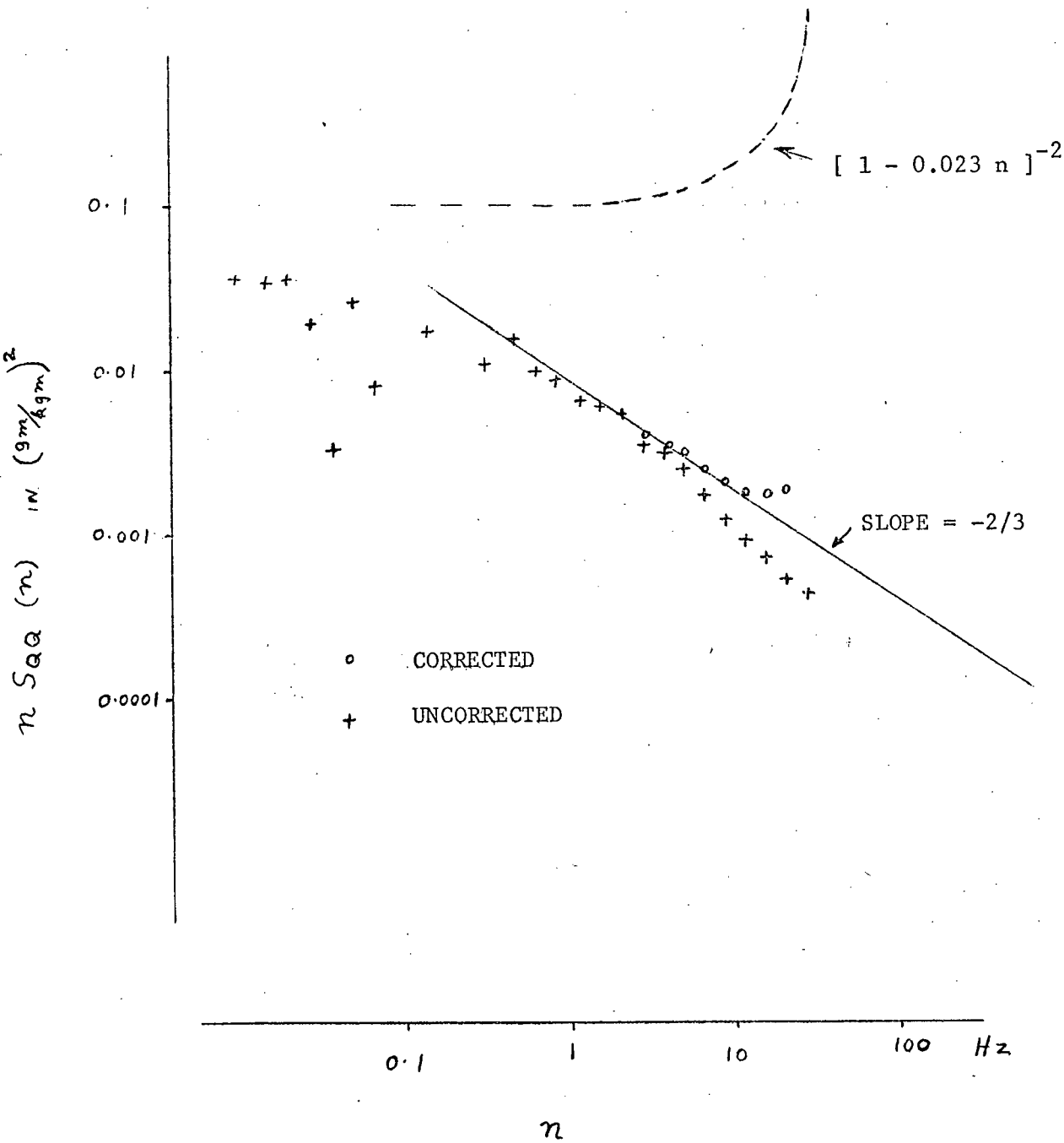

FIGURE 61. THE FREQUENCY RESPONSE OF THE HUMIDIOMETER

dew point hygrometer arises in its thermistor detection circuit; however, from the calibration curve it is evident that the non-linearity is not in excess of 2% for 10% deviations from the mean value. Hence the appropriate slope of the calibration curve was used to calibrate the spectrum of Figure 61, but the curve itself was used in the computation of the soundings of Figure 5.

The spectral comparison yields the humidiometer calibration in terms of dew point fluctuations. From the Clausius-Clapeyron equation the following approximate relations between the average (overbar) and fluctuating (primed) parts of the dew point and the specific humidity are obtained (see McBean, 1970):

$$\ln \frac{\bar{Q}\, P}{0.622} \doteq 1.81 + 19.9 \left(\frac{\bar{T}d}{273 + \bar{T}d} \right)$$

$$Q' \doteq 19.9 \left(\frac{\bar{Q}}{273 + \bar{T}d} \right) T'd$$

Where P is the atmospheric pressure in millibars.

Q is the specific humidity in Kgm/Kgm.

Td is the dew point in ^{0}C.

The humidiometer was mounted in the cabin and vented by means of an impact tube on the top of the fuselage (see Miyake et al, 1970 b). In the digital analysis the time delay due to the longitudinal separation of the humidiometer from the other turbulence sensors was removed by advancing the humidiometer record by the appropriate number of samples.

APPENDIX B

DATA PROCESSING

B.1 Introduction

All the spectra and time series presented herein were computed from the original analogue recorded data. Spectra for a few runs were computed from the data recorded digitally merely to check the calibration of the analogue tape recorder and subsequent conversion to digital format. In the following sections of this Appendix the method of selection of data segments is described, and the digitization and subsequent machine processing is outlined.

B.2 Selection of data segments

First the channels to be digitized were reproduced on a six pen chart recorder and examined for noise, dropout and changes of zero bias. Each data segment, or run, was selected between successive turns (roll angle) and/or to avoid all of these discontinuities in the data. In some cases, when bursts of noise in the temperature record were the only blots on an otherwise excellent run, the run was used anyway and the results involving temperature fluctuations were rejected. If the temperature record is applied to the input of an audio amplifier with speaker, the bursts of noise are recognised as radio pick-up from the Queen Air's UHF transmitter (1230 M Hz). In fact the pilot's voice is about as clear as it would be from a cheap portable radio. Evidently the thermistor probe and supports acted as an antenna, and the non-linearity of the thermistor itself partially rectified the carrier, thereby demodulating it.

The pitch angle record also played an important part in the selection of the start of each run. During the 90 degree turns the centrifugal

force on the gyroscope's bail rings introduced a spurious pitch angle deviation of about 1.5 degrees. Once level flight was resumed the gyroscope erected itself at a rate proportional to g sin θ' (see Miyake et al, 1970b). Thus a spurious exponential decay was imposed on the recorded pitch angle at the beginning of every run. Since in the analysis linear trends are rejected, the procedure used was to omit that part of the first half of each run in which the pitch angle's trace deviated appreciably from a straight line drawn through its trace in the second half.

B.3 Machine processing

Once the runs were selected the analogue data was quantized and written on digital tape. Figure 62 illustrates this in block diagram form and also outlines the subsequent processing steps.

The analogue to digital convertor (designed and built in this laboratory) accepts signal levels between $\pm$ 5.12 volts and quantizes them in 10 millivolts steps. To reduce the quantization noise effect some channels were pre-amplified. All the channels were low pass filtered with matched linear phase shift filters having a high frequency roll-off of 40 db/decade above the 3 db point at 160 Hz and phase shift of 0.45°/Hz up to 240 Hz. A linear phase shift is equivalent to a time delay, and so the wave forms are distorted only in regard to the amplitudes of the high frequency components, which are restored later in the program, 'SIMPLOT'.

The purpose of the filters is, of course, to reduce aliasing, and the sampling frequency of the A-D convertor was set at 320 Hz i.e. at twice the Nyquist frequency. Although this means an attenuation of only 3 db at the Nyquist frequency (160 Hz), it is adequate because the

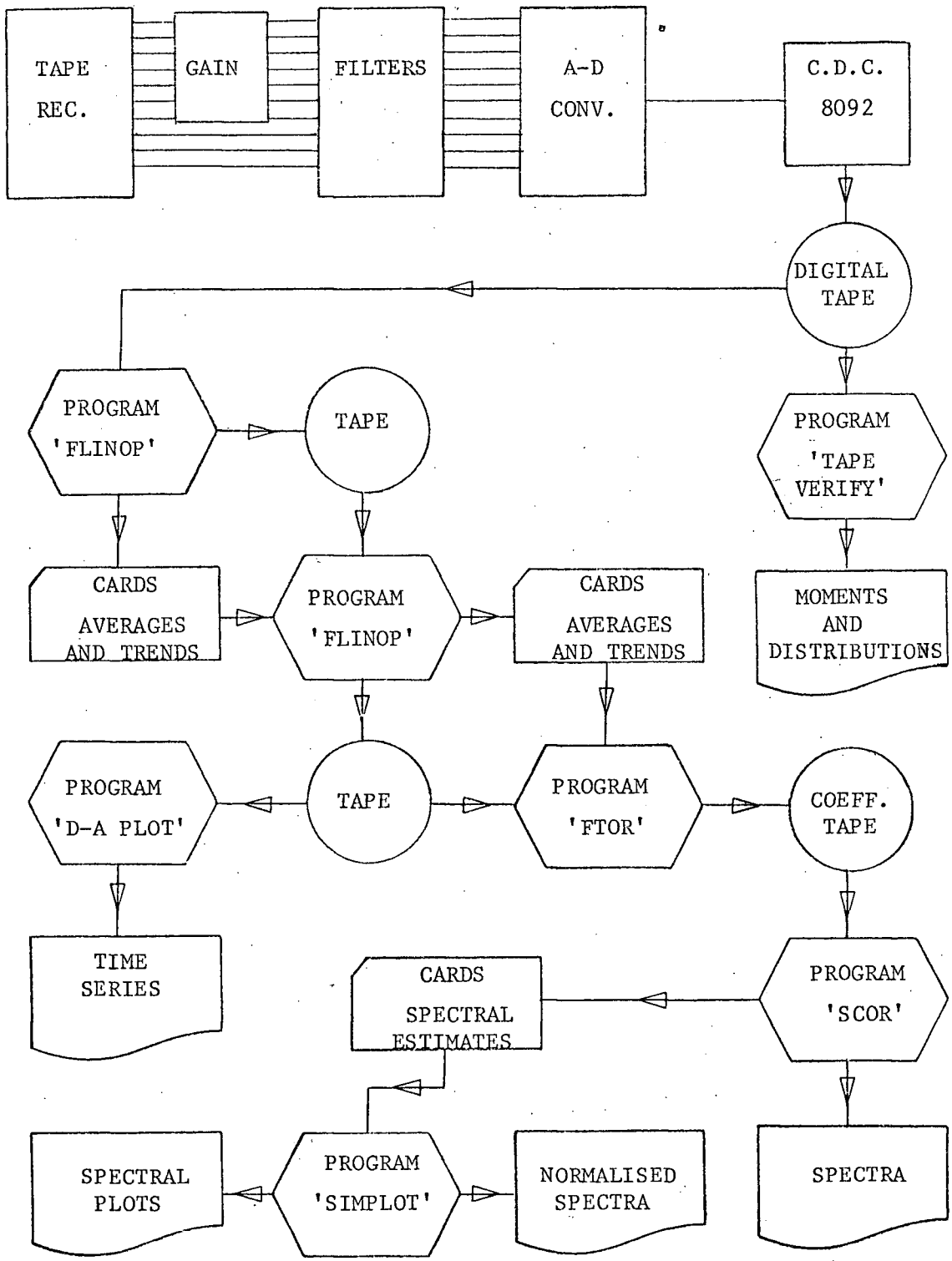

FIGURE 62. BLOCK DIAGRAM OF MACHINE PROCESSING STEPS

spectra of turbulence fall off rapidly with increasing frequency in this region. Thus, 320 times per second the convertor completed one 'cross channel sweep' of all ten channels, waiting only 45 micro-seconds between adjacent channels or 405 micro-seconds between first and last channels. All the data was digitized with the analogue tape recorder playing back at eight times the recording speed, and some of it was digitized a second time at real playback speed; i.e. the real time sampling frequencies were 40 Hz and 320 Hz respectively. Thus, the longest real time interval between sampling two channels is 3.3 milliseconds corresponding to a space lag of 23 cm.

A careful calibration of the tape recorder, amplifiers, filters and A-D convertor was performed both before and after each digitizion session.

A Control Data Corporation Computer (CDC 8902, see Figure 62) writes the sequentially sampled data on digital tape, which can then be handled by the IBM 360 system at U.B.C. Before proceeding with the processing of a digital tape it was prudent to ascertain whether or not the digitization process was successful. This was done by the program, 'TAPE VERIFY', written by R. Wilson of this Institute, in the form of voltage distributions for each channel and their first, second, third and fourth moments.

The lowest frequency estimate obtainable from a section of data of length $N\Delta t$ seconds is at $1/N\Delta t$ Hz. Thus, if the data contains an appreciable trend the energy associated with the trend will appear in the low frequency estimates (see Blackman and Tukey, 1959).

In view of the gyroscope's limitations and the fact that the acceleration signals have to be integrated, it is hardly reasonable to

expect the corrected velocities to be devoid of trend even if the actual velocity components were. Furthermore, due to aircraft range limitations, long flights at any level had to be sacrificed in favour of multi-level sampling; with the result that the short crosswind flights, at high altitudes in particular, reflect the presence of energy at scales larger than the total sample length. It was therefore decided that the most consistent approach would be to remove the averages and trends from all the channels both before computing the corrected velocity components and before determining the fourier coefficients of these components. Thus, the author undertook to write a program, 'FLINOP' which could be controlled to compute and remove averages and linear trends (in successive passes), perform all of the operations required for correction of aircraft motion, multiply time series together point by point and delay or advance any signal with respect to the others. These last two were required to produce time series of instantaneous fluxes and to advance the humidiometer signal by $d/V\Delta t$ samples respectively, where d is the downstream distance of the humidiometer from the nose, Δt is the interval between samples and V is the average air speed of the aircraft. The integration was done in staircase fashion and the differentiation by finite differences after first computing an equally weighted running mean over a selectable number of samples.

The tape written by the second pass through 'FLINOP' is reproduced on a Calcomp digital plotter in the form of time series using the program 'D-A PLOT', written by R. Wilson. These time series are displayed in many of the figures in this thesis.

The frequency domain is entered by means of the programme, 'FTOR' using the fast fourier transform algorithm, PK FORT 5DA 3465. The tape

of fourier coefficients which it produces is accepted by the programme, 'SCOR' which produces spectral and cross-spectral estimates, coherence and phases. Both of these programmes were written by J. Garrett of this Institute and are described in his Ph.D thesis (Garrett, 1970). However, because there is some divergence of nomenclature in the literature, the forms for the 'spectrum', 'coherence' and 'correlation coefficient', which are used here are explained:

Spectrum: $S_{xx}(n)$ is defined so that: $\overline{x^2} = \int_0^\infty S_{xx}(n)\,dn = \int_0^\infty nS_{xx}(n)\,d(\ln n)$

Coherence: $coh_{xy}(n) = \left(\frac{S^2_{xy}(n) + Q^2_{xy}(n)}{S_{xx}(n)\ S_{yy}(n)} \right) 1/2$

Correlation coefficient: $r_{xy}(n) = \frac{S_{xy}(n)}{\left(S_{xx}(n).S_{yy}(n)\right)^{1/2}}$

Where $S_{xy}(n)$ and $Q_{xy}(n)$ are the co-spectrum and quad-spectrum respectively.

The average correlation coefficient: $r_{xy} = \frac{\overline{x'y'}}{\sigma_x.\sigma_y}$

In 'FTOR' each run was divided into four or more blocks, and the coefficients computed for each block. This allowed the programme, 'SCOR' to compute the mean spectral estimate at each frequency, its standard deviation $\sigma(n)$ among the blocks and its trend throughout the run. The latter two provide an indication of the stationarity of the process. The block length was generally 1024 samples, but was reduced to 512 for a few of the very short runs.

Since the sequence of block averages of x(t) is itself a time

series in which the original data has been box-car averaged and sampled at intervals of $(N\Delta t)/K$ seconds (K is the number of blocks), a few spectral estimates ($\frac{K}{2}$ in number) can be obtained using the fast fourier transform algorithm. G. McBean of this Institute has extended 'SCOR' to do this (McBean, 1970). These 'low frequency' estimates also appear on the spectra, but, since there is only one estimate available, at each frequency, no observations of their variances are available. It is worth noting that these low frequency estimates contain so few degrees of freedom that only consistency in their values should be taken as a possible indication of the spectral shape.

The final stage of machine processing is the programme 'SIMPLOT' written by G. McBean of this Institute. 'SIMPLOT' accepts the spectral estimates from 'SCOR', corrects for the attenuation of the filters used in the digitization process and the path averaging of the sonic anemometer, obtains the cumulative integral under the spectra as a function of decreasing frequency, and plots (on a calcomp plotter) spectra and co-spectra on selectable axes.

APPENDIX C

COMPARISON OF SIMULTANEOUS MEASUREMENTS FROM FLIP AND THE AIRCRAFT

C.1 Introduction

During BOMEX the Queen Air made several flights around the specialized Research ship 'FLIP' (floating instrument platform, Rudnick, 1964), from which instrumentation similar to that on the aircraft was used to measure the vertical turbulent fluxes. One of these flights is presented here in an attempt to establish the validity of the airborne flux measurements. Inasmuch as FLIP is subject to wind and wave induced motion and since it is known to distort the mean flow, results from its use are also subject to doubt. However, since the likelihood of these two very different platforms yielding the same but erroneous result is small, agreement of the results will be taken as showing that measurements from both platforms are essentially correct.

C.2 Data outline

Table 5 provides a brief outline of the data sections to be compared. The duration of the data run from FLIP was 45 minutes, during which the mean wind was about 8.5 m/sec; while the upwind and downwind runs each yielded 4 minutes of usable data. Therefore, at the same height the upwind and downwind flights covered about the same scale sizes as the FLIP data. Furthermore, the data gathered from FLIP straddles the aircraft data in time. Hence, within the range of validity of Taylor's hypothesis, this comparison is over approximately the same scales; provided, of course, that conditions are homogeneous within about 50 km of FLIP.

PLATFORM	RUN	LOCAL TIME		HEIGHT OF INSTRUMENTS	DIRECTION OF FLIGHT	SYMBOL
		START	END			
FLIP	B-55/1	15.05	15.50	30 m		⊙
AIRCRAFT	4/3	15.33	15.37	15 m	DOWNWIND	×
AIRCRAFT	4/5	15.43	15.47	18 m	UPWIND	○

TABLE 5 THE DATA USED IN THE FLIP / AIRCRAFT COMPARISON

C.3 Spectra and cospectra

The analysis of the FLIP data presented some interesting problems, the solution of which are due in the main to the efforts of G. McBean of this Institute, who processed the FLIP data discussed herein.

The abscissa of Figures 63, 64 and 65 is the natural frequency f (=nZ/V). This similarity coordinate was used in order to be able to compare the spectra by direct superimposition. The values of V were 70 m/sec in the case of the aircraft and 8.5 m/sec in the case of FLIP; and the instruments were mounted 30 m above the surface on FLIP when the Queen Air flew by at an altitude of 18 m.

The instruments on the two platforms were independently calibrated, and so the ordinates of Figures 63, 64 and 65 are not normalized. It is seen that the n-spectra of vertical (Figure 63), horizontal (Figure 64) velocity fluctuations and the momentum n-cospectra (Figure 65) are very similar in amplitude and shape in all three cases presented: two airborne measurements in the vicinity of Flip and the concurrent Flip measurements.

In all three figures the Flip n-spectra display a 'bump' at f = 0.2, which is not in the aircraft n-spectra. This 'bump' coincides with the peak of the measured water wave spectrum, and is due to wave induced motion of Flip.

It seems that, apart from the wave induced bump in the Flip spectra and some scatter of the low frequency points, the agreement is excellent between the measurements made from Flip and those made from the aircraft. Thus, in view of the excellent correspondence of results from these two so different platforms, there cannot be much doubt of the validity of the conclusion that the Queen Air, equipped as it was, is an acceptable

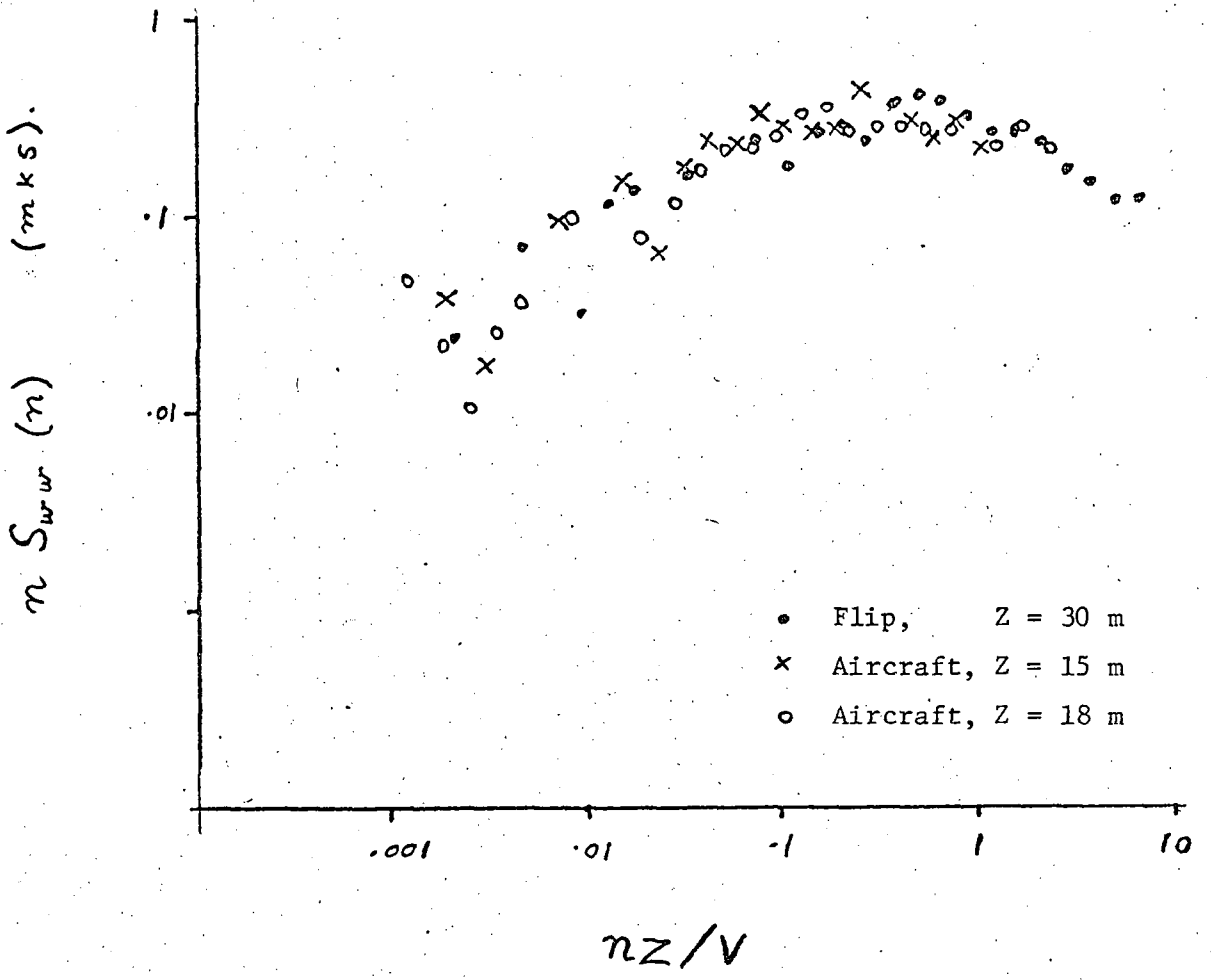

FIGURE 63. COMPARISON OF w´ SPECTRA FROM THE AIRCRAFT AND FLIP

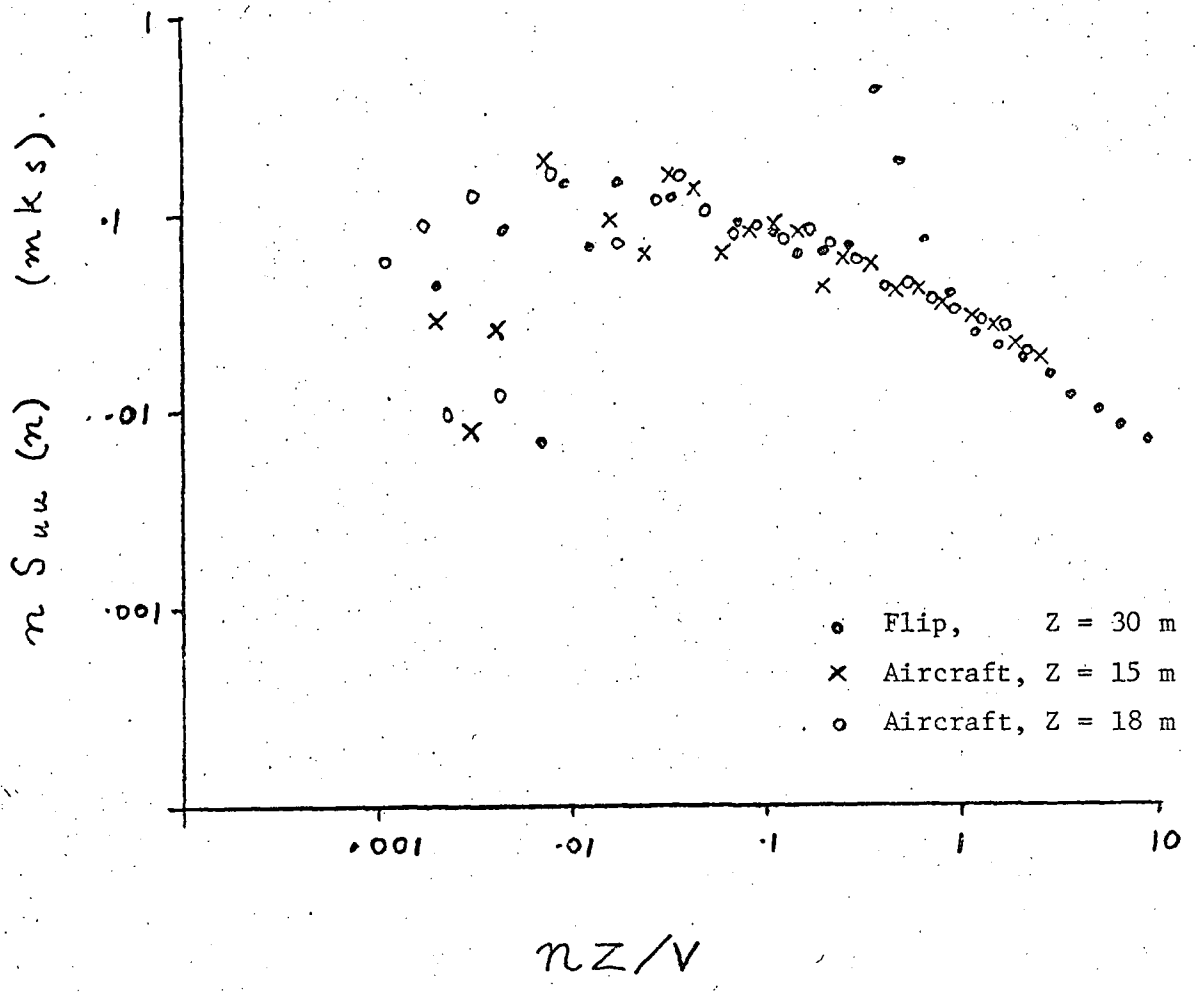

FIGURE 64. COMPARISON OF ú SPECTRA FROM THE AIRCRAFT AND FLIP

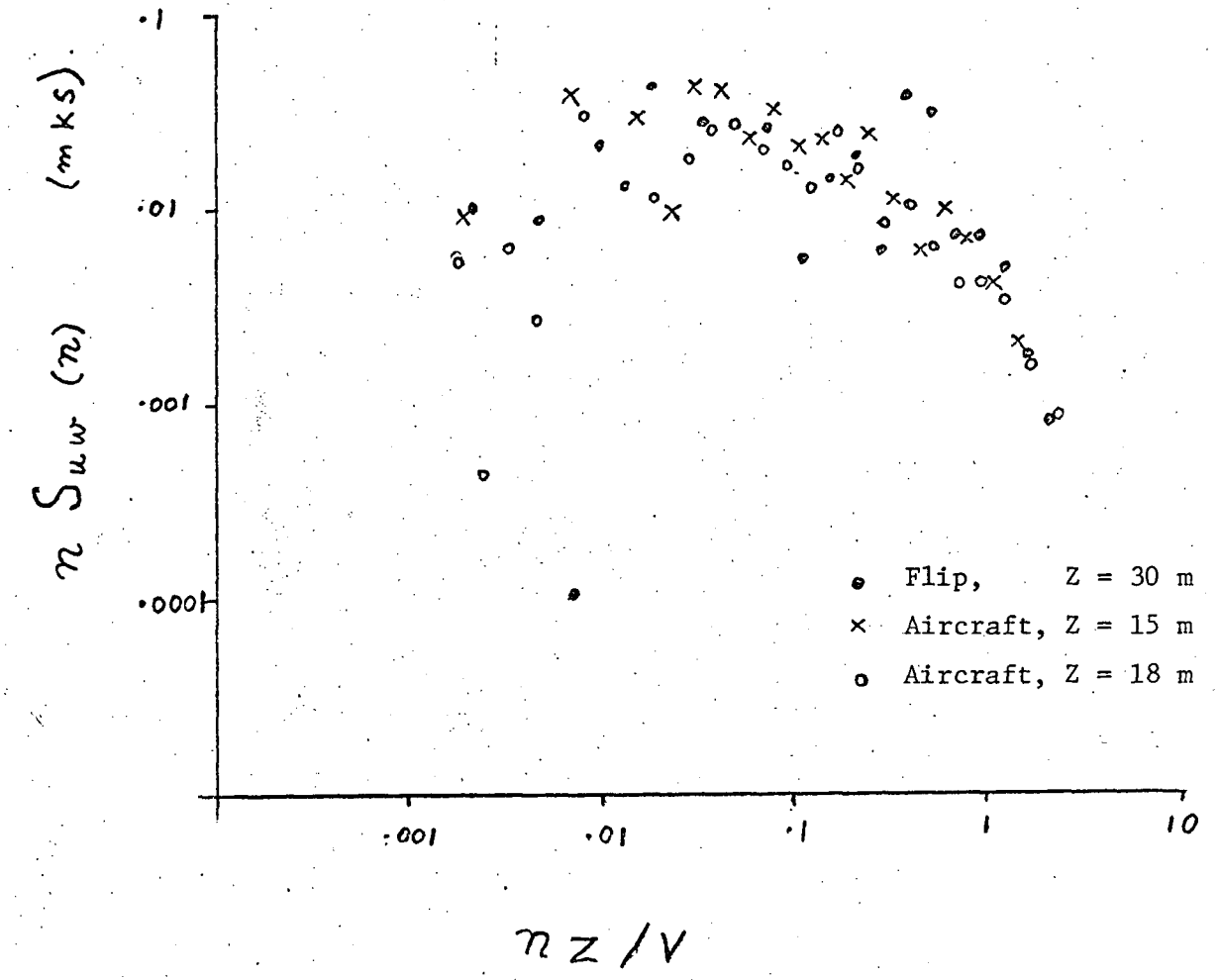

FIGURE 65. COMPARISON OF THE MOMENTUM COSPECTRA FROM THE AIRCRAFT AND FLIP

platform for the measurement of turbulence near the surface.

APPENDIX D

STATISTICS

RUN	σ_w cm/s	σ_u cm/s	σ_T C°	σ_Q gm/kgm	τ_{zx} $\frac{\text{dynes}}{\text{cm}^2}$	F_H mW/cm^2	F_Q mW/cm^2
1/6	30.8	52.2	.105	.291	.643	.77	10.30
1/3	31.0	37.8	.071	.188	.306	.75	9.49
1/7	47.3	38.5	.063	.223	.579	-.11	15.65
1/12	33.8	42.9	.155	.499	.079	-1.22	19.60
2/8	33.5	56.9	.128	.225	.985	2.47	13.19
2/7	30.3	43.8	.096	.246	.347	.34	8.97
2/4	33.5	46.0	.074	.171	.212	-.21	7.10
2/10	34.2	68.5	.411	.508	1.09	1.13	21.61
3/6	40.2	74.6	.117	.302	1.47	-.05	17.14
3/3	41.5	59.5	.093	.252	.921	.64	7.68
3/9	31.5	56.6	.066	.184	.789	.51	8.10
3/12	42.0	44.4	.527	.198	.504	--	9.27
4/5	37.7	73.5	.105	.255	1.28	.85	12.31
4/2	31.5	74.8	.073	.192	.478	.31	6.80
4/8	37.8	42.2	.069	.152	.401	-.48	4.54
4/9	24.3	45.9	.230	.226	.297	.13	3.56
5/2	37.0	76.6	.092	.277	1.34	.18	13.93
5/4	37.8	66.3	.093	.288	.905	.04	11.99
5/6	34.9	42.1	.071	.190	.375	-.07	7.78
5/8	34.9	36.7	.072	.152	.556	.52	8.42
6/2	39.7	66.4	.091	.245	1.49	.10	15.55
6/4	33.5	38.1	.102	.251	.272	-.12	8.42
6/6	40.2	39.2	.221	.649	.014	.39	11.34

TABLE 6 - VARIANCES

$$\frac{z\,k\,g\,\overline{w'\rho'}}{\rho\,u_*^3} = z/L = z/L_T + z/L_Q = \frac{-z\,k\,g\,\overline{w'T'}}{\bar{T}\,u_*^3} - \frac{z\,k\,0.61\,g\,\overline{w'Q'}}{u_*^3}$$

RUN	**	Z	u_*^2	$\overline{w'T'}$	$-Z/L_T$	$\overline{w'Q'}$	$-Z/L_Q$	$-Z/L$
		m	$(m/s)^2$	(m/s)C°		$(\frac{m}{s})$ $(\frac{gm}{kgm})$		
1/6	U	20	.0497	.0059	.14	.0318	.14	.28
1/3	U	43	.0237	.0058	.89	.0293	.83	1.72
1/7	D	150	.0448	-.00083	-.17	.0483	1.9	1.73
1/12	U	500	.0061	-.0094	-130.	.0605	150.	20.
2/8	D	18	.0762	.019	.21	.0407	.085	.30
2/7	U	46	.0268	.0026	.35	.0277	.69	1.04
2/4	U	150	.0164	-.0016	-1.5	.0219	3.8	2.3
2/10	D	460	.0842	.0087	2.1	.0667	3.0	5.1
3/6	U	18	.114	-.00042	-.025	.0529	.059	.034
3/3	U	49	.0712	.0049	.16	.0237	.15	.31
3/9	U	150	.061	.0039	.51	.0250	.61	1.12
3/12	U	500	.0391	--	--	.0286	4.4	4.4
4/5	U	18	.099	.0065	.048	.038	.053	.10
4/2	U	52	.037	.0024	.23	.021	.37	.60
4/8	U	150	.031	-.0037	-1.3	.014	.94	-.36
4/9	D	490	.023	.001	1.8	.011	3.7	5.5
5/2	U	26	.104	.0014	.014	.043	.08	.094
5/4	U	49	.070	.00034	.011	.037	.23	.24
5/6	U	88	.029	-.00052	-.12	.024	1.0	.88
5/8	U	140	.043	.0040	.81	.026	.98	1.79
6/2	U	29	.115	.00077	.007	.048	.086	.093
6/4	U	98	.021	-.0009	-.38	.026	2.00	1.62
6/6	U	480	.0011	.0030	520.	.035	1100.	1620.

** U = Upwind, D = Downwind

TABLE 7 - STABILITY

$$T_* = \frac{-\overline{w'T'}}{k\, u_*} \quad ; \quad Q_* = \frac{-\overline{w'Q'}}{k\, u_*}$$

RUN	u_*	$-T_*$	$-Q_*$	σ_w/u_*	σ_u/u_*	$-\sigma_T/T_*$	$-\sigma_Q/Q_*$
	cm/s	C°	gm/kgm				
1/6	22.3	.066	.357	1.38	2.34	1.59	.82
1/3	15.4	.094	.476	2.01	2.45	.76	.39
1/7	21.2	-.010	.570	2.33	1.82	-6.30	.39
1/12	7.8	-.301	1.939	4.33	5.50	-.51	.26
2/8	27.6	.172	.369	1.21	2.06	.74	.61
2/7	16.4	.040	.422	1.85	2.67	2.40	.58
2/4	12.8	-.031	.428	2.62	3.59	-2.39	.40
2/10	29.0	.075	.575	1.18	2.36	5.48	.88
3/6	33.8	-.003	.391	1.19	2.21	-39.0	.77
3/3	26.7	.046	.222	1.55	2.23	2.02	1.14
3/9	24.7	.039	.253	1.28	2.29	1.69	.73
3/12	19.8	--	.361	2.12	2.24	--	.55
4/5	31.5	.052	.302	1.20	2.33	2.02	.84
4/2	19.2	.031	.273	1.64	3.90	2.35	.70
4/8	17.6	-.053	.199	2.15	2.40	-1.30	.76
4/9	15.2	.016	.191	1.60	3.02	14.38	1.18
5/2	32.2	.011	.334	1.15	2.37	8.36	.83
5/4	26.5	.003	.349	1.43	2.50	31.00	.83
5/6	17.0	-.008	.353	2.05	2.48	-8.88	.54
5/8	20.8	.048	.313	1.68	1.76	1.50	.49
6/2	33.9	.006	.354	1.17	1.96	15.17	.69
6/4	14.5	-.016	.448	2.31	2.63	-6.38	.56
6/6	3.3	.227	2.65	12.18	11.88	.97	.24

TABLE 8 - SIMILARITY RATIOS

RUN	Z	$\frac{u_*^3}{\kappa z}$	$\frac{g\,\overline{w'T'}}{\bar{T}}$	$0.61g\,\overline{w'Q'}$	ϵ	D
	m	$\frac{cm^2}{s^3}$	$\frac{cm^2}{s^3}$	$\frac{cm^2}{s^3}$	$\frac{cm^2}{s^3}$	$\frac{cm^2}{s^3}$
1/6	20	13.86	1.93	1.90	10.81	-6.88
1/3	43	2.12	1.90	1.75	7.78	2.01
1/7	150	1.59	-0.27	2.89	3.81	-0.40
1/12	500	0.02	-3.07	3.62	1.86	1.29
2/8	18	29.20	6.21	2.44	18.23	-19.62
2/7	46	2.40	0.85	1.66	6.41	1.50
2/4	150	0.35	-0.52	1.31	3.54	2.40
2/10	460	1.33	2.84	3.99	5.86	-2.30
3/6	18	53.63	-0.14	3.17	51.58	-5.08
3/3	49	9.71	1.60	1.42	27.30	14.57
3/9	150	2.51	1.28	1.50	4.66	-0.63
3/12	500	0.39	-	1.71	5.95	3.85
4/5	18	43.41	2.13	2.27	68.39	20.58
4/2	52	3.40	0.78	1.26	19.73	14.29
4/8	150	0.91	-1.21	0.84	5.87	5.33
4/9	490	0.18	0.33	0.66	3.30	2.13
5/2	26	32.10	0.46	2.57	69.02	33.89
5/4	49	9.49	0.11	2.21	21.96	10.25
5/6	88	1.40	-0.17	1.44	6.97	4.30
5/8	140	1.61	1.31	1.56	7.69	3.21
6/2	29	33.58	0.25	2.87	28.76	-7.94
6/4	98	0.78	-0.29	1.56	4.25	2.20
6/6	480	0.00	0.98	2.09	2.56	-0.51

TABLE 9 - THE KINETIC ENERGY BUDGET